Mean-field theory of hard sphere glasses and jamming

Giorgio Parisi*

Dipartimento di Fisica, INFM-CNR SMC, INFN, Università di Roma "La Sapienza," Piazzale Aldo Moro 2, 00185 Roma, Italy

Francesco Zamponi†

Laboratoire de Physique Théorique, École Normale Supérieure, 24 Rue Lhomond, 75231 Paris Cedex 05, France

(Published 16 March 2010)

Hard spheres are ubiquitous in condensed matter: they have been used as models for liquids, crystals, colloidal systems, granular systems, and powders. Packings of hard spheres are of even wider interest as they are related to important problems in information theory, such as digitalization of signals, error correcting codes, and optimization problems. In three dimensions the densest packing of identical hard spheres has been proven to be the fcc lattice, and it is conjectured that the closest packing is ordered (a regular lattice, e.g., a crystal) in low enough dimension. Still, amorphous packings have attracted much interest because for polydisperse colloids and granular materials the crystalline state is not obtained in experiments for kinetic reasons. A theory of amorphous packings, and more generally glassy states, of hard spheres is reviewed here, that is based on the replica method: this theory gives predictions on the structure and thermodynamics of these states. In dimensions between two and six these predictions can be successfully compared with numerical simulations. The limit of large dimension is also discussed where an exact solution is possible. Some of the results presented here were published, but others are original: in particular, an improved discussion of the large dimension limit and new results on the correlation function and the contact force distribution in three dimensions. The main assumptions that are beyond the theory presented are clarified and, in particular, the relation between static computation and the dynamical procedures used to construct amorphous packings. There remain many weak points in the theory that should be better investigated.

DOI: 10.1103/RevModPhys.82.789 PACS number(s): 05.20.−y, 61.43.Fs, 64.70.Q−

CONTENTS

*giorgio.parisi@roma1.infn.it
†http://www.lpt.ens.fr/~zamponi

I. INTRODUCTION

The study of amorphous states of hard spheres is relevant for a large class of physical systems, including liquids, glasses, colloidal dispersions, granular matter, powders, and porous media. Therefore, after pioneering works done in the 1960s (Bernal and Mason, 1960; Bernal *et al.*, 1962; Scott, 1962; Mason and Clark, 1965, 1966; Scott and Kilgour, 1969; Finney, 1970), a large amount of precise numerical and experimental data is now available [see, e.g., Bennett (1972), Matheson (1974), Powell (1979), Berryman (1983), Pusey and Van Megen (1986), Lubachevsky and Stillinger (1990), Clarke and Jónsson (1993), Torquato (1995, 2002), Rintoul and Torquato (1996), Speedy (1998), O'Hern *et al.* (2002, 2003), Donev *et al.* (2005a), Krauth (2006), Silbert *et al.* (2006), Skoge *et al.* (2006), Angelani and Foffi (2007), Majmudar *et al.* (2007), Somfai *et al.* (2007), and Jerkins *et al.* (2008)]. Moreover, the sphere packing problem is related to many mathematical problems and arises in the context of signal digitalization and of error correcting codes, and it has been investigated in detail by the information theory community (Rogers, 1964; Conway and Sloane, 1993). Nevertheless, a satisfactory characterization of the amorphous states of a system of identical hard spheres is not yet available and the definition of amorphous close-packed states is still a matter of debate (Torquato *et al.*, 2000; O'Hern *et al.*, 2002; Kamien and Liu, 2007). From the rigorous point of view, for space dimension $d>3$ only some not very restrictive bounds have been obtained, and, in particular, it is still unclear whether the densest packings for $d\to\infty$ are amorphous or crystalline [see Sloane (2007) for a list of all known densest packings up to $d=128$].

Dense amorphous packings of hard spheres are usually produced according to some specific dynamical protocol. Typically one starts from an initial random configuration of the spheres, obtained, e.g., by throwing them into a container, and then shaking, tapping, or agitating in some way the spheres until a jammed structure is found (Scott and Kilgour, 1969; Bennett, 1972; Pusey and Van Megen, 1986; Torquato, 2002; Dauchot *et al.*, 2005; Schröter *et al.*, 2005; Abate and Durian, 2006; Daniels and Behringer, 2006; Majmudar *et al.*, 2007; Pica Ciamarra *et al.*, 2007; Jerkins *et al.*, 2008). In numerical simulations, amorphous packings are produced by inflating the particles while avoiding superposition either by molecular dynamics (Lubachevsky and Stillinger, 1990; Donev *et al.*, 2005a; Skoge *et al.*, 2006) or by using soft particles and minimizing the energy (Clarke and Jónsson, 1993; O'Hern *et al.*, 2002, 2003; Silbert *et al.*, 2006; Somfai *et al.*, 2007). As a matter of fact, most of these procedures, if crystallization is avoided, lead to final packing fractions close to 0.64 in $d=3$ and to 0.84 in $d=2$. These values of density, which are approximately 10% smaller than the values of the ordered close packing, have been called "random close-packing density."

Unfortunately, the algorithms (or procedures) that are used to create such packings are complicated *dynamical nonequilibrium* procedures. Obtaining analytical results for the properties of the final states requires an analytical solution of such complicated dynamical processes, which is very difficult even in the simplest theoretical models (Torquato and Stillinger, 2006a; Krzakala and Kurchan, 2007). The aim of this paper is then to identify a class of amorphous packings that might be described using *equilibrium* statistical mechanics, that is, in a *static* framework. These packings will be defined as the infinite

pressure limit of glassy states of hard spheres: such glassy states, if dense enough, are well-defined metastable states with very long lifetimes and should then be correctly described by equilibrium statistical mechanics. The idea of studying amorphous packings as the infinite pressure limit of a metastable state has been discussed (Biroli and Mézard, 2001; Pica Ciamarra *et al.*, 2003; Aste and Coniglio, 2004; Rivoire *et al.*, 2004; Tarzia *et al.*, 2004; Parisi and Zamponi, 2005; Kamien and Liu, 2007; Krzakala and Kurchan, 2007; Zamponi, 2007) and is appealing because it converts a difficult dynamical problem into a much simpler equilibrium problem.

Our approach to study glassy states will be based on the so-called random first-order transition (RFOT) theory of glasses, whose theoretical foundations were posed in a series of papers by Kirkpatrick, Thirumalai, and Wolynes (Kirkpatrick and Thirumalai, 1987; Kirkpatrick and Wolynes, 1987a) [see Cavagna (2009) for a detailed review]. In this theory the glass transition of particle systems is assumed to be in the universality class of the one-step replica symmetry breaking (1RSB) transition that happens in some mean-field exactly solvable spin-glass models (Gross and Mézard, 1984; Mézard *et al.*, 1987). Under this assumption, the glassy states of realistic finite-dimensional systems can be studied analytically, within some approximation, using equilibrium statistical mechanics by means of density-functional theory (Stoessel and Wolynes, 1984; Singh *et al.*, 1985; Kirkpatrick and Wolynes, 1987a; Dasgupta and Valls, 1999; Kim and Munakata, 2003; Chaudhuri *et al.*, 2005; Yoshidome *et al.*, 2007) and of the replica trick (Monasson, 1995; Mézard and Parisi, 1996). In particular, the replica method seems to give good quantitative estimates of the glass transition temperature (or density) and of the equation of state of the glass for Lennard-Jones systems (Coluzzi *et al.*, 1999; Mézard and Parisi, 1999a, 1999b, 2000) and hard spheres (Cardenas *et al.*, 1998, 1999; Parisi and Zamponi, 2005, 2006a).

Beside the large amount of numerical and experimental data available, there is an important advantage in working with hard spheres with respect to Lennard-Jones–like potentials. "Ground states" of hard spheres are obtained in the infinite pressure limit and correspond then to sphere packings that have interesting geometrical and topological properties, which can be investigated by looking at the network of contacts and at contact forces. This is very interesting because one can identify a set of geometrical observables that can be computed within the theory and directly compared with simulation and experiments. In this paper we show that this allows a precise test of the theory. Moreover, a more direct geometrical approach is possible; it has been largely exploited [see, e.g., Richard *et al.* (1999), Kansal *et al.* (2002), Aste (2005), Aste *et al.* (2005), Donev *et al.* (2005a, 2007), Lochmann *et al.* (2006), Skoge *et al.* (2006), Anikeenko and Medvedev (2007), Anikeenko *et al.* (2008), and van Meel *et al.* (2009)] and led to some important successes in the characterization of sphere packings. This is not possible for Lennard-Jones–like particles since the (zero-temperature) ground states of the system do not have special geometrical properties and indeed their structure is quite similar to typical liquid configurations. One might consider instead a soft potential that vanishes outside a finite radius; then the zero-energy ground states correspond to hard sphere configurations. In this way one obtains a system that displays the same geometrical properties of hard spheres at zero temperature and energy but at the same time becomes soft at finite temperature. This has been largely exploited (O'Hern *et al.*, 2002, 2003; Schreck and O'Hern, 2008; Berthier and Witten, 2009a, 2009b) to obtain important information on the properties of amorphous hard sphere packings. Therefore in this paper we focus on the hard sphere case and we discuss the limits of the theory and how it compares with numerical and experimental results. We show that despite the strong idealizations involved in the theory, the agreement with numerical data is surprisingly good. Moreover, we study the limit of large space dimension and obtain the asymptotic value of the density of amorphous packings.

Remarkably, a class of mean-field hard sphere models has recently been formulated for which the RFOT scenario is exact (Biroli and Mézard, 2001; Pica Ciamarra *et al.*, 2003; Rivoire *et al.*, 2004; Tarzia *et al.*, 2004; Sellitto *et al.*, 2005; Krzakala *et al.*, 2008; Mari *et al.*, 2009). These models allowed one to test the methods used here, confirming that they are reliable at least at the mean-field level. In particular, Mari *et al.* (2009) formulated a model in this class whose phase diagram is exactly the same as the one discussed below for finite-dimensional hard spheres.

It is worth noting that in experiments on granular systems and powders the role of friction is important (Dauchot *et al.*, 2005; Schröter *et al.*, 2005; Abate and Durian, 2006; Daniels and Behringer, 2006; Pica Ciamarra *et al.*, 2007; Shundyak *et al.*, 2007; Somfai *et al.*, 2007; Lechenault *et al.*, 2008), for instance, in determining the existence of loose packings (Onoda and Liniger, 1990; Jerkins *et al.*, 2008; Song *et al.*, 2008). Friction complicates a lot of the theoretical analyses of the packing problem since the system is intrinsically out of equilibrium and standard equilibrium statistical mechanics is, in principle, useless. Nevertheless, since the pioneering work of Edwards (Edwards and Oakeshott, 1989; Edwards, 1998), statistical mechanics ideas have been used to describe frictional systems, leading to remarkable results (Goldbart *et al.*, 2005). Comparison with experimental results is made difficult by the fact that in most experiments samples are polydisperse, often with a large range of particle sizes as in the case of many granulars.

For reasons of space, this paper is focused on our approach, that we will discuss in full detail; therefore, in the following we will consider mainly the statistical properties of a system of frictionless spheres, since our method is based on equilibrium statistical mechanics. We will not discuss in detail neither the geometrical properties (unless needed to compare numerical data with our results) of amorphous packings nor how their properties are influenced by the presence of friction. While in principle polydispersity can be included in our

theory, here we limit ourselves to the simple case of monodisperse systems, and only at the end we consider the case of binary mixtures. The literature on hard spheres, in general (and on the role of friction and geometry, in particular), is immense and covering it here would require a considerable effort; the reader is therefore referred to the original literature and to the existing books and reviews, e.g., Rogers (1964), Conway and Sloane (1993), Alexander (1998), Liu and Nagel (2001), Torquato (2002), Aste (2005), Goldbart *et al.* (2005), and Krauth (2006). Similarly, many excellent books and reviews on the physics of glasses and the glass transition exist [see, e.g., Ediger *et al.* (1996), Debenedetti and Stillinger (2001), Donth (2001), Binder and Kob (2005), Leuzzi and Nieuwenhuizen (2007), and Cavagna (2009), just to quote a few].

A. Organization of the paper (and how to read it)

This paper is organized as follows. Section II is devoted to a general discussion of the ideas that lead to the connection between packings that are produced by dynamic protocols and infinite pressure glassy states. In Sec. III the replica method is introduced in a general context and it is explained how it can be used to compute the phase diagram of glassy states. In Sec. IV a first implementation of the method, which works far from jamming, is discussed. Sections V–VIII contain the main results of the paper: the method is implemented in a way that works up to jamming and most of the results are presented. In particular, Sec. VI contains the discussion of the $d\to\infty$ limit. Many technical parts of the paper are in Appendixes A–E.

We tried where possible to make the different parts of the paper independent. There are different ways to read the paper:

- The discussion of Sec. II is self-contained. We suggest to the reader not interested in technical details to read only Sec. II, then skip the computations and look directly to the figures and tables that contain most of our results, and finally jump to the Conclusions. Each figure where results are presented contains a reference to the section where the corresponding calculations are discussed.
- The general discussion of the replica method in Sec. III is as self-contained as possible. This might be read together with Appendix A if one wants to obtain more insight into the method without going into the technical details of the computations.
- The technical sections, IV–VIII, are all independent one from the other; to understand one of them in detail one needs only to read Sec. III and Appendixes A–E.
- Finally, in Sec. IX we present results on the extension of the theory to binary mixtures, which are based on the method of Sec. VII.

It is important to stress that we present different implementations of the method separately, together with the corresponding results. Clearly, another possible choice would be to collect the results together in a separate section. Our choice has been made to stress that each approximation scheme gives slightly different results; although the qualitative picture stays the same, it is difficult to compare quantitatively different approximations. Moreover, each approximation has some advantages and disadvantages that we discuss in detail; in particular, some observables can be computed within some approximation and not within others. We leave to the reader the tasks to compare the different methods and to choose the best one according to their personal taste.

B. Notations

It is useful to give some definitions that will be widely used in the following. We consider a system of hard hyperspheres in d dimension with diameter D. We denote by

$$V_d(D) = \frac{\pi^{d/2}}{\Gamma(1+d/2)}D^d,$$
$$\Sigma_d(D) = dD^{-1}V_d(D) = 2\pi^{d/2}D^{d-1}/\Gamma(d/2) \tag{1}$$

the volume and surface of a sphere of radius D, respectively. It is also convenient to define

$$V_d = V_d(1) = \pi^{d/2}/\Gamma(1+d/2),$$
$$\Omega_d = \Sigma_d(1) = 2\pi^{d/2}/\Gamma(d/2). \tag{2}$$

Note that Ω_d is the d-dimensional solid angle.

Often, if there is no ambiguity, we use the symbols $x,y,\ldots$ to denote vectors in $\mathbb{R}^d$. If there is an ambiguity, we use the letter r and in this case we use $\vec{r}$ for a d-dimensional vector and $r=|\vec{r}|$ for its modulus. Correspondingly $\int d\vec{r}F(\vec{r})$ will indicate an integral over $\vec{r}\in\mathbb{R}^d$ while $\int_a^b drF(r)$ will indicate an integral over the real r. We use the notation $\delta(|\vec{r}|-D)$ for the distribution defined by $\int d\vec{r}F(|\vec{r}|)\delta(|\vec{r}|-D)=\Sigma_d(D)F(D)$, while $\delta(r-D)$ is defined by $\int_0^\infty drF(r)\delta(r-D)=F(D)$. They are related by $\delta(|\vec{r}|-D)=\Omega_d\delta(r-D)$.

For a generic potential $\phi(r)$ we define $b(r)=e^{-\phi(r)}$ and the Mayer function $f(r)=b(r)-1$. For the specific case of hard spheres we have $b(r)=\chi(r)=\theta(|r|-D)$.

Defining $\rho=N/V$ the number density of the spheres, we introduce as usual the packing fraction $\varphi=\rho V_d(D/2)$, i.e., the fraction of volume covered by the spheres. In the following, when talking about "density," we usually refer to the packing fraction.

II. A CLASS OF AMORPHOUS PACKINGS: INFINITE PRESSURE GLASSY STATES

In this section we define a class of "amorphous packings" of hard spheres that can be studied within the framework of equilibrium statistical mechanics. We start by discussing some algorithms that are commonly used to construct amorphous packings. Then we argue that

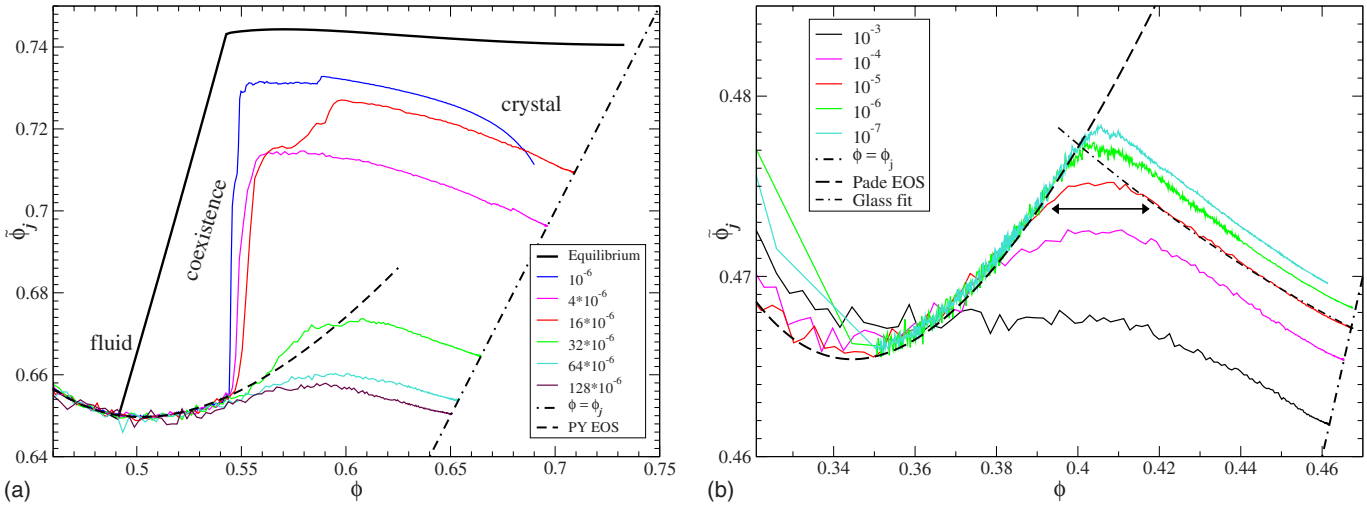

FIG. 1. (Color online) Evolution of the pressure during compression at rate γ in $d=3$ (left) and $d=4$ (right). The density φ is increased at rate γ and the reduced pressure $p(\varphi)=\beta P/\rho$ is measured during the process. See Skoge *et al.* (2006) for details. The quantity $\tilde{\varphi}_j(\varphi)=p(\varphi)\varphi/[p(\varphi)-d]$ is plotted as a function of φ. If the system jams at density φ_j, $p\to\infty$ and $\tilde{\varphi}_j\to\varphi_j$. Thus the final jamming density is the point where $\tilde{\varphi}_j(\varphi)$ intersects the dot-dashed line $\tilde{\varphi}_j=\varphi$. (Left) The dotted line is the liquid [Percus-Yevick (PY)] equation of state. The curves at high γ follow the liquid branch at low density; when they leave it, the pressure increases faster and diverges at φ_j. The curves for lower γ show first a drop in the pressure, which signals crystallization. (Right) All curves follow the liquid equation of state [obtained from Eq. (9) of Bishop and Whitlock (2005)] and leave it at a density that depends on γ. In this case no crystallization is observed. For $\gamma=10^{-5}$ the dot-dashed line is a fit to the high-density part of the pressure (glass branch). The arrow marks the region where the pressure crosses over from the liquid to the glass branch. From Skoge *et al.*, 2006.

the final states reached by these algorithms are well-defined metastable states whose properties can be investigated by a static computation (i.e., without any knowledge of the dynamical process that generated the packings). This point is very delicate and is receiving much attention in the context of optimization problems (Krzakala and Kurchan, 2007), where it has not yet been solved. The discussion that follows is tentative and the problem deserves further investigation.

A. Algorithms to construct amorphous packings

The usual way to construct amorphous packings in experiments or numerical simulations is to compress the system according to some protocol. In early experiments particles were thrown randomly in a box which was then shaken (Scott and Kilgour, 1969) or were deposited randomly around a small seed cluster (Bennett, 1972). In numerical simulations a common protocol (Lubachevsky and Stillinger, 1990) is to slowly increase, at a given rate γ, the particle diameter during a molecular dynamics run; it has recently been used extensively in three (Donev *et al.*, 2005a) and higher (Skoge *et al.*, 2006) dimensions to produce amorphous packings of $N\sim10^4$ spheres. Another possibility is to increase the diameter of the spheres until two of them overlap, then eliminate the overlap by following a gradient descent using some potential vanishing outside the radius of the particle (Xu *et al.*, 2005; Gao *et al.*, 2006) or, alternatively, to start from a random configuration and minimize the energy at fixed density, repeating the procedure while increasing the density until it becomes impossible to find a zero-energy final configuration (O'Hern *et al.*, 2002, 2003). These two procedures give similar results (Schreck and O'Hern, 2008). Other similar algorithms have been proposed and analyzed by Jodrey and Tory (1985), Clarke and Jónsson (1993), and Lochmann *et al.* (2006).

Based on standard concentration arguments, it is believed that, in the limit $N\to\infty$, the density of the final state is independent of the randomness built in the algorithm[1] (e.g., the initial configuration). This has been numerically verified for the soft-potential algorithms (O'Hern *et al.*, 2002, 2003; Xu *et al.*, 2005; Gao *et al.*, 2006); the final density is very close to 0.64 and has been called J point. It is a fact that for all algorithms that have been devised to construct amorphous packings of monodisperse frictionless spheres, for $N\to\infty$ the final density of the system converges to a value of φ close to 0.64 in three dimensions. It has been proposed to call the value $\varphi=0.64$ random close-packing density and different more precise definitions of this concept have been proposed. However, the precise numerical value of the latter quantity is found to depend on the details of the experimental protocol, and this led some authors to criticize the notion of random close packing (Torquato *et al.*, 2000).

To illustrate this difficulty, we concentrate on data obtained using the Lubachevsky-Stillinger procedure at different rates γ (Skoge *et al.*, 2006) and shown in Fig. 1. In this algorithm, during the compression, the (hard)

[1]Similar results have been shown for some classes of algorithms to solve optimization problems [see, e.g., Barthel *et al.* (2003) and Semerjian and Monasson (2003)].

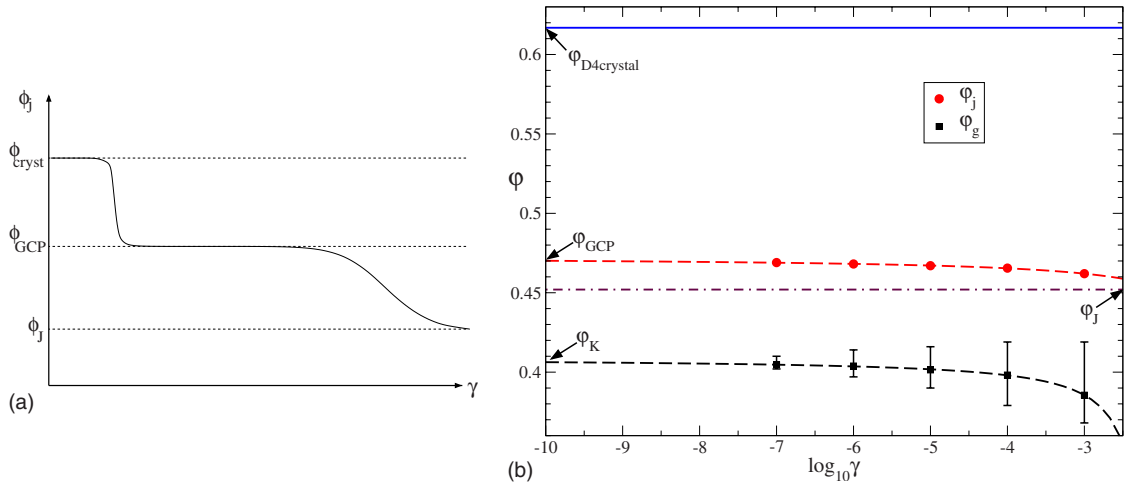

FIG. 2. (Color online) Jamming density $\varphi_j(\gamma)$ as a function of γ. (Left) Schematic plot of the jamming density $\varphi_j(\gamma)$ as a function of compression rate γ for the Lubachevsky-Stillinger algorithm. At quite high rates, the algorithm should be similar to the J-point procedure and converge to packings of density $\varphi_j(\gamma \text{ large}) \sim \varphi_J$. On decreasing γ the jamming density decreases (cf. Fig. 1) and reaches a *plateau* at $\varphi_j = \varphi_{\text{GCP}}$. For smaller γ the system is able to crystallize and $\varphi_j(0) = \varphi_{\text{crystal}}$. In $d=3$, crystallization is fast and the plateau is not observed, while in $d>3$ crystallization is so slow that it is not observed at all in numerical simulations (Skoge *et al.*, 2006). (Right) The same plot for hyperspheres in $d=4$. The solid line is the close-packing density achieved by the D4 crystal, $\varphi_{\text{D4}} = \pi^2/16$ (Conway and Sloane, 1993). Circles are values of $\varphi_j(\gamma)$ (the point where the curves intersect the dashed line in the right panel of Fig. 1). The dot-dashed line is the value of the J-point density (Schreck and O'Hern, 2008). In addition, we report the estimates of the glass transition density $\varphi_g(\gamma)$ (squares); error bars mark the amplitude of the crossover region and correspond to the arrow in the right panel of Fig. 1. Dashed lines are fits to $\varphi_j(\gamma) = 0.473 + 0.023/[\log_{10}(\gamma) + 0.85]$ and $\varphi_g(\gamma) = 0.409 + 0.02/[\log_{10}(\gamma) + 2.13]$.

spheres evolve according to molecular dynamics at some temperature; the value of the temperature is irrelevant and fixes the unit of time (Skoge *et al.*, 2006). One can measure the (kinetic) reduced pressure $p(\varphi) = \beta P/\rho$, where $\beta = 1/T$, during the evolution. This quantity is shown in Fig. 1 for different values of γ. One observes that, on compressing the low-density liquid at a constant rate γ, the pressure of the system follows the equilibrium pressure of the liquid up to some density $\varphi_g(\gamma)$ (often called glass transition density) around which the pressure starts to increase faster than in equilibrium and diverges on approaching a value of density $\varphi_j(\gamma)$, which is called jamming density. At this point the algorithm stops because the system cannot be compressed anymore: most of the spheres are in contact with their neighbors.[2] Values of $\varphi_j(\gamma)$ have been accurately measured by Skoge *et al.* (2006) as a function of γ. On the contrary, $\varphi_g(\gamma)$ is not precisely determined as long as $\gamma > 0$: the glass transition is smeared and happens in a crossover region $[\varphi_g^-(\gamma), \varphi_g^+(\gamma)]$ (marked by an arrow in the right panel of Fig. 1). However, the amplitude of the crossover interval seems to decrease[3] for $\gamma \to 0$ (see Fig. 1).

To characterize the typical configurations reached by the algorithm at $\varphi = \varphi_j(\gamma)$, one could try to solve the dynamics of the algorithm and compute, for instance, the correlation function $g(r)$ as a function of "time." This has been done for much simpler algorithms, such as the ghost random sequential addition algorithm (Torquato and Stillinger, 2006a), which, however, are unable to reach interesting densities.[4] More efficient algorithms such as the random sequential addition (RSA), where one attempts to add a sphere randomly and accepts the move only if there are no overlaps, already cannot be analyzed analytically and one has to resort to numerical investigation (Talbot *et al.*, 2000; Torquato *et al.*, 2006).

For this reason, in order to compute analytically the properties of jammed configurations, one would like to make use of a static computation. This can be justified as follows: If we plot the jamming density $\varphi_j(\gamma)$ as a function of γ, we obtain the plot reported in the right panel of Fig. 2. For $\gamma \to 0$, the algorithm is equivalent to an equilibrium compression and the pressure should follow the equilibrium equation of state; then the final state will be the most dense state, which is a crystal at least if the dimension is not very large. However, for small but nonzero γ, crystallization is not observed and the data of Skoge *et al.* (2006) suggest the existence of a *plateau* at some value of density, which we call φ_{GCP} for reasons that will be clear in the following. This is a hint of the existence of a long-lived metastable state; if this is the case, one can compute its properties by means of a thermodynamic computation by restricting the partition

[2]At low compression rates, crystallization is observed in $d=3$, but it seems to be strongly suppressed by kinetic effects in dimension $d>3$ so we neglect it for the moment.

[3]See Möller *et al.* (2006) for a recent theoretical discussion of these effects.

[4]For instance, in $d=3$ the limiting density for the algorithm is $\varphi = 0.125$.

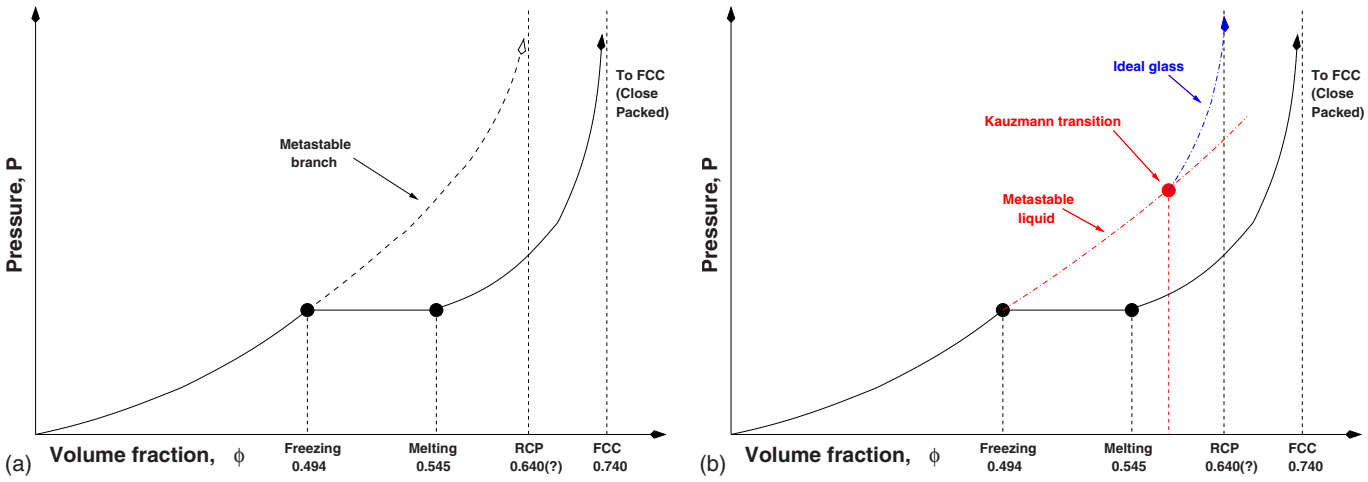

FIG. 3. (Color online) Schematic phase diagram of hard spheres in $\mathbb{R}^3$. (Left) Continuation of the liquid equation of state in the metastable region. (Right) Expected behavior in the presence of a thermodynamic glass transition.

function to the region of amorphous configurations. In Sec. II.B we discuss this issue in more detail.

It seems that many different algorithms that produce packings starting from a random configuration and without allowing the particles to relax much (O'Hern *et al.*, 2002, 2003; Xu *et al.*, 2005; Gao *et al.*, 2006) lead to close values of density (the J point). Therefore for large γ (but still small enough to allow for some minimal relaxation of the particles) the final density of the Lubachevsky-Stillinger algorithm should be close to the one reached by the J-point procedure, leading to the schematic plot reported in the left panel of Fig. 2. This is what indeed happens in a simple mean-field model (Cugliandolo and Kurchan, 1993) and seems confirmed by the data for spheres in $d=4$ reported in the right panel of Fig. 2. However, the validity of this statement is very debated for more general mean-field models (Krzakala and Kurchan, 2007). We will return to this point in the following.

Before concluding this section, we stress that here we focused only on the behavior of algorithms that are currently used to construct amorphous packings; these algorithms typically perform local moves in phase space. Many other algorithms to simulate hard spheres have been invented. Smarter algorithms can be designed, which are able to sample the equilibrium measure at higher density (Dress and Krauth, 1995; Grigera and Parisi, 2001; Krauth, 2006).

B. The equilibrium phase diagram

The equilibrium phase diagram of hard spheres in $\mathbb{R}^3$ is shown in Fig. 3, where the pressure is reported as a function of the packing fraction. At low density the system is in a liquid phase (as defined, e.g., by the low-density virial expansion); the maximum possible density is realized by the fcc lattice, as conjectured by Kepler and proven by Hales (2005). A first-order phase transition between the liquid phase and the fcc crystal phase is found by numerical simulations (Alder and Wainwright, 1957; Wood and Jacobson, 1957) and in experiments on colloidal systems (Pusey and Van Megen, 1986; Phan *et al.*, 1996). This is the equation of state that the system will follow if compressed at a really infinitesimal rate. We wish instead to focus on a small but finite rate in such a way to follow the liquid branch of the equation of state inside its metastability region.

1. What is the fate of the liquid above freezing?

The first ideas to define amorphous states of hard spheres at high density are to assume that the liquid phase can be continued above the freezing density φ_f and to look at its properties at large density (Aste and Coniglio, 2004; Kamien and Liu, 2007). For instance, one can choose a functional form that represents well the equation of state of the liquid below φ_f [e.g., the Carnahan-Starling or Percus-Yevick equation of state (Hansen and McDonald, 1986)] and assume that it describes the liquid phase also above φ_f. On increasing the density the pressure of the liquid increases as the average distance between particles decreases: one may expect that it diverges at a point where the particles get in contact with their neighbors and the system cannot be further compressed. Then one might identify this point with the random close-packing density (see the left panel of Fig. 3).

The first objection that has been raised against this proposal is that an intrinsic stability limit of the liquid (a spinodal point) might exist at a density above φ_f due to thermodynamic or kinetic reasons. It is probable that a thermodynamic spinodal does not exist because any reasonable continuation of the liquid equation of state does not predict such an instability (manifested, e.g., by an infinite compressibility). A kinetic spinodal, related to the existence of the crystal (Cavagna *et al.*, 2005), could instead exist at least in monodisperse systems. This would imply the impossibility of reaching amorphous jammed states if the compression rate is not very high. We will assume in the following that the metastable liquid can be compressed as slow as wished avoiding crystallization. This is not a very good assumption for mono-

disperse three-dimensional spheres but seems to be more close to reality for larger dimension (Skoge *et al.*, 2006) (see Fig. 1) or for suitably chosen binary mixtures. This point requires a better investigation, e.g., following the analysis of Cavagna *et al.* (2005), and we will not discuss it further here.

A second objection is that in the presence of a first-order phase transition the continuation of one phase into its metastable region is not well defined due to the appearance of essential singularities at φ_f. Many possible continuations of the low-density equation of state above φ_f are possible: the properties of the "liquid" above φ_f depend on the history of the sample, much as it happens for the hysteresis of a ferromagnetic system. Nevertheless, the ambiguity is expected to be exponentially small in the distance from φ_f, and as the distance between φ_f and the maximum density φ_{fcc} is not so large, one might expect to obtain a meaningful result in this way. Indeed, different possible continuations of the liquid equation of state (e.g., Carnahan-Starling, Percus-Yevick,and hypernetted chain) differ by less than 10% in the dense region around $\varphi \sim 0.64$ in $d=3$. Moreover, the ambiguity becomes smaller and smaller on increasing the dimension.

The extrapolation to infinite pressure can give very different results; Kamien and Liu (2007) showed that one can reasonably fit the pressure in the metastable region by a free volume equation of state and obtain a divergence of the pressure at $\varphi_{\mathrm{RCP}} \sim 0.64$ in $d=3$. On the other hand, all possible analytic continuations of the liquid equation of state, based on resummations of the virial series, predict a divergence of the pressure at unphysical large values of φ: e.g., the CS equation predicts a divergence in $\varphi=1$ which is clearly wrong since it is larger than the fcc value and implies that the available volume is completely covered by the spheres. Moreover, the $g(r)$ computed using these resummations do not show the characteristic features observed in amorphous jammed packings. Therefore, from a theoretical point of view it is difficult to justify the validity of the phenomenological free volume fit discussed by Kamien and Liu (2007) on the basis of an analytical continuation of the liquid equation of state. Clearly we cannot exclude that a more refined resummation of the virial series will give a continuation of the liquid branch with a divergence in 0.64 and a $g(r)$ similar to the one of amorphous packings; but such a theory has not been found yet. This motivates the study of different proposals, such as the existence of a phase transition in the liquid branch. This idea is also supported by accurate integral equations based on improvements of the PY equation that seem to indicate the existence of a phase transition at high density (Robles and de Haro, 2003).

2. The ideal glass transition

In this section we discuss the existence of a thermodynamic glass transition in the metastable liquid branch of the phase diagram (Woodcock and Angell, 1981; Stoessel and Wolynes, 1984; Speedy, 1994, 1998; Cardenas *et al.*, 1998). Such a transition can be expected for various reasons: it is predicted by mean-field models (Biroli and Mézard, 2001; Pica Ciamarra *et al.*, 2003; Rivoire *et al.*, 2004) and is suggested by the results of Robles and de Haro (2003). Moreover, from a dynamical point of view, an ergodicity breaking transition is predicted by mode-coupling theory (Bengtzelius *et al.*, 1984; van Megen and Underwood, 1993; Götze, 1999; Sellitto *et al.*, 2005), and a recently published set of accurate experimental and numerical data (Berthier and Witten, 2009a, 2009b; Brambilla *et al.*, 2009) on three-dimensional spheres strongly indicates a divergence of the equilibrium relaxation time in the metastable liquid phase at a density φ_0 at which the pressure is still finite. This supports the existence of a phase transition at φ_0 in three dimensions. In two dimensions the situation seems quite different (Santen and Krauth, 2000; Donev *et al.*, 2006; Tarzia, 2007).

The existence of an ideal glass transition in a finite-dimensional system is a matter of intense debate [see e.g., Santen and Krauth (2000), Xia and Wolynes (2001a, 2001b), Bouchaud and Biroli (2004), Brumer and Reichman (2004), Donev *et al.* (2006), Tarzia (2007), and Cavagna (2009)]. To avoid entering in this discussion, we take a more "pragmatic" point of view. We assume that a thermodynamic glass transition exists and investigate its consequences. It will become clear that for comparison with numerical and experimental data the existence of a true thermodynamic transition is not a key issue since in reality one is always stuck in metastable glassy states.

Assume again that the liquid phase can be continued above φ_f and neglect the (small) ambiguity in its definition due to its intrinsic metastability with respect to crystallization. We assume that at a density φ_K a thermodynamic glass transition (sometimes called ideal glass transition) happens.[5] The transition is signaled by a jump in the compressibility of the system. A simple qualitative argument to explain this is the following: in the dense liquid phase particles vibrate on a fast time scale in the cages made by their neighbors, while on a much larger time scale cooperative relaxation processes happen (structural relaxation). If we change the density by $\Delta\varphi$, the pressure will instantaneously increase by a ΔP_0; very rapidly the average size of the cages will decrease due to the increase in density and the pressure will relax to a

[5]The density φ_K has been associated with the name of Kauzmann, who first observed that in some molecular glasses extrapolating the liquid entropy at low temperature one would obtain at some point an entropy smaller than that of the crystal (Kauzmann, 1948). Based on the intuitive notion that a liquid should have more states than a crystal, hence more entropy, he concluded that some kind of transition should happen preventing the liquid entropy from crossing the crystal one. However, in the case of hard spheres, it is well known that the crystal entropy becomes bigger than that of the liquid at the freezing/melting transition. Hence the entropy of the liquid is smaller than that of the crystal in the whole metastable liquid branch. At φ_K the *complexity* (that will be introduced below) vanishes; but this quantity is different from the difference between liquid and crystal entropies in the case of hard spheres.

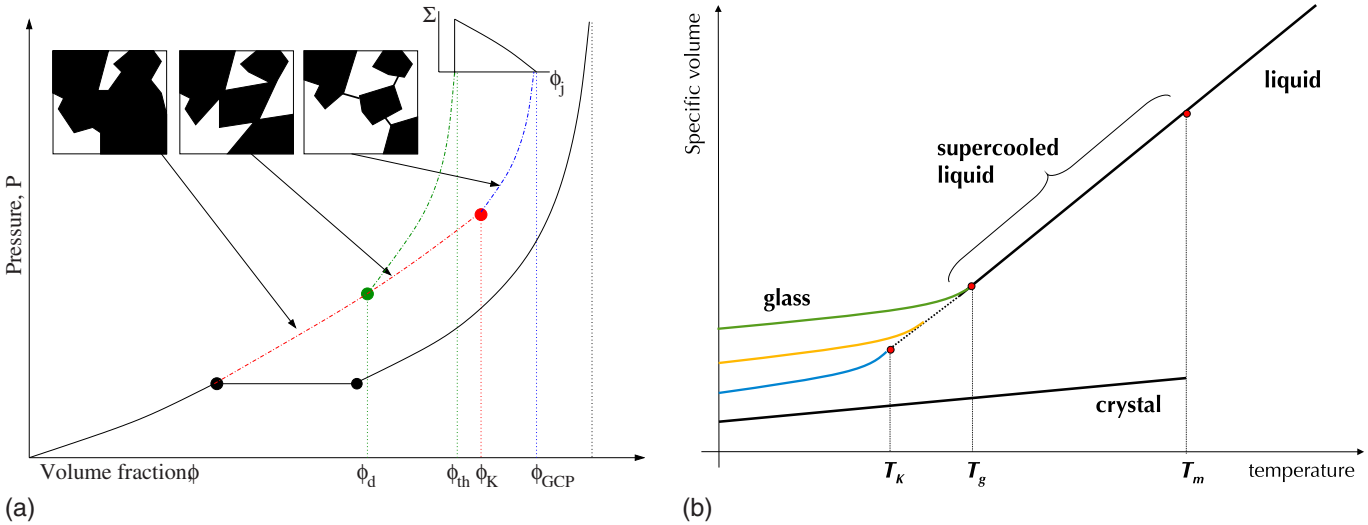

FIG. 4. (Color online) Schematic mean-field phase diagram of hard spheres in $\mathbb{R}^3$ (see the text for a detailed description). (Left) (P,φ) diagram: The full black line represents the equilibrium phase diagram with the liquid-solid transition (see Fig. 3). The metastable liquid is made by a single state below φ_d, while above this density it is the superposition of many glassy states. If the system is stuck in one of these states and compressed, it follows one of the glass branches of the phase diagram. At φ_K the system reaches the most dense states, and if further compressed it enters the ideal glass state. The pressure of the latter diverges at φ_{GCP}. In the inset, the complexity, i.e., the logarithm of the number of glassy states, is plotted as a function of the jamming density φ_j. The boxes show a picture of the (dN-dimensional) phase space of the system: black configurations are allowed; white ones are forbidden by the hard-core constraint. In the supercooled liquid phase the allowed configurations form a connected domain; however, on approaching φ_d the connections between different metastable regions become smaller and smaller. Above φ_K, they disappear in the thermodynamic limit and glassy states are well defined. (Right) For comparison, the standard glassy phase diagram for a soft potential (e.g., Lennard-Jones), specific volume vs temperature at fixed pressure, is reported (Ediger *et al.*, 1996; Debenedetti and Stillinger, 2001; Cavagna, 2009). The similarity is evident if one identifies $v\to 1/\varphi$ and $T\to 1/P$ (i.e., one should reflect the left diagram on a diagonal line joining the upper left corner and the lower right corner).

value $\Delta P_f < \Delta P_0$. Then, on the time scale of structural relaxation, the structure will change to follow the change in density and the pressure will relax further to a value $\Delta P_\infty < \Delta P_f$. We assume that at the glass transition the latter relaxation is frozen and the corresponding time scale becomes infinite: in other words, as usually done in the glass transition literature (Ediger *et al.*, 1996), we identify φ_K with the density φ_0 defined by Berthier and Witten (2009a, 2009b) and Brambilla *et al.* (2009). Thus, in the glass phase the increase in pressure following a change in density will be larger than in the liquid phase, leading to a smaller compressibility $K=\varphi^{-1}(\Delta\varphi/\Delta P)$.

The schematic phase diagram that we expect in the presence of a glass transition is shown on the right panel of Fig. 3. The existence of a glass transition can cure the behavior of the pressure of the liquid, which seems to diverge at a density bigger than the fcc density. The pressure of the glass diverges at a "glass close-packing" (GCP) density φ_{GCP} and we are tempted to identify φ_{GCP} with the RCP density. In next section we discuss a further complication: the existence of a large number of glassy states, in addition to the ideal (thermodynamic) glass, with different densities. Before concluding this section, we stress again that, although recent very accurate numerical data (Berthier and Witten, 2009b) support the existence of a glass transition of the type discussed for hard spheres, this remains one of the most debated problems in the community.

3. Many glassy states: The "mean-field" phase diagram

The glass transition, in the standard picture coming from the analysis of mean-field models, is related to the appearance of many metastable glassy states[6] in addition to the ideal glass one. These states appear in the liquid above some density φ_d and can be defined, for instance, as minima of a suitable density functional (Thouless *et al.*, 1977; Kirkpatrick and Wolynes, 1987a; Mézard *et al.*, 1987; Dasgupta and Valls, 1999; Chaudhuri *et al.*, 2005) (see Appendix A for a more detailed discussion). In the interval of densities $\varphi_d \leqslant \varphi \leqslant \varphi_K$, particles vibrate around these locally stable structures, which are visited subsequently on the scale of the structural relaxation. If we

[6]There are here two "types" of metastability: the first is the metastability of the whole amorphous branch with respect to crystallization. We are now discussing a second type of metastability, i.e., the existence of glassy states that have lower density (or smaller entropy) with respect to the glassy state with maximal density (the ideal one) and consequently they are metastable with respect to it. In order to avoid confusion, we indicate that some of the glassy states are metastable with respect to the ideal glass only when needed. Otherwise, we use "glassy states" to indicate both metastable glasses and the ideal glass. In any case these states will have a small but finite probability of decaying into the ideal state; this probability should go exponentially to zero when their density approaches the density of the ideal glassy state.

"artificially" freeze the structural relaxation and compress the system, the pressure increases faster than if the structure is allowed to relax for the same reason as above: the system is forced to reduce the size of the cages to respond to a change in density. The pressure diverges at the point where the particles contact their neighbors and the average size of the cages is zero. In this way, to each configuration of the liquid at a given density $\varphi \in [\varphi_d, \varphi_K]$ one can associate a jammed configuration at a density $\varphi_j(\varphi)$ that is obtained by compressing this configuration fast enough to avoid structural relaxation. A glass state can be thought of as a set of configurations leading to the same jammed configuration after a fast compression[7] (Speedy, 1998).

In the Lubachevsky-Stillinger protocol already discussed (see Fig. 1) one chooses *a priori* a compression rate γ and the system can equilibrate only up to a density $\varphi_g(\gamma)$ where the relaxation time becomes of the order of the compression rate. At this density the structure can no longer follow the compression and basically the system responds to the compression by reducing the cages up to the jamming density $\varphi_j(\gamma)$. Calling $\varphi_{\rm th}$ the value of the jamming density of the states that first appears at φ_d, it follows that (in the mean-field picture) we can produce *jammed* configurations in a whole range of densities $\varphi_{\rm th} \leqslant \varphi \leqslant \varphi_{\rm GCP}$ (Krzakala and Kurchan, 2007; Zamponi, 2007). The notation $\varphi_{\rm GCP}$ (glass close-packing density) is appropriate since $\varphi_{\rm GCP}$ is the highest possible density of infinite pressure glassy states.

Note that as the structural relaxation time scale is expected to diverge on approaching φ_K (Berthier and Witten, 2009a, 2009b; Brambilla *et al.*, 2009), at some point it will fall beyond any experimentally accessible time scale and necessarily the system will be frozen into a glassy state which is not the ideal glass. The *ideal* glass states are unobservable in practice: one will observe instead a *nonequilibrium* glass transition to a state that, again, will depend on the experimental protocol. This is very familiar in the structural glass literature, and in fact the diagram in Fig. 4 (left panel) is analogous to the usual specific volume versus temperature plot (right panel in Fig. 4) that characterizes structural glasses if one identifies φ with the inverse of specific volume and $1/P$ with temperature.

To summarize, the phase diagram inspired by mean-field models is shown in Fig. 4 and in Table I. It is characterized by the presence of the following phases and transitions:

TABLE I. Special points of the phase diagram obtained within the replica computation (see Fig. 4). For each special point, we list the densities defined in Table II associated to it. Note that φ_g and $\varphi_{\rm RCP}$ depend on the protocol used; hence they are not associated to any special point in the replica computation. The identification of φ_J and $\varphi_{\rm MRJ}$ with $\varphi_{\rm th}$ is tentative and probably not stricly true; still we expect these points to be quite close (see the text for details).

Point	Densities	Replica parameter
Dynamic transition	φ_d, $\varphi_{\rm MCT}$	$m=1$
Static transition	φ_K, φ_0	$m=1$
Glass close packing	$\varphi_{\rm GCP}$	$m=0$
Threshold states	φ_{th}, $\varphi_J(?)$, $\varphi_{\rm MRJ}(?)$	$m=0$

- At equilibrium, a low-density-liquid phase and a high-density crystal phase separated by a first-order transition, with corresponding freezing density φ_f and melting density φ_m (black full line and black dots in Fig. 4).
- A metastable dense liquid phase: above some density φ_d this phase is made by a collection of glassy states corresponding to locally stable configurations around which the system vibrates for a long time. Thus, φ_d is defined, in a static framework, as the density at which glassy states first appear[8] and for this reason is often called clustering transition density.[9]
- The liquid exists up to a density φ_K where an ideal glass transition happens. The ideal glass transition is signaled by a jump in the compressibility and by a divergence of the equilibrium relaxation time of the liquid[10] (Berthier and Witten, 2009a; Brambilla *et al.*, 2009).
- For each density $\varphi \in [\varphi_d, \varphi_K]$, a different group of glassy states dominates the partition function. These can be followed by compressing very fast, and each group is characterized by a jamming density $\varphi_j(\varphi)$. We call $\varphi_{\rm GCP}=\varphi_j(\varphi_K)$ the jamming density of the ideal glass state and $\varphi_{\rm th}=\varphi_j(\varphi_d)$ the jamming density of the less dense glassy states.

The number of glassy states corresponding to jamming densities $\varphi_j \in [\varphi_{\rm th}, \varphi_{\rm GCP}]$ grows exponentially with the size of the system, $\mathcal{N}(\varphi_j)=\exp[N\Sigma(\varphi_j)]$. The function $\Sigma(\varphi_j)$, usually called complexity or configurational

[7] In systems with soft potentials a similar procedure has been proposed by Stillinger and Weber (1982, 1985) in order to associate to each configuration of energy e a mechanically stable configuration or "inherent structure" of lower energy e_{IS}: starting from the reference configuration one quenches the system at zero temperature and finds a minimum of the potential, which is the corresponding inherent structure. We describe the same procedure, with energy replaced by (inverse) density and temperature by (inverse) pressure. See Speedy (1998) for details.

[8] At the mean-field level this point corresponds to the mode-coupling transition $\varphi_{\rm MCT}$.

[9] Glassy states are called clusters in optimization problems.

[10] Mode-coupling theory would predict a divergence of the relaxation time at the smaller density $\varphi_{\rm MCT} \sim \varphi_d$; however, in a finite-dimensional system there are strong arguments indicating that the liquid can be equilibrated up to φ_K, thanks to activated processes that allow a jump over the barriers separating metastable glassy states (see Appendix A).

entropy,[11] has the shape reported in the inset of Fig. 4: it jumps at a positive value at $\varphi_{\rm th}$ and vanishes at $\varphi_{\rm GCP}$ (therefore, the number of ideal glasses is not exponential in the system size). A more precise definition of this equilibrium complexity is presented in Appendix A.

4. Remarks on the static phase diagram

The striking similarity of the phase diagram in Fig. 4 with the numerical results[12] of Skoge *et al.* (2006) (see Fig. 1) makes it a good starting point to understand the physics of jammed amorphous states. However, one should keep in mind the following important remarks:

(1) This phase diagram is an idealization that discards many difficulties in the definition of amorphous packings, mainly related to *metastability*, either of metastable glass states with respect to the ideal glass state or of the ensemble of glassy states with respect to the crystal. The ambiguity in the definition of the liquid equation of state due to its metastability (Kamien and Liu, 2007) also affects the glass: the glass equation of state is theoretically not well defined, with an ambiguity of the order of 10%, depending on the equation of state one chooses to describe the liquid. Note that these difficulties might not be so important in some cases where the nucleation time of the crystal is very large, e.g., high-dimensional spheres or binary mixtures, as discussed. In particular, in the limit $d\to\infty$ we believe that the theory should be exact.

(2) In a finite-dimensional system, pure equilibrium states cannot exist in exponential numbers. In fact, the states corresponding to $\varphi_j<\varphi_{\rm GCP}$ can be stable only on a finite length scale and for a finite time in finite-dimensional systems as discussed originally by Kirkpatrick and Thirumalai (1987) and Kirkpatrick and Wolynes (1987a), in more detail by Kirkpatrick and Wolynes (1987b) and Kirkpatrick *et al.* (1989), and more recently by Mézard and Parisi (2000). Therefore the notion of complexity makes sense only on a finite time and length scale. The problem of evaluating this length and time scales has recently been reformulated in terms of a nucleation problem (Xia and Wolynes, 2001a, 2001b; Bouchaud and Biroli, 2004) and is probably the most active subject of research in the glass transition community. The subject is difficult and we cannot discuss it in detail here. The interested reader should look at the original literature (Xia and Wolynes, 2001a, 2001b; Bouchaud and Biroli, 2004; Franz, 2005; Montanari and Semerjian, 2006; Cavagna *et al.*, 2007). In the rest of this paper we neglect this difficulty and assume that mean-field states are stable on every length scale; however, we try to give a more precise definition of states in Appendix A, where we explicitly show the origin of the difficulties in finite dimension and explain why our theory might be a reasonable approximation of the real situation.

(3) The structure of the states close to $\varphi_{\rm th}$ might be more complicated than described here. In mean-field models processes such as state crossing, temperature (density) chaos, birth and death of states, etc., are known to happen. This complicates the analysis; unfortunately at present we cannot say much more on this important issue. More insight should come from the study of mean-field hard sphere models such as those discussed by Biroli and Mézard (2001), Krzakala *et al.* (2008), and Mari *et al.* (2009).

(4) For finite-dimensional systems, the transition to a metastable glass state is smeared and becomes a crossover, as seen in Fig. 1 [see also Ediger *et al.* (1996), and Möller *et al.* (2006)]. Only the ideal glass transition has a chance to survive as a real phase transition. For this reason the free volume fit of Kamien and Liu (2007), which describes the metastable liquid branch without assuming a phase transition, is not incompatible with the point of view presented here.

(5) When looking to actual configurations, it might be difficult to distinguish between a configuration representative of a pure glass state and one representative of a mixture of glass and crystal (Torquato *et al.*, 2000). Thus if one really wants to look at single configurations of finite systems, the definition of amorphous states discussed above is not very useful, and a definition based on order metrics may be more suitable (Torquato *et al.*, 2000). This leads to the concept of maximally random jammed (MRJ) packings, defined as follows: one chooses a function ψ that measures the order in some way, with $\psi=1$ corresponding to most ordered and $\psi=0$ to most disordered configurations. Then one defines $\varphi_{\rm MRJ}$ as the density of the jammed configurations that minimize ψ [see Torquato *et al.* (2000) for details]. This definition may be suitable when one studies single configurations, and it has been shown numerically that a value $\varphi_{\rm MRJ}\sim 0.64$ is obtained for many different order metrics. It is therefore important to stress that

[11] Although sometimes used as synonyms, in other cases these words denote different concepts: in fact, especially in the experimental literature the word configurational entropy denotes the difference between the entropy of a system in its liquid and crystalline phases. This difference is often used as an estimate of the complexity. Already in the case of soft potentials, this gives rise to a number of interpretation problems [see, e.g., Binder and Kob (2005) and Cavagna (2009) for detailed discussion]. In the particular case of hard spheres, the situation is even worse since energy is irrelevant and the liquid-crystal transition is completely driven by entropy; hence the crystal entropy is bigger than the liquid one above the melting density. It follows that the configurational entropy defined as the difference between liquid and crystal entropy has nothing to do with the complexity; in particular it will be negative at all densities above the melting density. Here, we will always use the word complexity in order to avoid confusion.

[12] Recall that in Fig. 1 the pressure has been rescaled.

the phase diagram above refers to *thermodynamic states* and not to configurations. Note that it is likely that the local order in the configurations typical of the infinite pressure states at density φ_j depends on φ_j, i.e., $\langle\psi\rangle(\varphi_j)$ is not constant; this does not necessarily mean that the packings at higher φ_j cannot be considered as amorphous since $\langle\psi\rangle(\varphi)$ increases with density also in the liquid state, which is definitely an amorphous state at all densities.

Before turning to the technical part, it is useful, having in mind this phase diagram, to return to the behavior of algorithms that are used to construct jammed amorphous packings, and to review some basic features that are observed in the structure of such packings.

C. On the protocol dependence of the random close-packing density

Up to now we discussed a specific algorithm: a molecular-dynamics simulation during which the system is compressed at a given rate, the Lubachevsky-Stillinger algorithm. In a more general setting, we can consider an algorithm or experimental protocol attempting to produce jammed amorphous configurations of a hard sphere system. The algorithm stops when the system is jammed: the final density is a random variable depending on the initial data and possibly on some randomness built in the algorithm itself. To investigate the probability $\mathcal{P}(\varphi_j)$ of reaching a final density φ_j, we make the assumption that when the system is jammed, each glassy state contains only one configuration.[13] Then the number $\mathcal{N}(\varphi_j)$ of jammed states with density φ_j is given by $\mathcal{N}(\varphi_j)\sim\exp[N\Sigma(\varphi_j)]$, where $\Sigma(\varphi_j)$ is the complexity introduced above.

We define also the probability $\mathcal{P}_a(\varphi_j)$ that the algorithm finds one particular configuration with density φ_j. This probability is related to the "basin of attraction" of configurations, i.e., to the number of trajectories of the algorithm that leads to the final configuration. Again, on the basis of concentration arguments, we expect the scaling $\mathcal{P}_a(\varphi_j)\sim\exp[Ns_a(\varphi_j)]$.

Note that $\mathcal{N}(\varphi_j)$ depends only on the geometrical properties of the configuration space of hard spheres, while $\mathcal{P}_a(\varphi_j)$ encodes the properties of the algorithm (Xu *et al.*, 2005; Krzakala and Kurchan, 2007). The resulting $\mathcal{P}(\varphi_j)=\mathcal{N}(\varphi_j)\mathcal{P}_a(\varphi_j)\sim\exp\{N[\Sigma(\varphi_j)+s_a(\varphi_j)]\}$ will be strongly peaked around a given value φ_j^a, the maximum of $\Sigma(\varphi_j)+s_a(\varphi_j)$ (Krzakala and Kurchan, 2007). The important point is that φ_j^a will depend on the particular algorithm through the function $s_a(\varphi_j)$, giving rise to the protocol dependence observed in experiments and numerical simulations (Xu *et al.*, 2005; Chaudhuri *et al.*, 2009).

Therefore it is highly nontrivial to associate the phase diagram of Fig. 1 to the behavior of a given algorithm or experimental protocol. The same problem has been discussed in the context of optimization problems, where a similar phase diagram is found, without yet reaching many conclusive statements. We can only make some remarks and conjectures:

(1) In the static computation, infinite pressure states are found only in the interval $[\varphi_{\rm th},\varphi_{\rm GCP}]$. One cannot exclude the existence of states with very small volume in phase space that are not seen in the static computation. However, due to the smallness of their volume, to observe them one should design a specific algorithm. Thus we assume that reasonable procedures, which allow for some exploration of phase space, will always find states with jamming density $\varphi_j\in[\varphi_{\rm th},\varphi_{\rm GCP}]$.

(2) In the case of equilibrium dynamics (e.g., a molecular-dynamics simulation with infinitely slow compression), the system is expected to equilibrate at each density. Thus, neglecting crystallization, we expect the system to follow the liquid branch up to φ_K and then the ideal glass branch up to $\varphi_{\rm GCP}$.

(3) The mode-coupling theory instead predicts a divergence of the relaxation time at $\varphi_{\rm MCT}<\varphi_K$. However, in the context of structural glasses it is well known that the mode-coupling transition is avoided and becomes a crossover to a nonequilibrium glass state at a compression-rate dependent φ_g. At the mean-field level, the mode-coupling transition corresponds to the point φ_d where the liquid state breaks into an exponential number of disconnected states.

(4) The equilibration is particularly slow above $\varphi_{\rm MCT}\sim\varphi_d$, being due to *activated processes* (Xia and Wolynes, 2001a, 2001b; Bouchaud and Biroli, 2004; Franz, 2005).[14] For moderately high rates, the system will leave the liquid branch close to φ_d and will jam at $\varphi_{\rm th}$. Thus the procedure of O'Hern *et al.* (2002), which corresponds to a fast compression, should produce packings around $\varphi_{\rm th}$. At the mean-field level one would have $\varphi_J\sim\varphi_{\rm th}$. However, one should keep in mind (see Appendix A) that states close to $\varphi_{\rm th}$ are particularly unstable in finite dimension and therefore $\varphi_{\rm th}$ is an ill-defined concept in this case.

(5) Remarkably, the value $\varphi_{\rm GCP}$ defined as the point where $\Sigma(\varphi_j)$ vanishes is a property of the system that does not depend on the algorithm (at least if one accepts the idealizations previously discussed, i.e., if one neglects the existence of the crystal).

(6) The behavior of more complex algorithms should be discussed on a case-by-case basis. Thus, if one de-

[13] If this assumption is false one should change the definition of complexity but the following argument would remain true (see Appendix A for a detailed discussion).

[14] In the constant-pressure ensemble the times are proportional to $\exp(P\Delta V)$, where ΔV is the volume barrier to go from one state to another state.

TABLE II. Summary of the relevant densities defined in the text. The values given in $d=3$ (for a monodisperse system) are indicative; more detailed values will be given in the following. The label MF indicates that the corresponding concept can be defined in mean-field theory but lacks an unambiguous operative definition in finite dimension.

Density	Definition	Type	Value in $d=3$
φ_{MRJ}	Maximally random jammed configurations (Torquato *et al.*, 2000)	Geometrical	~0.64
φ_d	The liquid state splits in an exponential number of states	MF, static	~0.58
φ_K	Ideal glass phase transition—jump in compressibility	static	~0.62
φ_{th}	Divergence of the pressure of the less dense states	MF, static	~0.64
φ_{GCP}	Divergence of the pressure of the ideal glass	static	~0.68
φ_{MCT}	Mode-coupling transition (van Megen and Underwood, 1993)	MF, dynamic	~0.58
φ_g	Glass transition density; depends on the compression rate	Dynamic	0.58–0.62
φ_0	Divergence of the equilibrium relaxation time	Dynamic	~0.62
φ_J	J point: final state of the algorithm of O'Hern *et al.* (2002)	Dynamic	~0.64
φ_{RCP}	No general agreement on the definition		~0.64

fines the random close-packing density as the final density for a given protocol, its value can be everywhere in $[\varphi_{\mathrm{th}},\varphi_{\mathrm{GCP}}]$ (and maybe outside this interval for very particular protocols). One would like to identify φ_{RCP} with φ_{GCP}, if one is thinking to slow quasiequilibrium compressions, or with $\varphi_{\mathrm{th}}\sim\varphi_J$, if one is thinking to fast quenches.

In Table II we summarize the different densities defined up to now.

D. Structural properties of amorphous states

Despite the difficulty in determining the final jamming density for a given experimental protocol, it turns out that many structural properties of the final state, manifested for instance in the pair-correlation function $g(r)$, are roughly independent of the protocol. This suggests that at least some of these properties are common to all amorphous packings in the range $\varphi_j\in[\varphi_{th},\varphi_{\mathrm{GCP}}]$ and are therefore characteristic of "random close-packed" structures. We are able to compute the correlation function $g(r)$ for these states; therefore it is interesting to review the main features that are observed in numerical simulations.

Detailed numerical and experimental results for $g(r)$ at jamming have been reported by Clarke and Jónsson (1993), O'Hern *et al.* (2002, 2003), Aste *et al.* (2005), Donev *et al.* (2005a, 2005b), Silbert *et al.* (2006), and Skoge *et al.* (2006). Depending on the procedure one approaches the jamming point φ_j from below, $\delta\varphi=\varphi_j-\varphi>0$ (Donev *et al.*, 2005a, 2005b; Skoge *et al.*, 2006) for hard particles, or from above, $\delta\varphi=\varphi-\varphi_j>0$, for soft particles (O'Hern *et al.*, 2002, 2003; Silbert *et al.*, 2006). The main features that are observed are the following:

(1) A delta peak close to $r=D$ due to particles in contact. One has $g(D)\sim\delta\varphi^{-1}$ and the width of the peak $\propto\delta\varphi$. The delta peak has the scaling form $g(r)/g(D)=f(\lambda)$, where $\lambda\propto(r-D)\delta\varphi^{-1}/D$, if $\varphi\to\varphi_j^-$ for hard particles (Donev *et al.*, 2005a), with $f(t)$ as a scaling function independent of $\delta\varphi$. The area of this peak gives the average number of particles in contact with a reference one, which is found to be $z=2d$ once rattlers (particles without contacts) are removed; this property is called *isostaticity*.

(2) A square-root singularity $g(r)\sim(r-D)^{-\alpha}$, with $\alpha=0.5$, close to $r=D$. This singularity is integrable and does not contribute to the number of contacts. The value of the exponent is debated: some claim that it is equal to 0.5 irrespective of the value of φ_j, the procedure, etc. (Silbert *et al.*, 2006). However, some dependence on the procedure has been claimed by Donev *et al.* (2005a), where a value $\alpha\sim0.4$ has been found.

(3) A dip around $r/D\sim1.2$ with respect to the liquid is observed. This is due to the particles of the first shell which are pushed toward contact ($r=D$) for $\delta\varphi\to0$.

(4) A split second peak in $r/D=\sqrt{3}$ (Donev *et al.*, 2005a; Silbert *et al.*, 2006). It is not clear what the exact behavior of $g(r)$ close to this peak is (Silbert *et al.*, 2006), in particular, if $g(r)$ is divergent or has only divergent slope for $r/D\to\sqrt{3}^-$. Even if $g(r)$ is not divergent for $r/D\to\sqrt{3}$, it has at least a jump in $\sqrt{3}$.

(5) A similar behavior is observed in $r/D=2$. Both features have been interpreted by Clarke and Jónsson (1993) and Silbert *et al.* (2006) as coming from the network of contacts. In fact, $r/D=2$ is the maximum distance at which two particles sharing one neighbor can be found, while $r/D=\sqrt{3}$ is the maximum distance for two particles sharing two neighbors.

(6) Long-range correlations [$h(r)\sim1/r^4$ and $S(k)\sim|k|$ for large r and small k] are found for hard particles (Donev *et al.*, 2005b) and seem to also be present in the soft particles case (Silbert *et al.*, 2006). This also

implies that $S(0)=0$, i.e., the packings are incompressible.

(7) A particularly intriguing property of jammed amorphous configurations is the presence of an excess of *soft modes*, i.e., vibrational modes with very small frequency. This has been shown numerically by O'Hern *et al.* (2003) and Silbert *et al.* (2005). Wyart (2005), Wyart, Nagel, and Witten (2005), and Wyart, Silbert, *et al.* (2005) argued that this excess of soft modes is related to the isostaticity property of the network of contact; moreover, a diverging length scale has been associated to these modes. It has also been proposed that the square-root singularity of $g(r)$ is related to these modes (Wyart, 2005). This set of results seems to suggest a "critical" nature of jammed amorphous packings that is currently receiving much interest (Hatano *et al.*, 2007; Majmudar *et al.*, 2007; Olsson and Teitel, 2007; Zeravcic *et al.*, 2008).

One of the main aims of the following discussion is to show that the class of packings obtained as infinite pressure glassy states shares at least some of these features, which are common to all disordered jammed packings produced with different protocols. We will be able to partially compute the $g(r)$ of these states and show that it is consistent with the properties described above. This fact supports the main assumption of this paper, that final states reached by typical algorithms belong to the class of infinite pressure glassy states.

III. THE METHOD

Assuming the phase diagram shown in Fig. 4 and neglecting the ambiguities associated to the existence of the crystal, the properties of the glass phase can be computed using a replica method inspired by mean-field models. The method has been described in great detail in a number of papers [see, in particular, Monasson (1995), Mézard and Parisi (1996, 1999a, 2000), and Mézard (1999)]; therefore we sketch it here, but the reader who is interested in the details and has no previous knowledge of the replica method should refer to the original papers for a more complete presentation.

An alternative route to compute the properties of glassy states is to use density-functional theory (Singh *et al.*, 1985; Kirkpatrick and Wolynes, 1987a; Dasgupta and Valls, 1999; Kim and Munakata, 2003; Chaudhuri *et al.*, 2005; Yoshidome *et al.*, 2007). In principle the two methods should be equivalent [see Castellani and Cavagna (2005) for pedagogical discussion in the case of mean-field models]; still it seems that the replica method gives more accurate quantitative results and for this reason we focus on this method in the following.

A. The replica method

The phase diagram shown in Fig. 4 is characterized by the existence of many glassy states at densities above φ_d. At constant density, states are characterized by their vibrational (or internal) entropy s, defined as the entropy of the system constrained to be in this state without relaxing toward different states. The derivative of the internal entropy with respect to density is the pressure of the states, which is plotted schematically in Fig. 4. Taking a constant φ slice of the phase diagram in Fig. 4, one will meet different states, depending on the pressure (or equivalently on the entropy). The number of states of entropy s at a given density φ is by definition $\mathcal{N}(s)=\exp[N\Sigma(s,\varphi)]$.

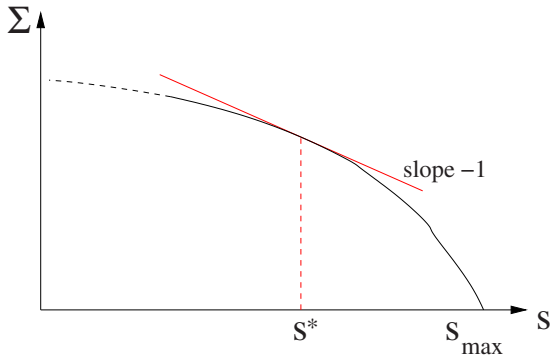

FIG. 5. (Color online) A schematic representation of $\Sigma(s,\varphi)$ at fixed φ. The behavior at small s depends strongly on the model and on the density [see Krzakala *et al.* (2007) for a more detailed discussion]. On increasing s, $\Sigma(s,\varphi)$ decreases and ultimately vanishes at a value $s_{\max}(\varphi)$. The value s^* is defined by $d\Sigma/ds=-1$. For $\varphi<\varphi_K$, $s^*<s_{\max}$, while for $\varphi\geqslant\varphi_K$ there is no solution and $s^*=s_{\max}$.

1. The ideal glass transition

The complexity $\Sigma(s,\varphi)$ (sketched in Fig. 5) is a concave function of s; it is reasonable to assume $\Sigma(s,\varphi)$ to be a decreasing function of s because at fixed density, states of higher entropy correspond to more compact structures (in order to have more free volume) and should be more rare. Moreover $\Sigma(s,\varphi)$ should continuously vanish at some value $s_{\max}(\varphi)$ corresponding to the entropy of the best amorphous structures at this density.[15] The partition function of hard spheres at density φ is just the total number of allowed configurations at that density. In the thermodynamic limit, each relevant configuration belongs only to one state and $\exp(Ns_\alpha)$ is the number of configurations belonging to the state α. Therefore one can write the partition function Z in the following way:

$$Z=e^{NS(\varphi)}\sim\sum_\alpha e^{Ns_\alpha}=\int_{s_{\min}(\varphi)}^{s_{\max}(\varphi)}ds e^{N[\Sigma(s,\varphi)+s]}\sim e^{N[\Sigma(s^*,\varphi)+s^*]},\tag{3}$$

where in the last line we performed a saddle-point ap-

[15] As discussed one can construct denser structures by allowing a small amount of local order: we are assuming to be able to avoid this in some well-defined way, which will be discussed in the following.

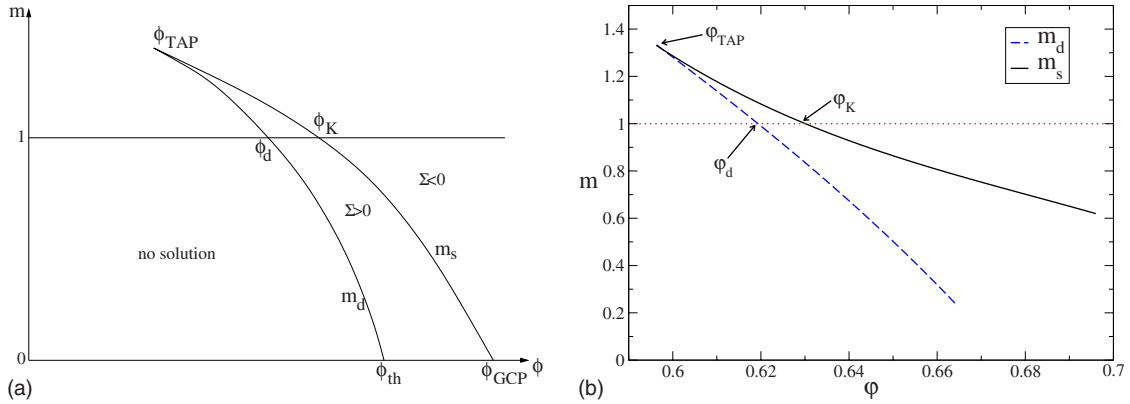

FIG. 6. (Color online) (m,φ) phase diagram. (Left) Schematic (m,φ) diagram: above the clustering line $m_d(\varphi)$ a nontrivial solution for the inter-replica correlation is found. This solution gives a positive complexity in the region enclosed between the lines m_d and m_s; therefore in this region glassy states are present. The line $m_s(\varphi)$ is defined by the condition $\Sigma(m,\varphi)=0$ and corresponds to the ideal glass state. The intersections of the line m_d (m_s) with $m=1$ and 0 define φ_d (φ_K) and $\varphi_{\rm th}$ $(\varphi_{\rm GCP})$, respectively. (Right) Phase diagram for $d=3$ as obtained by solving the replicated HNC equations (Sec. IV). Note that the static line has an unreasonable behavior at small m and that the densities φ_d and $\varphi_{\rm th}$ seem too big if compared with the accepted $\varphi_{\rm MCT}\sim 0.58$ and $\varphi_J\sim 0.64$ values.

proximation of the integral; $s^*(\varphi)$ is the point where $\Sigma(s,\varphi)+s$ assumes its maximum in the interval $[s_{\rm min},s_{\rm max}]$. Indeed, more compact structures have higher vibrational entropy (free volume) and lower complexity (their number), and the partition function is dominated by the best compromise, as expressed by the saddle-point evaluation of Eq. (3). For densities $\varphi_d<\varphi<\varphi_K$, the saddle point s^* falls inside the interval $[s_{\rm min},s_{\rm max}]$. The ideal glass transition is met at the density φ_K such that $s^*(\varphi_K)=s_{\rm max}(\varphi_K)$ or equivalently $\Sigma(s^*,\varphi_K)=0$. Above this density, the integral (3) is always dominated by the upper limit of integration; therefore we have

$$S(\varphi)=\begin{cases}\Sigma(s^*,\varphi)+s^*, & \varphi<\varphi_K\\ s_{\rm max}(\varphi), & \varphi>\varphi_K.\end{cases} \tag{4}$$

It is easy to see that [if $\Sigma(s,\varphi)$ is a smooth function] at φ_K a phase transition happens and is manifested by a discontinuity in the second derivative of $S(\varphi)$. Under our assumptions, close to $s_{\rm max}(\varphi)$ we have $\Sigma(s,\varphi)=\Sigma_1(\varphi)[s-s_{\rm max}(\varphi)]+\frac{1}{2}\Sigma_2(\varphi)[s-s_{\rm max}(\varphi)]^2+\cdots$. φ_K is defined by $\Sigma_1(\varphi_K)=-1$ and close to φ_K we have $s^*(\varphi)\sim s_{\rm max}(\varphi)-[1+\Sigma_1(\varphi)]/\Sigma_2(\varphi)$. The derivative of $S(\varphi)$ for $\varphi\to\varphi_K^-$ is given by $S'(\varphi)=\partial\Sigma(s^*,\varphi)/\partial\varphi\sim-\Sigma_1(\varphi)s'_{\rm max}(\varphi)\sim s'_{\rm max}(\varphi)$ which coincides with the derivative for $\varphi\to\varphi_K^+$. Therefore the pressure is continuous at φ_K, while it is easy to show that the compressibility jumps at φ_K, as discussed in Sec. II.B.2.

2. The replicated partition function and the (m,φ) phase diagram

The basic idea of the replica approach (Monasson, 1995; Mézard and Parisi, 1999a) is to introduce in Eq. (3) a parameter m conjugated to the internal entropy of the states. One can think of m as a control parameter that at fixed density allows us to select a given group of states.

In practice this can be done by considering m copies of the original system, constrained to be in the same state by a small attractive coupling (the practical implementation will be discussed in the following). The partition function of the replicated system is then

$$Z_m=e^{N\mathcal{S}(m,\varphi)}\sim\sum_\alpha e^{Nms_\alpha}=\int_{s_{\rm min}(\varphi)}^{s_{\rm max}(\varphi)}dse^{N[\Sigma(s,\varphi)+ms]}\sim e^{N[\Sigma(s^*,\varphi)+ms^*]}, \tag{5}$$

where now $s^*(m,\varphi)$ is such that $\mathcal{S}(m,s)=ms+\Sigma(s,\varphi)$ is minimum. The introduction of the coupled replicas has exactly the effect of giving a weight m to the vibrational entropy in Eq. (5). Only for integer m, the quantity Z_m has an explicit definition (and it can be evaluated by direct numerical simulations), but if m is allowed to assume real values,[16] the complexity can be estimated from the knowledge of the function $\mathcal{S}(m,\varphi)=ms^*(m,\varphi)+\Sigma(s^*(m,\varphi),\varphi)$. Indeed, it is easy to show that

$$\begin{aligned}s^*(m,\varphi)&=\frac{\partial\mathcal{S}(m,\varphi)}{\partial m},\\ \Sigma(m,\varphi)&=\Sigma(s^*(m,\varphi),\varphi)=-m^2\frac{\partial[m^{-1}\mathcal{S}(m,\varphi)]}{\partial m}\\ &=\mathcal{S}(m,\varphi)-ms^*(m,\varphi).\end{aligned} \tag{6}$$

The function $\Sigma(s,\varphi)$ can be reconstructed from the parametric plot of $s^*(m,\varphi)$ and $\Sigma(m,\varphi)$.

[16]This must be done by analytical continuation once the partition function for integer m has been computed using some approximation. In principle, the analytic continuation might not be well defined, but it has been verified explicitly in mean-field models that the procedure gives the correct results [see Mézard *et al.* (1987), Monasson (1995), Mézard (1999), Mézard and Parisi (1999a), Talagrand (2003), and Franz and Tria (2006)] for detailed general discussion of the replica method].

For each density, one can define a point $m_s(\varphi)$ as the solution[17] of $\Sigma(m,\varphi)=0$ (see left panel of Fig. 6). On the line $m_s(\varphi)$, from Eq. (5) we see that $\mathcal{S}(m,\varphi)=ms_{\max}(\varphi)$, then

$$S_{\text{glass}}(\varphi) \equiv s_{\max}(\varphi) = \frac{\mathcal{S}(m_s(\varphi),\varphi)}{m_s(\varphi)}. \tag{7}$$

This simple prescription allows us to compute the entropy of the glass once $\mathcal{S}(m,\varphi)$ is known.[18]

Generically, the entropy $\mathcal{S}(m,\varphi)$ turns out to be the maximum of a functional of some order parameter, which typically represents the inter-replica correlation functions, and is obtained by maximizing the functional (explicit examples will be given in the following). For each density, the inter-replica correlations are nonzero only above some value $m_d(\varphi)$, and in this case the replicas are in the same state. In this region we obtain nontrivial values of $\Sigma(m,\varphi)$; thus $m_d(\varphi)$ corresponds to the minimum value $s_{\min}(\varphi)$ below which there are no states and $\Sigma=0$. We call $m_d(\varphi)$ the clustering line because above this line the space of configuration is disconnected in many clusters corresponding to the glassy states. The two lines $m_d(\varphi)$ and $m_s(\varphi)$ in the plane (m,φ) define a phase diagram which is schematically shown in Fig. 6 and mirrors the (P,φ) phase diagram. In fact, m is conjugated to the entropy, which is related to the pressure; the two phase diagrams are related by a Legendre transform. The lines m_s and m_d touch at some value φ_{TAP} below which there are no states except the liquid one. Above φ_{TAP}, states are found for $m_d(\varphi)\leqslant m\leqslant m_s(\varphi)$. When the line $m_d(\varphi)$ reaches the line $m=1$, states begin to be present in the liquid phase: this corresponds to the point φ_d. When the static line m_s crosses $m=1$, the liquid ceases to exist and the ideal glass transition is met.

3. The equation of state of metastable glassy states

The replica method allows us to compute, for a given density, the function $\Sigma(s,\varphi)$. But to access the equation of state of the metastable glassy states we must follow the evolution of each state at different densities. This is, in general a complicated problem already at the mean-field level. Therefore in order to be able to perform the computation, we make a strong additional assumption on the phase-space structure of the model, namely, that each state is labeled uniquely by its maximum possible density or jamming density φ_j. This is the maximum value of density for this given structure, corresponding to infinite pressure, where particles are in contact with their neighbors. We assume that if one starts from the jammed structure at φ_j and slowly decreases the density, the particles are allowed to vibrate slightly around the original structure but the state maintains its identity until it merges with the liquid. In other words, we assume that there are no bifurcations of states, and states can disappear only at φ_j.

If one starts in a jammed state at density φ_j and slightly decompresses the system, the state acquires a finite entropy $s(\varphi,\varphi_j)$. We can invert this relation to get $\varphi_j(s,\varphi)$. If there are no bifurcations and we denote the logarithm of the number of structures with jamming density φ_j as $\Sigma_j(\varphi_j)$, we have the simple relation

$$\Sigma(s,\varphi) = \Sigma_j(\varphi_j(s,\varphi)). \tag{8}$$

This is a consequence of our assumption[19] because if states cannot bifurcate or die, their number remains constant; this implies that we can label the states equivalently by their jamming density φ_j or by their complexity Σ_j.

Then the procedure to extract $s(\varphi,\varphi_j)$ from Eq. (6) is the following: we fix a value Σ_j and solve

$$\Sigma(m,\varphi) = \Sigma_j \tag{9}$$

to get $m(\varphi,\Sigma_j)$. Then we have $s(\varphi,\Sigma_j)=s^*(m(\varphi,\Sigma_j),\varphi)$. As shown below, in the limit $m\to 0$ we find $s^*(m,\varphi)\to-\infty$, i.e., the pressure diverges. The jamming limit then corresponds to $m\to 0$, and the relation between φ_j and Σ_j is simply

$$\Sigma_j(\varphi_j) = \lim_{m\to 0}\Sigma(m,\varphi_j). \tag{10}$$

Inverting this equation we obtain $\varphi_j(\Sigma_j)$, which we can substitute in $s(\varphi,\Sigma_j)$ to obtain $s(\varphi,\varphi_j)$.

To summarize, under our assumption, in the (m,φ) plane of Fig. 4, we can draw many lines, each defined by $\Sigma(m,\varphi)=\Sigma_j$. Each line identifies a group of states that share the same jamming density φ_j, which is the point where the line crosses $m=0$, and the same complexity Σ_j. For a given line, we can compute the internal entropy of the corresponding states as $s(\varphi,\varphi_j)=s^*(m(\varphi,\varphi_j),\varphi)$, and differentiating this with respect to φ we get the pressure

[17]Note that the condition $\Sigma(m,\varphi)=0$ is equivalent to $\partial(\mathcal{S}/m)/\partial m=0$, which corresponds to the usual optimization of the free energy with respect to m in the 1RSB computations.

[18]An important remark (Mézard and Parisi, 1999a) is that the entropy of the replicated liquid $\mathcal{S}(m,\varphi)$ is analytic as long as $m<m_s(\varphi)$. In fact, the introduction of m shifts the phase transition that happens for $\varphi=\varphi_K$ at $m=1$ to higher values of density for $m<1$ (see Fig. 6). Therefore $\mathcal{S}(m,\varphi)$ can be computed, in the whole interesting glassy region, by analytic continuation of the low-density (replicated) liquid entropy.

[19]For this reason it is often called "isocomplexity" assumption in the spin-glass literature. It holds for the simplest spin glass the spherical p-spin glass, with a single value of p (Cugliandolo and Kurchan, 1993), but for more general models (e.g., spherical spin glasses with interactions involving sets of p and q spins with $p\neq q$ or Ising spin glasses) its exact validity is debated (Barrat *et al.*, 1997; Montanari and Ricci-Tersenghi, 2004; Krzakala *et al.*, 2008); still there is a general agreement that isocomplexity is approximately correct.

of the states, as drawn in the right panel of Fig. 4. Clearly if we choose $\Sigma_j=0$ we recover the ideal glass state as previously discussed.

B. The molecular liquid

The m copies are assumed to be in the same state. This can be implemented by constraining each particle of a given replica to be close to a particle of each of the other $m-1$ replicas. The liquid is made of *molecules* of m atoms, each belonging to a different replica of the original system, or in other words, the atoms of different replicas stay in the same cage. The replica method allows us to define and compute the properties of the cages in a purely equilibrium framework in spite of the fact that the cages have been defined originally in a dynamic framework.[20] The problem is then to compute the free energy of a molecular liquid where each molecule is made of m atoms. The m atoms are kept close to each other by a small inter-replica coupling that is switched off at the end of the calculation, while each atom interacts with all other atoms of the same replica via the original pair potential.

Note that the free energy of the replicated liquid is assumed to be analytic in the whole region $m<m_s(\varphi)$ as the only phase transition happens at $m_s(\varphi)$ when the complexity vanishes. Thus we can use approximations valid in the liquid phase to compute the free energy up to $m_s(\varphi)$. This is enough because the free energy is continuous on the transition line, and therefore the free energy of the glass can be computed by approaching the line $m_s(\varphi)$ from below, as discussed above. Note also that we are interested in the regime of fairly high densities where we expect the cages to be small and the motion of atoms inside a state to be quite localized. Thus, if all replicas are in the same state, inter-replica correlations remain strong when we switch off the coupling. Our task is then to compute the entropy of the replicated liquid in a small cage regime when atoms in a molecule are quite close to each other.

1. The partition function

We start from the grand canonical partition function of the replicated system of molecules of coordinates $\bar{x}=(x_1,\ldots,x_m)$ in a volume V, and we put a harmonic attraction between particles in a molecule. Particles belonging to the same replica interact via the hard sphere potential. The replicated partition function is

$$Z_m(\epsilon)=\sum_{N=0}^{\infty} z^N \int_V \frac{d^N x_1 \cdots d^N x_m}{N!} \prod_{i<j}\prod_a \chi(x_{ai}-x_{aj}) \times \prod_i \exp\left(-\frac{\epsilon}{m}\sum_{a<b}(x_{ai}-x_{bi})^2\right) = \sum_{N=0}^{\infty}\int_V \frac{d^N\bar{x}}{N!}\prod_i z(\bar{x}_i)\prod_{i<j}\bar{\chi}(\bar{x}_i,\bar{x}_j), \tag{11}$$

where $\chi(x-y)=\theta(|x-y|-D)$, $\bar{\chi}(\bar{x},\bar{y})=\Pi_a\chi(x_a-y_a)$, and

$$z(\bar{x})=z\exp\left(-\frac{\epsilon}{m}\sum_{a<b}(x_a-x_b)^2\right). \tag{12}$$

It is clear that the derivative of $\mathcal{S}(m,\varphi;\epsilon)\equiv\langle N\rangle^{-1}\ln Z_m(\epsilon)$ with respect to ϵ gives the average cage radius, which is defined as the average distance of atoms in two replicas $a\neq b$:

$$A\equiv\frac{1}{2Nd}\left\langle\sum_i (x_{ai}-x_{bi})^2\right\rangle = \frac{1}{m(m-1)d}\left\langle\sum_{a<b}(x_a-x_b)^2\right\rangle = -\frac{1}{(m-1)d}\frac{d\mathcal{S}(m,\varphi;\epsilon)}{d\epsilon}. \tag{13}$$

Note that this cage radius could also be measured as the large time limit of the mean-square displacement of a single system (Angelani and Foffi, 2007). We are interested in the limit of zero coupling between the replicas. If there is only one thermodynamic state, the liquid, then the replicas will decorrelate for $\epsilon\to 0$ and $A(0)=\infty$. On the contrary, if there are many stable states, an infinitesimal coupling will be enough to send the replicas into the same state; this will produce a correlation between the replicas and A will be of the order of the cage radius inside one state. This phenomenon can be better understood in term of the Legendre transform of $\mathcal{S}(m,\varphi;\epsilon)$ with respect to ϵ, which is a function of A defined by[21]

$$\mathcal{S}(m,\varphi;A)=\min_{\epsilon}[\mathcal{S}(m,\varphi;\epsilon)+(m-1)dA\epsilon], \tag{14}$$

and is schematically shown on the right panel of Fig. 7. As $(m-1)d\epsilon=d\mathcal{S}(m,\varphi;A)/dA$, the stationary points of $\mathcal{S}(m,\varphi;A)$ correspond to zero coupling and in fact $\mathcal{S}(m,\varphi)=\max_A\mathcal{S}(m,\varphi;A)$. In the liquid phase, $\mathcal{S}(m,\varphi;A)$ will have a single maximum in $A=\infty$, while when glassy states are present, $\mathcal{S}(m,\varphi;A)$ will have a secondary maximum at finite A. See Mézard and Parisi (2000) for detailed discussion of the Legendre transform with respect to ϵ.

We discuss in the following some approximation schemes to compute $Z_m(\epsilon)$. For the moment, we try to give a "pictorial" representation of this method. A way

[20]Note that it has been pointed out that, already at the MCT level, "cages" are in fact extended objects in the sense that single atoms can always hop out of their local cage and only groups of many atoms can be really blocked: strictly speaking only when the number of atoms goes to infinity is the group blocked. Depending on the approximation, we may or may not be able to take into account this effect.

[21]Due to a global $m-1$ factor, maxima and minima are exchanged for $m<1$ in the following discussion.

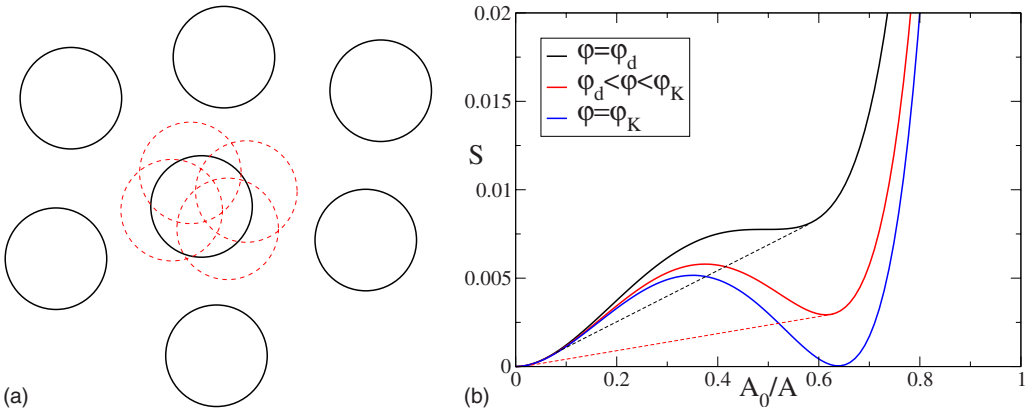

FIG. 7. (Color online) The molecular liquid. (Left) A molecule of the replicated liquid: each full (black) sphere of the original liquid is replicated m times (dashed spheres), and the m copies vibrate around the reference one. (Right) Replicated entropy as a function of the order parameter A/A_0, where A_0 is some reference value and $m<1$. The full line is the mean-field curve, while the dashed line takes into account the finite-dimensional nature of the system (see Appendix A).

to visualize the partition function $Z_m(\epsilon)$ [Eq. (11)] is that the original system is represented by the reference coordinates x_{1i} of the first replica; around each reference particle, $m-1$ other particles vibrate on a small scale $\sim 1/\sqrt{\epsilon}$. They are shown in Fig. 7 as dashed spheres. The interaction is such that dashed spheres belonging to the same replica cannot overlap.

Alternatively, the system can be thought of as a "molecular liquid" in which each molecule is built by the m replicated particles vibrating around their center of mass $X=m^{-1}\Sigma_a x_a$. The entropy of the replicated system is given in Eq. (6) by $\mathcal{S}(m,\varphi)=\Sigma(s^*(m,\varphi),\varphi)+ms^*(m,\varphi)$. In this picture, the entropy of the molecular system $\mathcal{S}(m,\varphi)$ is given by the entropy of the centers of mass $\Sigma(m,\varphi)$ plus the contribution due to the vibrations of the m particles in a molecule around the center of mass, which is m times the vibrational entropy $s^*(m,\varphi)$, i.e., the volume of a typical cage of the centers of mass system. Note that for generic m, s^* slightly depends on m since the m replicas are not independent.

This representation of $Z_m(\epsilon)$ shows that a consistent way to remove the crystal state in this computation is to describe the system of the centers of mass by a low-density virial expansion, as done in the following (see Appendix B). In other words, we assume that the centers of mass X represent structures that are typical of the liquid state. This is our operational definition of amorphous states and for this reason in our computation partially crystallized states do not appear.

2. Correlation functions

The replicated liquid is characterized by the density $\rho_a(x)=\langle\Sigma_i\delta(x_{ia}-x)\rangle$ of each replica and by the correlation function

$$\rho_{ab}(x,y)=\left\langle\sum_{ij}\delta(x_{ai}-x)\delta(x_{bj}-y)\right\rangle, \tag{15}$$

where the sum is over all ij if $a\neq b$ and over $i\neq j$ if $a=b$. If there is symmetry between the replicas, $\rho_a(x)=\rho$ and the two relevant correlations are the intrareplica correlation $g(x,y)=\rho_{aa}(x,y)/\rho^2$ and the inter-replica correlation $\tilde{g}(x,y)=\rho_{a\neq b}(x,y)/\rho^2$. In the following we show that $g(x,y)$ has a quite different shape in the liquid and in the glass at high pressure. Hence, we denote by $g_G(x,y)$ the pair distribution function in the glass phase, while we keep the notation $g(x,y)$ for the one of the liquid. To avoid confusion, we stress that $g(x,y)$ and $g_G(x,y)$ refer to the same observable in different phases, while $g(x,y)$ and $\tilde{g}(x,y)$ are different observables.

If there are no correlations between different replicas, $\tilde{g}=1$. This happens for $m<m_d(\varphi)$, where no glassy states are present. In the region $m\geqslant m_d(\varphi)$, there are glassy states. Each state α is characterized by a frozen density profile $\rho_\alpha(x)$ and by its correlation function $\rho_\alpha(x,y)$. The density profile can be computed, in principle, as the minimum of a suitable density functional $F[\rho(x)]$ (Singh *et al.*, 1985; Kirkpatrick and Wolynes, 1987a; Dasgupta and Valls, 1999; Kim and Munakata, 2003; Chaudhuri *et al.*, 2005; Yoshidome *et al.*, 2007).

We are interested in averages over the states. Due to translational invariance, $\overline{\rho_\alpha(x)}=\rho$, and for the intra-replica correlation we have simply

$$g(x-y)=\rho^{-2}\overline{\rho_\alpha(x,y)}, \tag{16}$$

where the overbar denotes the average over the states.

We assumed that the coupling between different replicas is able to force them all to be in the same state. Apart from that, in the limit of vanishing coupling no other correlations are induced. Thus

$$\tilde{g}(x-y)=\rho^{-2}\overline{\rho_\alpha(x)\rho_\alpha(y)}. \tag{17}$$

3. Nonergodicity factor

Equation (17) allows us to relate the inter-replica correlations to the so-called *nonergodicity factor* of mode-coupling theory. We sketch here the connection but the reader is referred to Bengtzelius *et al.* (1984), van Megen and Underwood (1993), and Götze (1999) for more de-

tails. In mode-coupling theory it is usual to work in Fourier space; the Fourier-transformed density reads

$$\rho_\alpha(q) = \int dx e^{iqx} \rho_\alpha(x) = \left\langle \sum_i e^{iqx_i} \right\rangle_\alpha , \tag{18}$$

where $\langle\cdot\rangle_\alpha$ denotes the thermal average in state α. The main object of mode-coupling theory is the coherent normalized scattering function

$$F(q,t) = \frac{1}{NS(q)} \left\langle \sum_{ij} e^{iq[x_i(t)-x_j(0)]} \right\rangle, \tag{19}$$

where $S(q)=N^{-1}\Sigma_{ij}e^{iq(x_i-x_j)}=1+\rho h(q)$ is the structure factor, which is related to the Fourier transform of $h(r)=g(r)-1$ (Hansen and McDonald, 1986) and $x_i(t)$ is the position of particle i at time t assuming that the position at time $t=0$ has been extracted from the Gibbs distribution (mode-coupling theory is a theory of the equilibrium dynamics of glasses). By definition, $F(q,0)=1$; in the glass phase $F(q,t)$ develops a plateau that becomes infinite at the mode-coupling transition $\varphi_{\rm MCT}$. Hence for $\varphi>\varphi_{\rm MCT}$ the long-time limit of $F(q,t)$ is nonzero; this is called nonergodicity factor f_q:

$$f_q \equiv \lim_{t\to\infty} F(q,t). \tag{20}$$

In the replica interpretation, the fact that $F(q,t)$ does not vanish in the long-time limit (or, in other words, that density fluctuations cannot relax completely) signals the appearance of metastable states. Even for $t\to\infty$, the system cannot escape from the metastable state in which it was at time $t=0$. However, it can decorrelate inside the state. Therefore, in the long-time limit one has

$$\left\langle \sum_{ij} e^{iq[x_i(t)-x_j(0)]} \right\rangle_\alpha \sim \left\langle \sum_i e^{iqx_i(t)} \right\rangle_\alpha \left\langle \sum_j e^{-iqx_j(0)} \right\rangle_\alpha = \rho_\alpha(q)\rho_\alpha(-q), \tag{21}$$

and, taking into account that the initial condition (hence the initial state α) has been extracted from the Gibbs distribution, one finally obtains

$$f_q = \frac{\overline{\rho_\alpha(q)\rho_\alpha(-q)}}{NS(q)} = \frac{\rho\tilde{h}(q)}{S(q)}, \tag{22}$$

where $\tilde{h}(q)$ is the Fourier transform of $\tilde{h}(r)=\tilde{g}(r)-1$.

IV. THE REPLICATED LIQUID: HYPERNETTED CHAIN (HNC) EQUATIONS

The simplest way to compute the property of the replicated liquid is the following. We consider the system of the m replicas as an m-component mixture, which is then described by the number density ρ_a of type a particles, and by the correlation function $g_{ab}(x,y)$ which is the probability of finding a particle of type b in y given that there is a particle of type a in x.

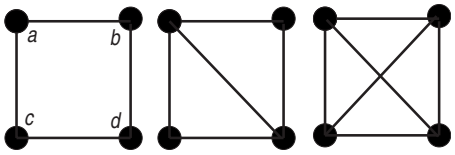

FIG. 8. The three diagrams contributing to order four in density to the replicated free-energy functional. Each vertex is associated to a density ρ_a, while each line is associated to a $h_{ab}(x_i,x_j)=g_{ab}(x_i,x_j)-1$ factor; $a,b=1,\ldots,m$ are replica indices. The value of the diagram is obtained by integrating over x_i and summing over the replica indices. Only the leftmost diagram is kept in the HNC approximation (Hansen and McDonald, 1986); the other two are two-line irreducible.

A. Replicated HNC equations

The entropy of the replicated liquid can be expressed as a functional of these quantities (Morita and Hiroike, 1961; De Dominicis and Martin, 1964; Hansen and McDonald, 1986):

$$\begin{aligned}\mathcal{S}[\rho_a,g_{ab}(x,y)] = &-\frac{1}{2}\sum_{ab}\int dxdy\rho_a\rho_b[g_{ab}(x,y)\ln g_{ab}(x,y) \\ &- g_{ab}(x,y) + g_{ab}(x,y)\beta\phi_{ab}(x,y) + 1] \\ &- V\sum_a \rho_a[\ln\rho_a - 1] \\ &- \frac{1}{2}\sum_{n\geqslant 3}\frac{(-1)^n}{n}\mathrm{Tr}[\rho h]^n \\ &- \{\text{two-line irreducible diagrams}\},\end{aligned} \tag{23}$$

and $g_{ab}(x,y)$ have to be determined by maximizing the entropy. In Eq. (23) we assume that the inter-replica coupling has already been sent to zero and look for nontrivial solutions for the inter-replica correlation. As an example, the diagrams contributing at order four in density are shown in Fig. 8.

The simplest approximation that allows us to obtain a treatable functional amounts to neglecting two-line irreducible diagrams; in this way one obtains the HNC equations for g_{ab}:

$$\ln g_{ab}(x,y) + \beta\phi_{ab}(x,y) = h_{ab}(x,y) - c_{ab}(x,y), \tag{24}$$

where c is defined by the Ornstein-Zwenicke relation

$$h_{ab}(x,y) = c_{ab}(x,y) + \sum_c \int dz h_{ac}(x,z)\rho_c c_{cb}(z,y). \tag{25}$$

The interaction potential is $\phi_{ab}(x,y)=\phi(x-y)\delta_{ab}$, where $\phi(x)$ is the hard-core potential. Using translational invariance and a replica symmetric structure, we have $\rho_a=\rho$, $g_{aa}(x,y)=g(x-y)$, and $g_{a\neq b}(x,y)=\tilde{g}(x-y)$. The replicated entropy becomes[22]

[22]We can set $\beta=1$ as temperature is irrelevant for hard spheres. Note that the term $\int d\vec{r}\phi(r)g(r)=0$.

$$\mathcal{S}(m,\varphi) = \frac{\mathcal{S}}{N} = -\frac{\rho}{2}\int d\vec{r}\{mg(r)[\ln g(r)-1] + m(m-1)\tilde{g}(r)[\ln \tilde{g}(r)-1] + m^2 + m\phi(r)g(r)\} - m(\ln\rho - 1) + \frac{1}{2\rho}\int \frac{d\vec{q}}{(2\pi)^d}\Big\{(m-1)\times\ln\{1+\rho[h(q)-\tilde{h}(q)]\} + \ln\{1+\rho[h(q) + (m-1)\tilde{h}(q)]\} - m\rho h(q) + \frac{m\rho^2 h(q)^2}{2} + \frac{m(m-1)\rho^2\tilde{h}(q)^2}{2}\Big\}, \tag{26}$$

where $h(q)$, $\tilde{h}(q)$ are the Fourier transforms of $h(r)$, $\tilde{h}(r)$. The HNC equations can be written as

$$\ln g(r) = -\phi(r) + W(r),$$
$$\ln \tilde{g}(r) = \tilde{W}(r), \tag{27}$$

where $W(r)$,$\tilde{W}(r)$ are defined by their Fourier transforms

$$W(q) = \frac{1}{m}\frac{\rho[h(q)+(m-1)\tilde{h}(q)]^2}{1+\rho[h(q)+(m-1)\tilde{h}(q)]} + \frac{m-1}{m}\frac{\rho[h(q)-\tilde{h}(q)]^2}{1+\rho[h(q)-\tilde{h}(q)]},$$
$$\tilde{W}(q) = \frac{1}{m}\frac{\rho[h(q)+(m-1)\tilde{h}(q)]^2}{1+\rho[h(q)+(m-1)\tilde{h}(q)]} - \frac{1}{m}\frac{\rho[h(q)-\tilde{h}(q)]^2}{1+\rho[h(q)-\tilde{h}(q)]}. \tag{28}$$

Using Eq. (6), the free energy and complexity of the states are

$$s^*(m) = \frac{\partial\mathcal{S}(m)}{\partial m} = -\frac{\rho}{2}\int d\vec{r}\{g(r)[\ln g(r)-1] + (2m-1)\tilde{g}(r)[\ln\tilde{g}(r)-1] + 2m + \phi(r)g(r)\} - \ln\rho + 1 + \frac{1}{2\rho}\int\frac{d\vec{q}}{(2\pi)^d}\Big\{\ln\{1+\rho[h(q)-\tilde{h}(q)]\} + \frac{\rho\tilde{h}(q)}{1+\rho[h(q)+(m-1)\tilde{h}(q)]} - \rho h(q) + \frac{\rho^2 h(q)^2}{2} + \frac{(2m-1)\rho^2\tilde{h}(q)^2}{2}\Big\}, \tag{29}$$

$$\Sigma(m) = -m^2\frac{\partial[\mathcal{S}(m)/m]}{\partial m} = \frac{\rho m^2}{2}\int d\vec{r}\{\tilde{g}(r)[\ln\tilde{g}(r)-1]+1\} - \frac{1}{2\rho}\int\frac{d\vec{q}}{(2\pi)^d}\Big\{\ln\{1+\rho[h(q)-\tilde{h}(q)]\} - \ln\{1+\rho[h(q)+(m-1)\tilde{h}(q)]\} + \frac{m\rho\tilde{h}(q)}{1+\rho[h(q)+(m-1)\tilde{h}(q)]} + \frac{m^2\rho^2\tilde{h}(q)^2}{2}\Big\}.$$

The advantage of this formulation is that Eqs. (27) are relatively easy to solve numerically and give direct access to both the thermodynamic property of the glass (entropy and pressure), the structure factor $g(r)$, and the nonergodic parameter $\tilde{g}(r)$.

B. Results

The above equations were used by Mézard and Parisi (1996) and Cardenas *et al.* (1998, 1999) to compute the properties of amorphous states of hard spheres. We now reproduce these calculations for illustration.[23]

1. Phase diagram

The (m,φ) phase diagram for $d=3$ is shown in Fig. 6. The values of $\varphi_K=0.63$ and $\varphi_d=0.619$ are reasonable even if φ_d is a bit too large if compared to $\varphi_{\mathrm{MCT}}\sim 0.58$ (van Megen and Underwood, 1993). Also, the value of $\varphi_{\mathrm{th}}\sim 0.67$ that one can guess from the extrapolation of m_d to $m=0$ is larger than the accepted value $\varphi_J\sim 0.64$ from numerical simulations.

Moreover, one immediately notices that the static line does not seem to extrapolate to zero at reasonable densities.[24] This was already observed by Mézard and Parisi (1996) and was one of the major problems of the HNC approximation. Before discussing this issue in detail, we discuss the results for the correlation functions.

2. Correlation functions

Clearly, in the liquid phase $m=1$ and the correlation function of the liquid coincides with the one obtained

[23]The HNC equations were solved by an iterative Picard scheme using an initial Gaussian guess for $\tilde{c}(x)$. We used a grid defined by imposing a cutoff $r<L=8D$ and discretizing space with a step $a=D/128$. We checked the stability of the reported results by doubling the cutoff and inverse step.

[24]It is worth noting at this point that on increasing the density, long-range correlations seems to develop and short-range singular behavior emerges in $g(r)$ as expected from numerical simulations. Thus one is forced to increase the cutoff and inverse step used in the discretization of the HNC equations. We checked that in the range shown in Fig. 6 the resulting m_s, m_d are not affected by discretization corrections.

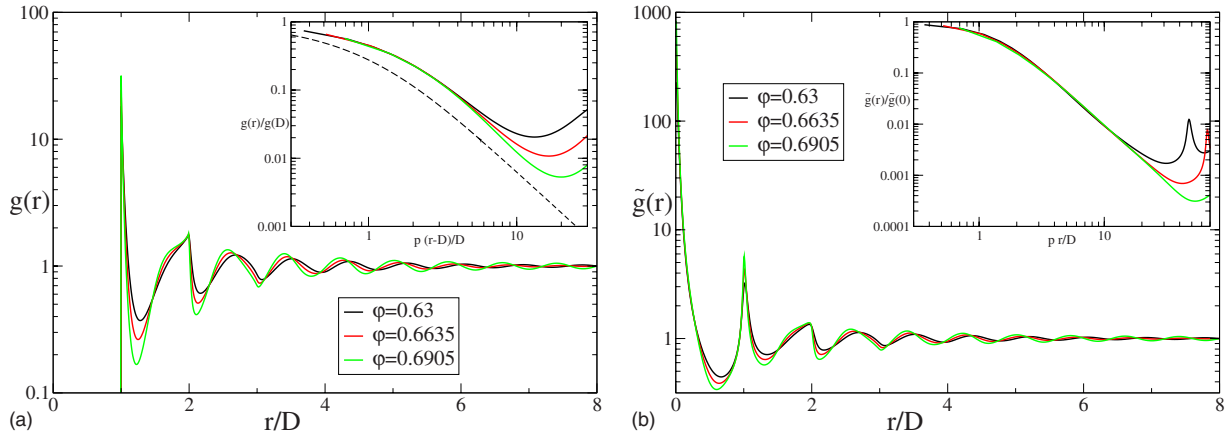

FIG. 9. (Color online) $g_G(r)$ and $\tilde{g}(r)$ along the ideal glass line $m_s(\varphi)$ at three different densities, computed using the replicated HNC equations (Sec. IV). Inset: Scaled plot of $g_G(r)/g_G(D)$ vs $p(r-D)/D$ and $\tilde{g}(r)/\tilde{g}(0)$ vs pr/D, where $p=1+4\varphi g_G(D)$.

within the nonreplicated HNC approximation. The result for $g_G(r)$ along the line $m_s(\varphi)$ (i.e., for the ideal glass) is shown in Fig. 9. Many interesting features expected from numerical simulations (see Sec. II.D) are observed: First, $g_G(r)$ develops a delta peak close to $r=D$, whose shape (inset of the left panel) is quite similar to the one observed by Donev *et al.* (2005a). Moreover, a dip for $r\sim 1.2$ is developed due to particles of the first shell getting closer to the reference one. Another interesting feature is the jump that develops in $r=2D$ and the cusp in $r=3D$, which are in fact related to the delta peak in $r=D$. Finally, we observe that on increasing the density $g_G(r)$ develops long-ranged oscillations for large r, even if a systematic study of these correlations would require the investigation of smaller values of m at which the approximation gives inconsistent results.

As for $\tilde{g}(r)$, the most interesting feature is the peak close to $r=0$ that describes the particle of replica b which is in the same molecule of the reference particle of replica a. Its shape has a clear scaling form on decreasing m: the cage radius, i.e., the scale on which the delta peak is rounded, decreases and goes to 0 for $m\to 0$, as previously anticipated. The behavior for larger r is similar to the one of $g(r)$, "rounded" by the fluctuations inside each molecule of particles of different replicas. Finally, in Fig. 10 we show the nonergodicity factor f_q [Eq. (22)], which is a central object of mode-coupling theory. The shape of f_q obtained with replicas is qualitatively similar to the one obtained within MCT (Bengtzelius *et al.*, 1984; van Megen and Underwood, 1993; Götze, 1999) and experiments (van Megen *et al.*, 1991), although from the quantitative point of view marked differences are present.

C. Discussion

The replicated HNC equation gives interesting qualitative indications on the phase diagram and correlations functions and is not too bad from the quantitative point of view. However, the value $\varphi_d=0.619$ is too large compared with numerical estimates, and the nonergodicity factor is quite far from the measured values. Another unsatisfactory feature of the HNC approximation is that it gives a complexity Σ of the order of 0.01, which is two orders of magnitude smaller compared to what is observed in simulations and experiments, where $\Sigma\sim 1$. As for the correlation of the glass, this approximation misses the peak at $r=\sqrt{3}D$ (which should be encoded in the diagrams that have been neglected) and the square-root singularity close to $r=D$ but well reproduces the other characteristic features of jammed disordered packings.

Unfortunately, the results of the HNC approximation definitely become bad at small values of m, i.e., deep inside the glass phase on approaching jamming. This can be understood quite easily by inspecting the diagrams that have been neglected in the HNC approximation, already at the lowest nontrivial order in density; these are shown in Fig. 8. The argument goes as follows: As discussed, when the pressure is high (or m is small) the cage becomes very small, and the peak in $\tilde{g}(r)$ close to $r=0$ approaches a delta function. Consider the contribution to the diagrams in Fig. 8 when the replica indices are all different, $a\neq b\neq c\neq d$; then on each link there is

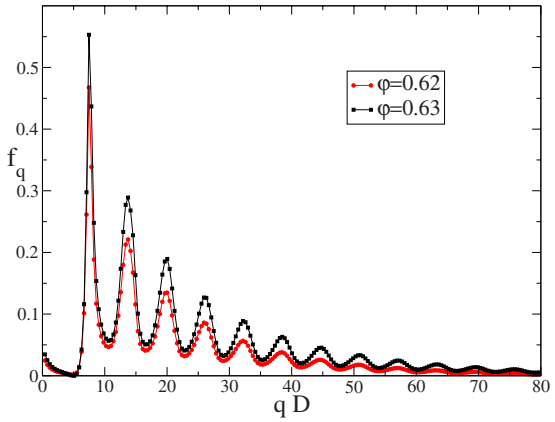

FIG. 10. (Color online) Nonergodicity factor, defined in Eq. (22), computed using the replicated HNC equations (Sec. IV) at $\varphi=0.62\sim\varphi_d$ and $\varphi=0.63\sim\varphi_K$.

a factor $\tilde{g}(x_i-x_j)$. We focus on the small x_i-x_j behavior; then $\tilde{g}(x_i-x_j)\sim\delta(x_i-x_j)$ and the leftmost diagram has a contribution

$$\int dx_1dx_2dx_3dx_4\delta(x_1-x_2)\delta(x_2-x_3)$$
$$\times\delta(x_3-x_4)\delta(x_4-x_1)\sim\delta(0) \tag{30}$$

since three delta functions are enough to constrain the four integration variables to be close to each other. The notation $\delta(0)$ here is a formal way to indicate that the contribution above will diverge roughly as the maximum of the peak of $\tilde{g}(r)$. Now, the other two diagrams in Fig. 8 have more links; performing the same computation as above, we find that they diverge as $\delta(0)^2$ and $\delta(0)^3$. But these diagrams are not included in the HNC and this makes the approximation bad at high pressure. Actually, this reasoning shows that the HNC is keeping the less divergent diagrams at each order, while the maximally divergent diagrams are the completely connected ones, at least as far as the contribution with different replica indices is concerned. Therefore to study the jamming limit we need to treat correlations inside a molecule in a more appropriate way. We discuss next a different approximation scheme that fixes this problems by taking into account all correlations between different replicas (in some sense, resumming the contribution of completely connected diagrams).

The argument above is supported by the fact that we were not able to derive analytically the limit $m\to 0$ of the HNC equations, and we have a strong feeling that they become pathological in this limit. The same problem is present in the limit $d\to\infty$ and should be connected to the fact that the cage radius is very small in this limit, as shown below. In summary, the HNC approximation does not work for small cage radius: multiple correlation functions in the replica sector become important.

V. THE REPLICATED LIQUID: EFFECTIVE POTENTIALS

A way to compute the replicated free energy for a system of Lennard-Jones particles in a more accurate way, by taking into account multiple correlations inside a molecule, has been described by Mézard and Parisi (1999b). The idea is to write the free energy as a function of the cage radius A and expand systematically in powers of A, which is assumed to be small. Thus we expect this method to work well in the dense region and for $m\sim 0$, where the HNC approximation fails. The method is successful but cannot be extended straightforwardly to hard spheres because at some stage in their work Mézard and Parisi (1999b) assumed that vibrations were harmonic, an approximation that clearly breaks down for hard-core potentials. In this section we discuss a general method that allows us to map the replicated free energy onto the nonreplicated free energy of a liquid of particles interacting via some effective potentials to be computed below. The method is similar in spirit to the self-consistent phonon theory used by Stoessel and Wolynes (1984) and Hall and Wolynes (2003, 2008) to study the stability of a glass state. This will allow us to derive in a simple way the small cage expansion for the case of hard spheres. Moreover, the correlation function of the glass turns out to be the correlation function of the effective liquid, thus simplifying much of its computation. Similar ideas have been recently used by Stevenson *et al.* (2008).

A. Entropy as a functional of the single-molecule density

We wish to compute the entropy as a functional of the order parameter A, the cage radius, whose expected behavior has been schematically shown in Fig. 7. Instead of directly expanding the partition function (11) for large ϵ and then Legendre transform with respect to ϵ as in Eq. (14), we will first use standard liquid theory to perform a Legendre transform of Eq. (11) with respect to the full function $z(\bar{x})$. In this way we obtain the entropy as a functional of the single-molecule density

$$\rho(\bar{x})=\left\langle\sum_i\delta(\bar{x}-\bar{x}_i)\right\rangle, \tag{31}$$

where $\delta(\bar{x}-\bar{x}_i)=\Pi_a\delta(x_a-x_{ai})$, and of the interaction function $\bar{\chi}(\bar{x},\bar{y})$,

$$\mathcal{S}[\rho(\bar{x}),\bar{\chi}(\bar{x},\bar{y})]=\int d\bar{x}\rho(\bar{x})[1-\ln\rho(\bar{x})]$$
$$+\sum(\text{a class of diagrams}). \tag{32}$$

The class of diagrams contributing to Eq. (32) is defined precisely by Morita and Hiroike (1961), De Dominicis and Martin (1964), and Hansen and McDonald (1986) but is not important here. What is important is that a diagram $\mathcal{D}$ represents an integral of the form

$$\mathcal{D}=\frac{1}{S}\int\prod_i\rho(i)d\bar{x}_i\prod_\ell[\bar{\chi}(\ell)-1], \tag{33}$$

where i are the vertices of the diagram and $\ell=(i<j)$ are the links, and to shorten the notation we defined $\rho(i)=\rho(\bar{x}_i)$ and $\bar{\chi}(\ell)=\bar{\chi}(\bar{x}_i,\bar{x}_j)$. S is the symmetry factor of the diagram, i.e., the number of equivalent relabelings of the vertices of the diagram.

The reason why we start from Eq. (32) instead of Eq. (11) is that the single-molecule density $\rho(\bar{x})$ is directly related to the order parameter A we want to study. In particular, we can make a simple Gaussian ansatz[25]

[25]This simple ansatz assumes that all particles have the same cage radius $\sqrt{A}$. However, at very high pressure, it is well known that most of the particles are immobile, while a small fraction (typically ~5%) can vibrate in a cage that remains finite even at infinite pressure. These particles are called "rattlers" in the literature on jamming. Our ansatz completely neglects rattlers. One could think to improve it by introducing two cage radii, one associated to jammed particles and the other to rattlers: we did not explore this possibility.

$$\rho(\bar{x}) = \frac{\rho m^{-d/2}}{(2\pi A)^{(m-1)d/2}} \exp\left(-\frac{1}{2mA}\sum_{a<b}(x_i^a - x_i^b)^2\right)$$
$$= \frac{\rho}{(2\pi A)^{md/2}} \int dX \exp\left(-\frac{1}{2A}\sum_a (x_a - X)^2\right)$$
$$= \rho \int dX \prod_a \frac{e^{-(1/2A)(x_a - X)^2}}{(2\pi A)^{d/2}}$$
$$\equiv \rho \int dX \prod_a \gamma_A(x_a - X), \tag{34}$$

where $\gamma_A(x)$ is a normalized Gaussian with variance A; we then have $\int d\bar{x}\rho(\bar{x}) = \rho V = N$; therefore ρ has the interpretation of the number density of molecules (note that having Legendre transformed we are now working at fixed N).

The Gaussian ansatz for $\rho(\bar{x})$ is not equivalent to the Gaussian ansatz (12) for the single-molecule activity; in fact $\rho(\bar{x})$ is a sum of diagrams containing $z(\bar{x})$ and the interaction function, so it is Gaussian at lowest order in ϵ but has corrections coming from higher orders. The corrections are singular because of the singularity of the interaction. For this reason it is convenient first to Legendre transform with respect to $z(\bar{x})$ and then to make the Gaussian ansatz for $\rho(\bar{x})$: the resulting small A expansion has a better behavior.

The Gaussian form (34) allows us to compute exactly the ideal-gas term of the entropy:

$$\frac{1}{N}\int d\bar{x}\rho(\bar{x})[1 - \ln \rho(\bar{x})]$$
$$= 1 - \ln\rho - \frac{d}{2}(1-m)\ln(2\pi A) - \frac{d}{2}(1 - m - \ln m)$$
$$\equiv 1 - \ln\rho + S_{\text{harm}}(m,A), \tag{35}$$

where we defined

$$S_{\text{harm}}(m,A) = \frac{d}{2}(m-1)\ln(2\pi A) + \frac{d}{2}(m - 1 + \ln m). \tag{36}$$

We want to find a simple way to rewrite the replicated entropy exploiting the fact that A is small.

B. The effective nonreplicated liquid

Before proceeding to the formal computation, it is better to understand intuitively what the result will be. To this aim, note that we assumed that the vibrations of the m copies of the particles, $x = (x_1, \ldots, x_m)$, are described by the Gaussian distribution (34), corresponding to harmonic vibrations.

The width A is a variational parameter and we maximize the entropy with respect to it at the end; for the moment we assume that A is small. The idea is to choose a replica (say, replica 1) as a reference and consider the vibrations of the other $m-1$ particles around the reference one. At the zeroth order in A, the $m-1$ copies essentially coincide with the reference one, and $\mathcal{S}(m,\varphi;A) \equiv N^{-1}\mathcal{S}[\rho(\bar{x}),\bar{\chi}(\bar{x},\bar{y})]$ is given by the entropy $S(\varphi)$ of the nonreplicated liquid (corresponding to replica 1) plus the free energy of $m-1$ harmonic oscillators of spring constant A:

$$\mathcal{S}^{(0)}(m,\varphi;A) = S(\varphi) + S_{\text{harm}}(m,A). \tag{37}$$

We see indeed that the ideal-gas term (35) corresponds to Eq. (37) where $S(\varphi)$ has been approximated by the ideal-gas contribution.

A first-order approximation is obtained by considering the effective two-body interaction induced on the particles of replica 1 by the coupling to $m-1$ copies. We consider two particles x_1 and y_1 of replica 1 belonging to two molecules $\bar{x}$ and $\bar{y}$. Each particle of a given replica a interacts with the other particles of the same replica via the hard-core potential $\phi(r)$. The effective interaction between particles in replica 1 is obtained by averaging this interaction over the probability distribution $\rho(\bar{x})$ of the two molecules $\bar{x}$ and $\bar{y}$:

$$e^{-\phi_{\text{eff}}(x_1 - y_1)} = \int dx_{2,m} dy_{2,m} \rho^{-2}\rho(\bar{x})\rho(\bar{y}) \prod_{a=1}^{m} e^{-\phi(x_a - y_a)}$$
$$\equiv e^{-\phi(x_1 - y_1)} \left\langle \prod_{a=2}^{m} e^{-\phi(x_a - y_a)} \right\rangle_{x_1, y_1}. \tag{38}$$

As an example, the potential $\phi_{\text{eff}}(r)$ for hard spheres in $d=3$ is shown in Fig. 11 for some values of A and m (see Appendix C for its calculation). A first-order approximation to $\mathcal{S}(m,\varphi;A)$ is then obtained by substituting to the entropy $S(\varphi)$ of the simple hard sphere liquid the free energy of a liquid of particles interacting via the potential $\phi_{\text{eff}}(r)$,

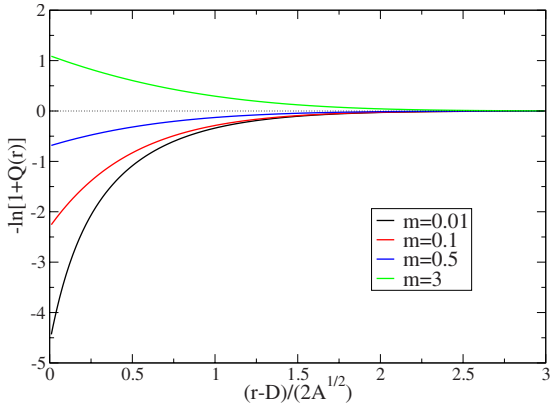

FIG. 11. (Color online) The non-hard-core part of the effective potential $\phi_{\text{eff}}(r) - \phi(r) = -\ln[1+Q(r)]$ [Eq. (38)] as a function of $(r-D)/\sqrt{4A}$ for $r \geq D$ for different values of $m = 0.01, 0.1, 0.5, 3$ (from bottom to top) in $d=3$. Note that the range of the potential is $O(\sqrt{A})$ and that it is attractive for $m < 1$ and repulsive for $m > 1$. The strength of the potential diverges for $m \to 0$.

$$\mathcal{S}^{(1)}(m,\varphi;A) = -\beta F[\varphi;\phi_{\rm eff}(r)] + S_{\rm harm}(m,A). \quad (39)$$

It is now evident that we can obtain better approximations of the true function $\mathcal{S}(m,\varphi;A)$ by also considering the three-body interactions induced on particles of the replica 1 and so on.

This procedure can be justified more formally by introducing a diagrammatic expansion in powers of A and resumming a class of diagrams: this is discussed in detail in Appendix B. The result is the following: the replicated entropy (32) can be *exactly* rewritten as

$$\mathcal{S}(m,\varphi;A) \equiv N^{-1}\mathcal{S}[\rho(\bar{x}),\bar{\chi}(\bar{x},\bar{y})] = S_{\rm harm}(m,A) - \beta F_{\rm eff}[\varphi;\phi_{\rm eff},\phi^{(2)}_{\rm eff},\phi^{(3)}_{\rm eff},\dots], \quad (40)$$

where the effective potentials $\phi^{(n)}_{\rm eff}$ depend on both A and m. The correlation function of the glassy states as a function of A and m is just the correlation function of the liquid described by $F_{\rm eff}$.

The effective potential $\phi^{(n)}_{\rm eff}$ is constructed as follows: one constructs all possible connected diagrams with n links and such that one pair of vertices is not connected by more than one link. Then one numbers the vertices $x_1,x_2,\dots$. The effective potential $\phi^{(n)}_{\rm eff}$ for one chosen diagram depends on the variables $x_1,x_2,\dots$ (whose numbers depend on the diagram). For $n=1$, we have only one possibility, $\phi_{\rm eff}$ depends only on $\vec{r}=x_1-x_2$ by translation invariance and is given by Eq. (38). Also, for $n=2$ we have only one possibility where the two links share one vertex; the resulting potential depends on $\vec{r}=x_1-x_2$ and $\vec{s}=x_1-x_3$ (denoting by x_1 the common vertex), and we have

$$e^{-\phi^{(2)}_{\rm eff}(x-y,x-z)} = \frac{\left\langle \prod_{a=2}^{m} e^{-\phi(x_a-y_a)} e^{-\phi(x_a-z_a)} \right\rangle_{x,y,z}}{\left\langle \prod_{a=2}^{m} e^{-\phi(x_a-y_a)} \right\rangle_{x,y} \left\langle \prod_{a=2}^{m} e^{-\phi(x_a-z_a)} \right\rangle_{x,z}}, \quad (41)$$

where the brackets denote averages similar to the one in Eq. (38) (see Appendix B for details). There it is also shown that the correlation function $g_G(r)$ of the glass is given by the correlation function $g_{\rm eff}(r)$ of the effective liquid.

C. Properties of the effective potentials

The effective potentials have the following general properties, which are discussed in Appendix B:

(1) If for at least one of the links the distance $r=|x_i-x_j|$ is such that $|r-D|\gg\sqrt{A}$, the potential vanishes exponentially as $e^{-(r-D)^2/A}$.

(2) For the reason above, we can argue that they contribute $O(A^{n/2})$ to the free energy, where n is the number of links in the potential. This is because the potential is nonvanishing only if, for all links, $|r-D|\sim\sqrt{A}$, and this region has volume $O(A^{n/2})$.

(3) One can show that the leading order of the potentials vanishes if the unit vectors of the links are orthogonal. Then, one can argue that in the limit $d\to\infty$ where the links are almost always orthogonal, the potentials for $n\geqslant 2$ give vanishing contributions.

(4) All potentials are $O(m-1)$ for $m\to 1$. Thus in this limit they can be treated as perturbations of the hard-sphere liquid.

(5) In the opposite limit $A\to 0$ with $A=\alpha m$ (jamming limit, see below), the potentials tend to become delta functions around $r=D$.

In the following we use these properties to derive the glass equation of state and its structure factor as a function of the dimensionality.

Before concluding we remark that in the case of a smooth potential it might be preferable to use the center of masses as reference positions instead of the coordinates of replica 1. The expansion of Appendix B can be carried out similarly in this case and leads to analogous expressions for the effective potentials. The difference is that in the case of a smooth potential the small cage expansion starts with a term of order A and one can show that if the center of masses is chosen as reference positions, the n-body potential is of order A^{n-1}. Conversely, if one uses replica 1 as a reference, all potentials are of order A. The advantage of using replica 1 as a reference is that the correlation function of the effective liquid is directly the correlation function of the glass. In the case of hard spheres the expansion is well behaved because of the properties above. One should keep in mind that depending on the problem at hand, one expansion might be better than the other.

VI. THE LIMIT OF LARGE SPACE DIMENSION

We begin by the study of the limit $d\to\infty$ because in this limit all expressions simplify and we are able to obtain a consistent solution in all regions of the phase diagram. Moreover, this limit is interesting because metastability effects should be less important in high dimension: the limit $d\to\infty$ is a kind of mean-field limit where the surface and the volume are of the same order of magnitude and nucleation becomes almost impossible. As discussed in the Introduction, the limit $d\to\infty$ also has interesting applications in the digitalization of signals [see Conway and Sloane (1993)].

A. The liquid in $d\to\infty$

The problem of computing the entropy of the hard-sphere liquid for $d\to\infty$ was addressed by Frisch and Percus (1999) and Parisi and Slanina (2000), where the same result was obtained in two independent ways. Frisch and Percus (1999) showed that the ring diagrams dominate

the virial series order by order in ρ for large d. The resummation of these diagrams gives

$$S(\varphi) = 1 - \ln\rho + \frac{\rho}{2}\int d\vec{r} f(r) - \frac{1}{2\rho}\int \frac{d\vec{q}}{(2\pi)^d} \times \left[\ln[1-\rho\hat{f}(q)] + \rho\hat{f}(q) + \frac{[\rho\hat{f}(q)]^2}{2}\right], \quad (42)$$

where $\hat{f}(q)$ is the Fourier transform of the Mayer function $f(r)=\chi(r)-1$,

$$\hat{f}(q) = -V_d\Gamma\left(\frac{d}{2}+1\right)\left(\frac{2}{q}\right)^{d/2} J_{d/2}(q). \quad (43)$$

The key observation is that, up to a density $\varphi_{\max}^{\mathrm{HS}} = \exp[d(1-\ln 2)/2]/2^d$, the logarithm does not have poles so that the above expression is well defined. If $2^d\varphi$ is not exponentially large, the nonring diagrams are conjectured to give only exponentially small corrections (Frisch and Percus, 1999), and one can show that the last term is exponentially small (Frisch and Percus, 1999). Therefore, if $2^d\varphi$ does not grow exponentially with d, $S(\varphi)$ is given by the ideal-gas term plus the first virial correction (i.e., by the van der Waals equation) up to exponentially small corrections,

$$S(\varphi) = 1 - \ln\rho - 2^{d-1}\varphi + O(e^{-d}),$$
$$g(r) = \chi(r)[1 + O(e^{-d})]. \quad (44)$$

Parisi and Slanina (2000) introduced simple equations for the pair-correlation function $g(r)$ and solved in the limit $d\to\infty$; it was shown that one obtains the same result, up to $\varphi_{\max}^{\mathrm{HS}}$, meaning that Eq. (44) might be a reasonable analytic continuation of the liquid equation of state up to $\varphi_{\max}^{\mathrm{HS}}$ which is exponentially larger than 2^d. At this value of the density a pole develops at finite q that seems to correspond to a liquid instability [the Kirkwood instability (Frisch and Percus, 1999)].

The physical meaning of this instability is not clear. Although interesting from the mathematical point of view [maybe also in relation to the problem of finding the most dense lattices (Parisi, 2008)], this question is not physically relevant in this context. We show later that the glass transition indeed preempts this instability that is therefore in a nonphysical region of the density: this system becomes unstable toward replica symmetry breaking at a density $\varphi\sim 2^{-d}d$ before reaching the Kirkwood instability.

B. The effective liquid: The Baxter model in $d\to\infty$

To compute the free energy of the replicated liquid, we will neglect all the potentials but the two-body one. This is because, as discussed above, we have indications that the corrections coming from the many-body potentials vanish in this limit. However, this point deserves a more careful investigation.

1. Two-body potential in large dimension

The calculation of the two-body potential was already done at first order by Parisi and Zamponi (2005); in Appendix C it is carried out at any order. The resulting effective potential [Eq. (38)] is shown in Fig. 11 for $d=3$. Note that at fixed m the effective potential is a function of $(r-D)/\sqrt{4A}$ only.

In the limit $d\to\infty$ the correlations of the liquid vanish and its $g(r)$ approaches a step function $\theta(r-D)$; on the contrary, as shown below, the cage radius in the relevant region is very small (of the order of $1/d$). Then, as the two-body potential vanishes on a scale $\sqrt{A}$, it is reasonable to approximate it with a delta function in $r=D$: this leads to the Baxter model (Baxter, 1968) where

$$e^{-\phi_{\mathrm{eff}}(r)} = \chi(r)[1+Q(r)] \to \chi(r)[1 + DG_m(A)V_d(1)\delta(r-D)], \quad (45)$$

where $G_m(A)$ is related to the integral of $Q(r)$ by Eq. (C4) of Appendix C,

$$G_m(A) = \frac{1}{V_d(D)}\int d\vec{r}\chi(r)Q(r) = \frac{d}{D^d}\int_D^\infty dr r^{d-1}Q(r). \quad (46)$$

We show below that the natural scale for A in this limit is $\hat{A}=d^2A/D^2$ which is of order 1 at the glass transition. With this scaling it is possible to compute the leading expression in the limit $d\to\infty$ [see Eq. (C32) in Appendix C],

$$\lim_{d\to\infty} G(m, D^2\hat{A}d^{-2}) \equiv \mathcal{G}_m(\hat{A}) = \int_{-\infty}^{\infty} dy e^y \left[\Theta\left(\frac{y+\hat{A}}{\sqrt{4\hat{A}}}\right)^m - \theta(y)\right], \quad (47)$$

where $\Theta(t)=\frac{1}{2}[1+\mathrm{erf}(t)]$.

2. The Baxter liquid in large dimension

We have then to solve the Baxter model in the limit $d\to\infty$. To do this it is enough to observe (Parisi and Slanina, 2000) that the Fourier transforms of $\delta(r-D)$ and $\theta(D-r)$ coincide at the leading order in the limit $d\to\infty$. Using the results of Parisi and Slanina (2000) it is easy to show that

$$\hat{f}_{\mathrm{eff}}(q) = [1-\mathcal{G}_m(\hat{A})]\hat{f}(q), \quad (48)$$

where $\hat{f}_{\mathrm{eff}}$ is the Mayer function corresponding to the Baxter potential (45). Note that this relation is exact for $q=0$. It is possible to show (e.g., by direct numerical computation) that, for all m and $\hat{A}$, $\mathcal{G}_m(\hat{A})<1$; therefore the coefficient $1-\mathcal{G}$ is positive and the only difference between the Baxter liquid and the hard sphere liquid is in an $O(1)$ renormalization of the density. Therefore, up

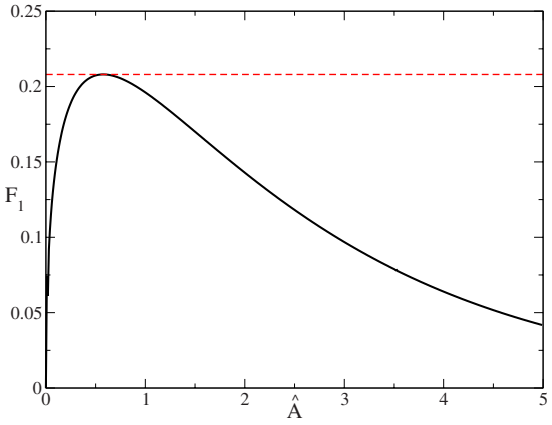

FIG. 12. (Color online) The function $\mathcal{F}_1(\hat{A})$.

to a density $\varphi_{\max}^{\text{Baxter}} = \varphi_{\max}^{\text{HS}}/[1-\mathcal{G}_m(\hat{A})]$, the free energy of the Baxter liquid is given by

$$-\beta F_{\text{Baxter}}(m,\varphi;\hat{A}) = 1 - \ln\rho - 2^{d-1}\varphi[1-\mathcal{G}_m(\hat{A})]. \tag{49}$$

We will see that the replica instability happens for $\varphi < \varphi_{\max}^{\text{Baxter}}$, so this expression will be enough for our purposes. The replicated entropy is finally given by substituting Eqs. (49) and (47) into Eq. (39),

$$\begin{aligned}\mathcal{S}(m,\varphi;A) &= S_{\text{harm}}(m,A) + 1 \\ &\quad - \ln\rho - 2^{d-1}\varphi(1-\mathcal{G}_m(\hat{A})) \\ &= S(\varphi) + S_{harm}(m,A) + 2^{d-1}\varphi\mathcal{G}_m(\hat{A}) \\ &= 1 - \ln\rho - 2^{d-1}\varphi - \frac{d}{2}(1-m)\ln(2\pi\hat{A}/d^2) \\ &\quad - \frac{d}{2}(1-m-\ln m) + 2^{d-1}\varphi \\ &\quad \times \int_{-\infty}^{\infty} dy e^y \left[\Theta\left(\frac{y+\hat{A}}{\sqrt{4\hat{A}}}\right)^m - \theta(y)\right]. \end{aligned} \tag{50}$$

From this expression (that might be exact in the large dimension limit) it is possible to derive the phase diagram of the system.

C. The equation for A and the clustering transition

From Eq. (50) we obtain the equation for A from the condition $\partial\mathcal{S}/\partial A = 0$,

$$\frac{d}{2^d\varphi} = \frac{\hat{A}}{1-m}\frac{\partial\mathcal{G}_m(\hat{A})}{\partial\hat{A}} \equiv \mathcal{F}_m(\hat{A}). \tag{51}$$

The solution to this equation must be substituted into Eq. (50) to obtain the replicated entropy $\mathcal{S}(m,\varphi)$. For generic m, $\mathcal{F}_m(\hat{A})$ has the shape shown in Fig. 12 for $m=1$. Therefore a solution exists only if

$$\varphi \geqslant \frac{d}{2^d}\frac{1}{\max_{\hat{A}}\mathcal{F}_m(\hat{A})} \equiv \varphi_d(m), \tag{52}$$

which defines the clustering transition density $\varphi_d(m)$. As $\max_{\hat{A}}\mathcal{F}_m(\hat{A})$ is a quantity of order 1 for all m, the scale of the clustering transition is $\varphi_d \sim d/2^d$. The same result was obtained by Kirkpatrick and Wolynes (1987a) by means of density-functional theory. Moreover, this result compares well with the results of Torquato *et al.* (2006) who found that simple algorithms are able to construct packings up to this scale of density.

For $\varphi > \varphi_d(m)$, the equation for $\hat{A}$ admits two solutions, the physical one being the smallest, which correspond to a maximum of the free energy for $m<1$, as usual in the replica computations. This solution has the right physical behavior as the cage radius becomes smaller on increasing the density. While the full curve $\varphi_d(m)$ can easily be computed numerically from Eq. (52), we focus in the following on the special cases $m=1$ and 0 that define the equilibrium clustering transitions φ_d and φ_{th}, respectively.

1. The clustering (mode-coupling) transition

For $m=1$, the clustering transition can be identified with the usual dynamical (or mode-coupling) transition. This is because when the liquid splits into an exponential number of glassy states, we expect the dynamics to become very slow as the system must cross barriers to change state. In $d\to\infty$ these barriers become very high and we expect a real dynamical transition characterized by a divergence of the relaxation time at φ_d. It would be interesting to check this conjecture by investigating the mode-coupling equations in the limit $d\to\infty$.

We have from Eqs. (47) and (51), taking[26] the limit $m\to 1$,

$$\mathcal{F}_1(\hat{A}) = -\hat{A}\frac{\partial}{\partial\hat{A}}\int_{-\infty}^{\infty} dy e^y \Theta\left(\frac{y+\hat{A}}{\sqrt{4\hat{A}}}\right)\ln\Theta\left(\frac{y+\hat{A}}{\sqrt{4\hat{A}}}\right). \tag{53}$$

This function can be easily computed numerically: the result is shown in Fig. 12. It has a maximum for $\hat{A}=0.576$ where $\mathcal{F}_1=0.208$; the corresponding value for the clustering transition is

$$\varphi_d = \varphi_d(1) = 4.8d/2^d, \quad d\to\infty. \tag{54}$$

Note that this value is somehow larger (but not too much) than the saturation density $\varphi_{\text{RSA}} = d/2^d$ (Torquato *et al.*, 2006) of the random sequential addition process in which spheres are added sequentially at random.

[26]Before taking the limit it is convenient to substitute in Eq. (47) $\theta(y)\to\Theta((y+\hat{A})/\sqrt{4\hat{A}})$, it can be shown that the integral is unchanged. This is due to the property $\int d\vec{r}[q_A(r)-\chi(r)]=0$ (see Appendix C).

2. The J point in $d\to\infty$

In the limit $m\to 0$ the cage radius A that optimizes the free energy goes to 0. Therefore the jammed states are obtained in the double limit $m\to 0$, $\hat{A}\to 0$, $\hat{A}=\hat{\alpha}m$, as discussed in Sec. VI.D. Using the results of Appendix C, in particular Eq. (C35), one can show that Eq. (51) for $\hat{A}$ becomes in this limit

$$\frac{d}{2^d\varphi}=\mathcal{F}_0(\hat{\alpha})=\frac{1}{4\hat{\alpha}}\int_0^\infty dy y^2 e^{-y-y^2/4\alpha}. \tag{55}$$

The function $\mathcal{F}_0(\hat{\alpha})$ has the same qualitative shape of $\mathcal{F}_1(\hat{A})$ (see Fig. 12) and assumes its maximum for $\hat{\alpha}=0.302$ with $\mathcal{F}_0=0.160$. This gives the leading order in $d\to\infty$ of the clustering density for $m=0$,

$$\varphi_{\rm th}=\varphi_d(0)=6.26d/2^d,\quad d\to\infty. \tag{56}$$

As discussed this density corresponds to the first appearance of jammed states at infinite pressure and we conjecture that it coincides with the J-point density, at least in this large dimension limit.

D. The ideal glass state

Once Eq. (51) has been solved, one can obtain the entropy and complexity of glassy states from Eqs. (6) and (50),

$$\begin{aligned} s^*(m,\varphi)&=-d\ln d+\frac{d}{2}\left[\ln(2\pi\hat{A})+1+\frac{1}{m}\right]\\ &\quad+2^{d-1}\varphi\partial_m\mathcal{G}_m(\hat{A}),\\ \Sigma(m,\varphi)&=\frac{d}{2}\ln d-\frac{d}{2}[1+\ln(\hat{A}/m)]\\ &\quad-2^{d-1}\varphi[1+m^2\partial_m m^{-1}\mathcal{G}_m(\hat{A})]\\ &\quad-\ln(2^d\varphi)-\frac{1}{2}\ln(\pi d)+1, \end{aligned} \tag{57}$$

where we used the Stirling formula to expand the gamma function appearing in V_d. In the region of the clustering transition we showed that $2^d\varphi\sim d$ and $\hat{A}=O(1)$; thus the first term in Σ always dominates and gives a positive complexity.

To find the solution to $\Sigma(m,\varphi)=0$ we have then to choose $\varphi=d\hat{\varphi}/2^d$ and look to $\hat{\varphi}\to\infty$. In this case the solution for $\hat{A}$ vanishes. For small $\hat{A}$, the function $\mathcal{G}_m(\hat{A})\sim\sqrt{4\hat{A}Q_0(m)}$ (see Appendix C). Substituting into Eq. (51) we get $\hat{A}\propto\hat{\varphi}^{-2}$, and substituting this into Eq. (57)

$$\Sigma(m,\hat{\varphi})=\frac{d}{2}\ln d-\frac{d}{2}[\hat{\varphi}+O(\ln\hat{\varphi})]. \tag{58}$$

Then we see that the leading behavior is $\hat{\varphi}=\ln d$ independently of m. The dependence on m comes from the subleading terms [see Parisi and Zamponi (2006b) for an analysis of these terms]. Therefore, both the Kauzmann and glass close-packing density scale as

$$\varphi_K,\varphi_{\rm GCP}=d\ln d/2^d,\quad d\to\infty \tag{59}$$

for $d\to\infty$. Note that in the limit $m\to 0$, $\hat{A}=\hat{\alpha}m$, the vibrational entropy goes to $-\infty$ due to the term $\ln\hat{A}$ in Eq. (57). In summary, for $m\to 0$ the cage radius goes to 0, the entropy goes to $-\infty$, and the pressure diverges: the particles get in contact and the system is jammed.

E. The correlation function

The correlation function of the glass is given by the correlation function of the effective Baxter liquid. In the ring resummation for hard spheres [Eq. (42)], we get

$$\begin{aligned} g(r)&=\frac{2}{\rho}\frac{\delta S}{\delta\ln\chi(r)}=\chi(r)y(r),\\ y(r)&=1+\int\frac{dq}{(2\pi)^d}e^{-iqr}\frac{\rho\hat{f}(q)}{1-\rho\hat{f}(q)}, \end{aligned} \tag{60}$$

where $\hat{f}(q)$ is given by Eq. (43). For the Baxter effective liquid one has to substitute $\hat{f}(q)\to\hat{f}_{\rm eff}(q)$ and $\chi(r)\to e^{-\phi_{\rm eff}(r)}$. In both cases, for $d\to\infty$, the analysis of Parisi and Slanina (2000) or a direct investigation of Eq. (60) shows that $y(r)=1+e^{-(d/2)\hat{y}(r)}$, where the function $\hat{y}(r)$ can be determined [see Parisi and Slanina (2000)]. Ignoring this exponentially small corrections[27] we are left with $g_G(r)=e^{-\phi_{\rm eff}(r)}$. Therefore the correlation function of the glass is essentially given by a step function plus a peak in $r=D$, which becomes a delta function in the jamming limit $m\to 0$, $A=\alpha m$. We can compute the weight of the delta peak $\chi(r)Q(r)$, which is related to the average number of contacts per sphere z by

$$z=\rho\int dr\chi(r)Q(r)=\frac{\rho\Omega_d D^d}{12\tau}=2^d\varphi G_m(A). \tag{61}$$

In the jamming limit $\mathcal{G}_m(\hat{A})\to\mathcal{G}_0(\hat{\alpha})$ [see Eq. (C36)] and $\hat{\alpha}=\hat{\alpha}(\varphi)$ is the solution of Eq. (55), so that

$$z=d\left.\frac{\mathcal{G}_0(\hat{\alpha})}{\mathcal{F}_0(\hat{\alpha})}\right|_{\hat{\alpha}=\hat{\alpha}(\varphi)}, \tag{62}$$

where $\mathcal{F}_0(\hat{\alpha})=\hat{\alpha}d\mathcal{G}_0(\hat{\alpha})/d\hat{\alpha}$ is defined in Eq. (55). In the limit $\hat{\alpha}\to 0$, which corresponds to random close packing, we have $\mathcal{G}_0(\hat{\alpha})\propto\sqrt{\hat{\alpha}}$ which implies $z\to 2d$, i.e., the packings are *isostatic*. However, for $\hat{\alpha}>0$, Eq. (62) gives $z>2d$, with $z\sim 3.6d$ at the threshold density.

This strange result might be due to different reasons: (i) subleading corrections that we neglected might affect the result in some subtle way; (ii) the states corresponding to finite $\hat{\alpha}$ might be unstable; it is possible that only

[27] That, however, is necessary to ensure that $S(q)\geqslant 0$ for all q and that $S(0)=0$ (Parisi and Slanina, 2000).

states with $\hat{\alpha} \sim (\ln d)^{-2}$ are stable; and (iii) it is possible that other contributions, e.g., those of the square-root singularity in lower dimension, are merged with the true contacts on the scale of the delta peak. This point deserves further investigation.

F. Discussion

We showed that for $d \to \infty$ the model can be almost completely solved, at least within our initial assumptions, i.e., that there is a clustering transition where the configuration space splits into many disconnected clusters without further structure[28] and the phase diagram is computed in full detail.

To further check the consistency of the small cage expansion, it is interesting to estimate the Lindemann ratio in the glass phase when $2^d\varphi \sim d \ln d$. The Lindemann ratio L for a given solid phase is the ratio between the typical amplitude of vibrations around the equilibrium positions and the mean interparticle distance. In our framework it can be defined as

$$L \equiv \rho^{1/d}\sqrt{A}. \tag{63}$$

Using $\sqrt{\hat{A}} = d\sqrt{A}/D \propto 1/\hat{\varphi} \propto (\ln d)^{-1}$ as derived in Sec. VI.D, and $2^d\varphi = \rho V_d(D) \sim d \ln d$, one has

$$L \sim 1/(\sqrt{d} \ln d) \ll 1, \tag{64}$$

which is consistent with the assumption that vibrations are small.

We can compare our prediction for the glass close packing $\varphi_{\mathrm{GCP}} \sim 2^{-d} d \ln d$ with the best available bounds on the density of crystalline packings. A classical lower bound for the close packing density is the Minkowsky bound, $\varphi \sim 2^{-d}$. It has been improved by Ball (1992) where, for the case of lattice packings, it is proved that $\varphi \geqslant 2d2^{-d}$ [see also Krivelevich *et al.* (2004) where a procedure to construct packings achieving this bound has been discussed]. The best currently known upper bound is reported by Kabatiansky and Levensthein (1978) and has the asymptotic scaling $\varphi \sim 2^{-0.5990\ldots d}$ Our result for φ_{GCP} lies between these bounds (it is only a factor $\ln d$ better than the lower bound) so we cannot give an answer to the question whether the densest packings of hard spheres in large d are amorphous or crystalline. Hopefully better bounds on the density of crystalline packings will address this question in the future. The values of densities of crystalline laminated lattices (Conway and Sloane, 1993) up to $d=50$ seem to suggest that there are lattices where $2^d\varphi$ grows exponentially in d. It is, however, quite possible that this is a preasymptotic effect [see Parisi (2008) for detailed discussion]. It would be interesting to find the density of laminated lattices in larger dimensions. Finally, it is worth noting that Torquato and Stillinger (2006b) proposed that it is possible to achieve packings having density exponentially higher than the Minkowsky lower bound and actually very close to the upper bound cited above. Trying to prove (or disprove) this conjecture is a challenge for future research.

[28] In replica jargon this corresponds to a 1RSB solution. Unfortunately we cannot study the instability of this solution toward more complicated replica symmetry-breaking solutions.

VII. FINITE DIMENSION: FIRST ORDER IN THE SMALL CAGE EXPANSION

In this section we discuss the simplest approximation that works well in finite dimension, namely, a first-order expansion in the cage radius $\sqrt{A}$. Despite its simplicity, we see that it is able to reproduce many of the available numerical data with good accuracy. Its main drawback is that it does not allow us to access the clustering transition nor the full shape of $g(r)$ in the glass phase. In Sec. VIII, we discuss different ways to try to improve over this approximation.

A. First-order replicated free energy

We focus on the first correction in the expansion of Eq. (40) in powers of $\sqrt{A}$. Then, we can neglect all $n \geqslant 3$-body potentials that give contributions $O(A)$ (see Appendix B). Moreover, at fixed m the two-body potential is $O(\sqrt{A})$ and we can treat it as a perturbation. Note that in the limit $m \to 0$ this is not true, as in fact the expansion parameter is A/m and not A. However, we are interested in the limit $m \to 0$ with $A = \alpha m$. Taking the limit $m \to 0$ of the first-order term in $\sqrt{A}$ will then give the first-order term in $\sqrt{\alpha}$.

1. The small cage expansion

Taking into account only the two-body potential, Eq. (40) reduces to Eq. (39), where

$$-\beta F_{\mathrm{eff}}[\varphi;\phi_{\mathrm{eff}}(r)] = N^{-1}\mathcal{S}[\varphi;\chi(r)[1+Q(r)]], \tag{65}$$

where $\mathcal{S}[\varphi;b(r)]$ is the entropy functional (32) for a nonreplicated liquid with interaction $b(r) = e^{-\phi_{\mathrm{eff}}(r)}$. It is easy to show, using standard liquid theory (Hansen and McDonald, 1986), that for a translationally invariant system

$$\frac{1}{N}\frac{\delta\mathcal{S}[\varphi,b(r)]}{\delta \ln b(r)} = \frac{\rho}{2}g(r), \tag{66}$$

where $g(r)$ is the pair distribution function of the liquid. Using this relation to expand Eq. (65) for small $Q(r)$ and calling $S(\varphi) = N^{-1}\mathcal{S}[\varphi;\chi(r)]$ the entropy of the nonreplicated hard sphere liquid, the first-order expression for the entropy is obtained from Eq. (40),

$$\mathcal{S}(m,\varphi;A) = N^{-1}\mathcal{S}[\rho(\bar{x}),\bar{\chi}(\bar{x},\bar{y})] = S_{\mathrm{harm}}(m,A) + S(\varphi) + \frac{\rho}{2}\int dr g(r)Q(r). \tag{67}$$

To compute the correlation function of the glass, we start from Eq. (B12); we use Eq. (67) substituting $\chi \to \chi e^{-v}$ and we get

$$\frac{\rho^2}{2} g_G(x,y) = \frac{\rho^2}{2} g(x,y) + \frac{\rho^2}{2} \int du dv \frac{\delta g(u,v)}{\delta \ln \chi(x,y)} Q(u,v), \tag{68}$$

and using Eq. (D9) of Appendix D,

$$\frac{\delta g(u,v)}{\delta \ln \chi(x,y)} = g(x,y)\delta(x-u)\delta(y-v) + (\text{other terms}) \tag{69}$$

(where the other terms contain basically the connected four-point function), we get

$$g_G(r) = g(r)[1 + Q(r)] + (\text{other terms}), \tag{70}$$

which is the result already obtained for Parisi and Zamponi (2005) in a completely different way. One can argue that the contribution of the other terms is negligible for $r \sim D$; therefore Eq. (70) allows us to access the shape of the contact peak in $g_G(r)$.

If $\sqrt{A} \ll D$, we can assume that the function $g(r)$ is essentially constant[29] on the scale $\sqrt{A}$, $g(r) \sim g(D)\chi(r)$ for $r - D \sim O(\sqrt{A})$. Then we have

$$\int dr g(r) Q(r) \sim g(D) \int dr \chi(r) Q(r) \equiv g(D) V_d(D) G_m(A) \tag{71}$$

and

$$\mathcal{S}(m,\varphi;A) = S_{harm}(m,A) + S(\varphi) + g(D) 2^{d-1} \varphi G_m(A), \tag{72}$$

which resembles the expression for the Baxter model in $d \to \infty$ [Eq. (50)] except for the factor $g(D)$ in front of the last term. The expansion in powers of $\sqrt{A}$ is easily obtained from Eq. (C23) in Appendix C,

$$\mathcal{S}(m,\varphi;A) = S_{\text{harm}}(m,A) + S(\varphi) + 2^d \varphi g(D) \frac{d\sqrt{A}}{D} Q_0(m). \tag{73}$$

This result has been obtained by Parisi and Zamponi (2005, 2006a).

2. Optimization with respect to the cage radius

We finally have to optimize with respect to A in Eq. (73) to get the free energy at the minimum. Note that the derivative of Eq. (73) is a linear function of $\sqrt{A}$, therefore it always allows a solution independently of the values of φ and m. Therefore investigating the dynamic transition, i.e., the point at which the solution for A disappears, is not possible within this approximation. This is because the function $F_m(A)$ has a shape similar to the one in Fig. 12: if we expand it for small A and keep only the leading $\sqrt{A}$ term, we lose the maximum in Fig. 12 and are left with a continuously increasing function. Therefore the equation $F_m(A) = \text{const}$ will have the solution for all values of the constant, i.e., of the density.

Keeping this in mind, we obtain for the replicated free energy

$$\mathcal{S}(m,\varphi) = S(\varphi) - \frac{d}{2}(1-m)\ln[2\pi A^*] - \frac{d}{2}(m - 1 - \ln m), \tag{74}$$

$$\sqrt{A^*(m)} = \frac{1-m}{Q_0(m)} \frac{D}{\rho V_d(D) g(D)} = \frac{1-m}{Q_0(m)} \frac{D}{2^d \varphi Y(\varphi)},$$

where[30] $Y(\varphi) \equiv g(D)$. Applying Eq. (6) we get

$$s^*(m,\varphi) = \frac{\partial \mathcal{S}(m,\varphi)}{\partial m} = \frac{d}{2} \ln[2\pi A^*(m)] + d(1-m)\frac{Q_0'(m)}{Q_0(m)} + \frac{d}{2}\frac{m+1}{m}, \tag{75}$$

$$\Sigma(m,\varphi) = \mathcal{S}(m,\varphi) - m s^*(m,\varphi) = S(\varphi) - \frac{d}{2}\ln[2\pi A^*(m)] - dm(1-m)\frac{Q_0'(m)}{Q_0(m)} + \frac{d}{2}\ln m - dm.$$

The important remark is that the only input in the expressions above is the entropy of the liquid $S(\varphi)$; the only other quantity is $Y(\varphi)$ appearing in $A^*(m)$ [see Eq. (74)], but the latter is related to $S(\varphi)$ by the general relation

$$p \equiv \frac{\beta P}{\rho} = 1 + 2^{d-1}\varphi g(D) = -\varphi \frac{dS(\varphi)}{d\varphi}, \tag{76}$$

where p is the reduced pressure.

Given $S(\varphi)$, the density φ_{GCP} is the solution of $\Sigma_j(\varphi) = \lim_{m\to 0} \Sigma(m,\varphi) = 0$; using Eq. (75) and the asymptotic behavior of $Q_0(m) \sim \sqrt{\pi/4m}$ (see Appendix C), we obtain the condition

$$\Sigma_j(\varphi) = \lim_{m\to 0} \Sigma(m,\varphi) = S(\varphi) - d\ln\left[\frac{\sqrt{8}}{2^d \varphi Y(\varphi)}\right] + \frac{d}{2} = 0, \tag{77}$$

while the Kauzmann density is the solution of $\Sigma_{\text{eq}}(\varphi) = \Sigma(1,\varphi) = 0$, which gives the condition

[29] In fact this assumption is false: it will turn out at the end of the computation that $\sqrt{A}/D \sim 0.01$ but on this scale $g(r)$ still has structure close to contact. However, this assumption gives consistently the first order in the small cage expansion.

[30] The reason for this notation is that $y(r) = e^{\phi(r)} g(r)$ is continuous in $r = D$ (Hansen and McDonald, 1986) and $Y(\varphi) = y(D) = g(D)$.

$$\Sigma_{\rm eq}(\varphi) = S(\varphi) - d\,\ln\left[\frac{\sqrt{2\pi}}{2^d Q_0 \varphi Y(\varphi)}\right] = 0, \tag{78}$$

with $Q_0 \equiv -Q_0'(m=1) = 0.638\ldots$.

As $Q_0(m) \sim m^{-1/2}$ for $m \to 0$, from the second equation in Eq. (74) one can show that in the limit $m \to 0$, $A \propto m$, and the first equation in Eq. (75) shows that the vibrational entropy and the pressure both diverge. This is consistent with the identification of the limit $m \to 0$ and the jamming limit, as discussed in Sec. VI.D.

It has been shown by Parisi and Zamponi (2005, 2006a) that these first-order expressions already give quantitative predictions that are in good agreement with numerical simulations. In the following we review these results.

B. Equation of state of the glass and complexity of the liquid

Once an equation of state for the liquid is given, Eq. (75) give access to the phase diagram except for the dynamic transition. In this section we discuss the results in different space dimensions.

1. $d=1$

In dimension $d=1$ we do not expect any glass transition. Indeed, the particles are always in a "state": apart from the trivial symmetries (permutations and global translations), they vibrate around the "configuration" $x_1 < x_2 < \cdots < x_N$. The packing fraction is $\varphi = \rho D$. The diameter of the cages is given by $2R = D(1-\varphi)/\varphi$, and it is easy to show that the distribution of the cage radii is exponential. Therefore in this case we expect our Gaussian approximation to be very inaccurate.

The entropy can be computed exactly and is given by $S(\varphi) = 1 + \ln(2R) = 1 - \ln(\varphi/D) + \ln(1-\varphi)$. The value of the correlation function at contact is $Y(\varphi) = 1/(1-\varphi)$ and diverges at close packing $\varphi = 1$.

In our approach, as there is only one state, we expect to have $Z_m = \exp[mNS(\varphi)]$, then $\mathcal{S}(m,\varphi) = -N^{-1}\ln Z_m = -mS(\varphi)$, and $s^*(\varphi) = -\partial_m \mathcal{S}(m,\varphi) = S(\varphi)$, i.e., the vibrational entropy is equal to the total entropy and the complexity is $\Sigma = 0$. Indeed, substituting the expressions above for $S(\varphi)$ and $Y(\varphi)$ in Eq. (75) we easily find

$$\begin{aligned} 2\sqrt{A^*(1)} &= D\frac{1}{0.638}\frac{1-\varphi}{\varphi}, \\ s^*(\varphi) &= \frac{1}{2}\ln[2\pi A^*(1)] \\ &= \ln\frac{\sqrt{2\pi}}{2(0.638)} - \ln(\varphi/D) + \ln(1-\varphi). \end{aligned} \tag{79}$$

Thus the theory reproduces the exact result apart from a (small) constant shift of the entropy (corresponding to a multiplicative factor in front of the cage radius). This is probably due to the Gaussian approximation, which is clearly wrong as the distribution of the cage is exponential, and to the small cage approximation. Indeed, for $\varphi \sim 1$, where the cages are small, the leading term of the entropy is correctly reproduced by the expressions above.

2. $d=2$

In dimension $d=2$ we can use either the Henderson expression for $Y(\varphi)$ (Henderson, 1975),

$$Y_H(\varphi) = \frac{1 - 7\varphi/16}{(1-\varphi)^2}, \tag{80}$$

or the improved expression of Luding (2001),

$$Y_L(\varphi) = Y_H(\varphi) - \varphi^3/2^7(1-\varphi)^4, \tag{81}$$

with small quantitative differences. In the first case we find[31] $\varphi_K = 0.816$ and $\varphi_{\rm GCP} = 0.874$, while in the second we find $\varphi_K = 0.811$ and $\varphi_{\rm GCP} = 0.873$.

Note that in $d=2$ the existence of an ideal glass transition has recently been the object of an intense debate (Santen and Krauth, 2000, 2001; Brumer and Reichman, 2004; Donev *et al.*, 2006; Tarzia, 2007). In fact, amorphous packings of monodisperse two-dimensional spheres are particularly unstable (Brito and Wyart, 2006). For this reason, in the following we focus on $d \geqslant 3$.

3. $d \geqslant 3$

In $d=3$ we used the Carnahan-Starling expression (Hansen and McDonald, 1986) for the entropy $S(\varphi)$, which reproduces very well the numerical data for the equation of state of the hard sphere liquid. In $d>3$ the Carnahan-Starling equation of state can be generalized to (Song *et al.*, 1989),

$$\begin{aligned} Y(\varphi) &= \frac{(1-\alpha\varphi)}{(1-\varphi)^d}, \\ \alpha &= d - 2^{d-1}(B_3/b^2), \end{aligned} \tag{82}$$

where $Y(\varphi) = g(D)$ is the value of the radial distribution function at contact and b and B_3 are the second and third virial coefficients, whose exact expression is known (Song *et al.*, 1989). The entropy of the liquid $S(\varphi)$ is obtained by integrating the exact expression (76). In $d=4$ this equation is not very accurate (see Fig. 15) and an equation of state based on Padé approximants (Bishop and Whitlock, 2005) seems more accurate (see Fig. 1). Still the error is not so large and for simplicity in the analytic computations we use the Carnahan-Starling approximation for all $d \geqslant 3$.

Using this expression for $S(\varphi)$, Eqs. (77) and (78) can be easy solved numerically to get the values of $\varphi_{\rm GCP}$ and φ_K for any given value of d. The results are reported in Table III for $d \leqslant 8$ and compared with $\varphi_{\rm MRJ}$ as reported

[31] Note that Zamponi (2007) erroneously stated that in $d=2$ the present method predicts the absence of a glass transition. We thank F. Caltagirone for pointing out the error and providing the correct values of φ_K and $\varphi_{\rm GCP}$.

TABLE III. Values of φ_K and $\varphi_{\rm GCP}$ from the first-order small cage expansion of Sec. VII (only values for $d\leqslant 8$ are reported for brevity; values for $d\geqslant 8$ are in Fig. 13) compared with the available numerically measured values of φ_J (O'Hern *et al.*, 2003; Xu *et al.*, 2005; Schreck and O'Hern, 2008) and $\varphi_{\rm MRJ}$ (Skoge *et al.*, 2006). The last two columns give the values of φ_K and $\varphi_{\rm GCP}$ extrapolated from the fits of the data of Skoge *et al.* (2006) shown in Fig. 2. The large-d scaling of $\varphi_{\rm MRJ}$ has been conjectured by Skoge *et al.* (2006).

d	φ_K (theory)	$\varphi_{\rm GCP}$ (theory)	φ_J (num.)	$\varphi_{\rm MRJ}$ (num.)	φ_K (extr.)	$\varphi_{\rm GCP}$ (extr.)
2	0.8165	0.8745				
3	0.6175	0.6836	0.640	0.64		
4	0.4319	0.4869	0.452	0.46	0.409	0.473
5	0.2894	0.3307		0.31		
6	0.1883	0.2182		0.20		
7	0.1194	0.1402				
8	0.0739	0.0877				
∞	$2^{-d}d\ln d$	$2^{-d}d\ln d$		$2^{-d}d$?		

by Skoge *et al.* (2006). The latter quantity is the density of the maximally random (according to some measure of "order") collectively jammed packings of the system [see Torquato *et al.* (2000) for the precise definition; it is estimated by Skoge *et al.* (2006) by the jamming density $\varphi_j(\gamma)$ for finite but small γ, see Sec. IV of Skoge *et al.* (2006) for detailed discussion]. As $\varphi_j(\gamma)$ is expected to increase on decreasing γ and $\varphi_{\rm GCP}=\lim_{\gamma\to 0}\varphi_j(\gamma)$ (see Fig. 2), it follows that $\varphi_{\rm MRJ}$, as estimated by Skoge *et al.* (2006) should be strictly lower than $\varphi_{\rm GCP}$, but close to it consistently with the data in Table III. A plot of φ_K and $\varphi_{\rm GCP}$ for d up to 19 is shown in Fig. 13. Note that it has been suggested by Skoge *et al.*, (2006) that $2^d\varphi_{\rm MRJ}\sim c_1+c_2 d$ and indeed, given that the compression rates used in numerical simulation are not very small, $\varphi_{\rm MRJ}$ should be quite close to $\varphi_{\rm th}$, which scales as $d/2^d$ [see Eq. (56)]. Recalling that $2^d\varphi_K, 2^d\varphi_{\rm GCP}\sim d\ln d$, we expect that at some point $\varphi_{\rm MRJ}$ will become smaller than φ_K even if this is not observed for $d\leqslant 6$.

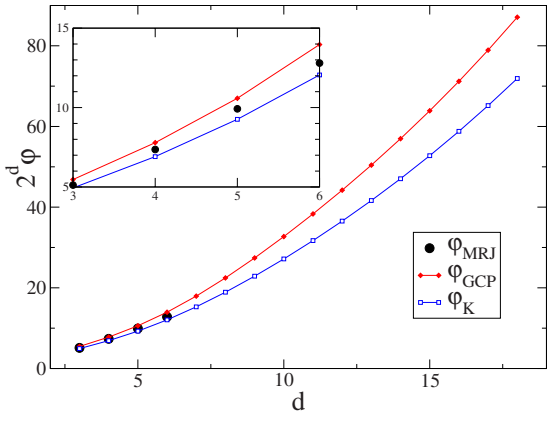

FIG. 13. (Color online) Plot of φ_K [open squares, obtained solving Eq. (78)], $\varphi_{\rm GCP}$ [full diamonds, Eq. (77)], and $\varphi_{\rm MRJ}$ (full circles, numerical estimate of Skoge *et al.*, 2006) as a function of the dimension. Both φ_K and $\varphi_{\rm GCP}$ scale as $2^d\varphi\sim d\ln d$ for large d, while their distance scales as $2^d(\varphi_{\rm GCP}-\varphi_K)\sim d$. In the inset the same plot for $3\leqslant d\leqslant 6$ (compare with Fig. 6 of Skoge *et al.*, 2006).

The very nice data for $d=4$ reported by Skoge *et al.* (2006) and shown in Fig. 1 allow for a more precise comparison of the numerical and theoretical results: the value of $\varphi_j(\gamma)$ has been measured for five different values of $\gamma=10^{-3}$, 10^{-4}, 10^{-5}, 10^{-6}, and 10^{-7} (see Fig. 2). A standard procedure to extrapolate to $\gamma\to 0$ is to fit the data to a Vogel-Fulcher law,

$$\gamma(\varphi_j)=\gamma_0 10^{-D/(\varphi_{\rm GCP}-\varphi_j)} \Leftrightarrow \varphi_j(\gamma)=\varphi_{\rm GCP}+\frac{D}{\log_{10}[\gamma/\gamma_0]}.$$

Such extrapolations are often ambiguous; however, the fit is good (see Fig. 2) and gives $\varphi_{\rm GCP}=0.473$. A similar extrapolation of $\varphi_g(\gamma)$ (defined roughly as the point where the curves in Fig. 1 leave the liquid equation of state) to $\gamma=0$ gives $\varphi_K=0.409$. The final results differ by $\sim 10\%$ from the theoretical values (see Table III). This is a very good result given the ambiguities that are present both in the numerical data (numerical error and extrapolation) and in the theory (the choice of a particular expression for the equation of state of the liquid that is not exact and the small cage expansion). Note that a similar extrapolation is not possible in $d<4$ due to crystallization and for $d>4$ due to lack of numerical data. Hopefully new data for $d>4$ will also allow for a similar comparison in this case.

In Figs. 14 and 15 we report the inverse reduced pressure as a function of the packing fraction for $d=3$ and $d=4$. We plot the numerical data of Skoge *et al.* (2006) reproduced in Fig. 1, and we choose two among the smallest compression rates available. We see that the numerical data are far from the ideal glass pressure and are better described by metastable glassy states corresponding to a complexity $\Sigma\sim 1$. Indeed, it is well known from numerical simulations of structural glass formers that the system falls out of equilibrium when $\Sigma\sim 1$. The overall agreement of the theoretical predictions with the data of Skoge *et al.* (2006) is very good.

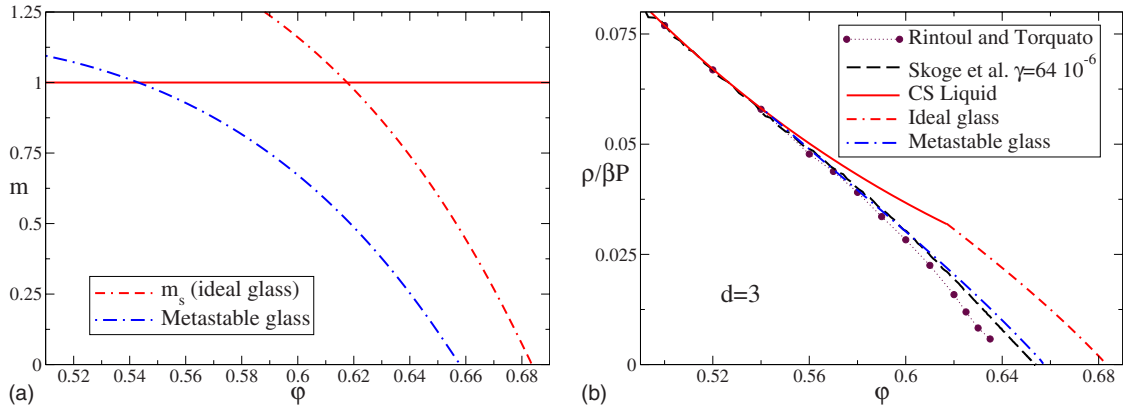

FIG. 14. (Color online) Equation of state in $d=3$ using the Carnahan-Starling equation of state to describe the liquid and in the small cage approximation (Sec. VII). (Left) (m,φ) phase diagram (compare with Fig. 6). The line $m_s(\varphi)$ (dot-dash-dashed line) separates the liquid and glass regions. The glass transition density is defined by $m_s(\varphi_K)=1$ and the glass close-packing density by $m_s(\varphi_{\mathrm{GCP}})=0$: we find $\varphi_K=0.62$ and $\varphi_{\mathrm{GCP}}=0.68$. The dot-dashed line refers here to a metastable glassy state defined by $\Sigma(m,\varphi)=\Sigma_j$ (here we chose $\Sigma_j=1.2$) with jamming density $\varphi_j=0.659$. (Right) Inverse reduced pressure as a function of density. Full line is the CS equation of state; dot-dash-dashed line is the ideal glass; dot-dashed line is the same metastable glass of left panel. Data from Rintoul and Torquato (1996) (full circles) and more recent ones from Skoge *et al.* (2006) (dashed black line, same data as in Fig. 1, left, for $\gamma=64\times10^{-6}$) are shown for comparison.

Finally, in Fig. 16 we show the equilibrium complexity $\Sigma_{\mathrm{eq}}(\varphi)=\Sigma(1,\varphi)$ as a function of φ. Numerical data from Speedy (1998) and Angelani and Foffi (2007) are available, and the agreement is again very good.

C. Scaling close to jamming

In this section we derive asymptotic relations for the behavior of the glassy states at $\varphi\to\varphi_j$. This is interesting because close to φ_j the correlation function shows interesting features that have been studied in detail numerically (see Sec. II.D).

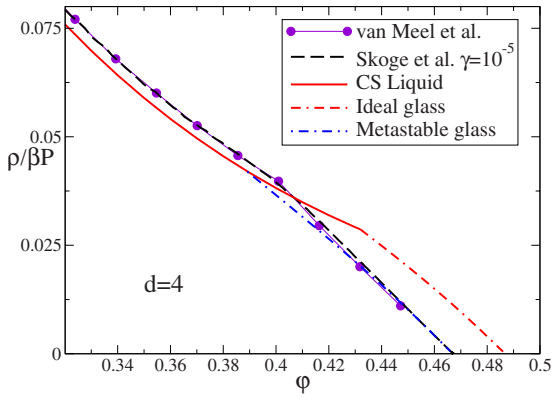

FIG. 15. (Color online) Inverse reduced pressure as a function of density in $d=4$ using the Carnahan-Starling equation of state (full line) to describe the liquid and in the small cage approximation (Sec. VII). Data from Skoge *et al.* (2006) (black dashed line, same data as in Fig. 1, right, for $\gamma=10^{-6}$) and from van Meel *et al.* (2009) are reported for comparison. The reported metastable glass (dot-dashed line) corresponds to $\Sigma_j=1.44$ and has a jamming density $\varphi_j=0.467$. In this case the Carnahan-Starling equation is less accurate; nevertheless, the overall quantitative agreement is still good. The ideal glass branch is reported as a dot-dash-dashed line.

1. Scaling of the pressure

First we compute the scaling of the pressure close to φ_j. It is convenient to recall the procedure already discussed in Sec. III.A.3. To each group of glassy states of jamming density φ_j we can associate a complexity Σ_j given by Eq. (77). Then one has to solve Eq. (9) to obtain $m(\varphi,\Sigma_j)$ or equivalently $m(\varphi,\varphi_j)$. The function $m(\varphi,\varphi_j)$ represents a group of glassy states in the (m,φ) plane of Fig. 6, left panel. Once substituted into Eq. (75), it gives the entropy of the states[32] labeled by φ_j as a function of φ.

We are interested in the equation of state of these states close to $m=0$ or $\varphi=\varphi_j$. Then we need to compute $m(\varphi,\varphi_j)$ at first order in $\varphi_j-\varphi$. To this aim we have to linearize $\Sigma(m,\varphi)-\Sigma_j(\varphi_j)$ at first order in m and $\varphi_j-\varphi$; after some computation (see Appendix E) we get

$$\Sigma(m,\varphi)-\Sigma_j(\varphi_j)\sim-\left[S'(\varphi_j)+d\frac{Y'(\varphi_j)}{Y(\varphi_j)}+\frac{d}{\varphi_j}\right](\varphi_j-\varphi)-dm, \tag{83}$$

which gives, expressing $S'(\varphi)$ in terms of $Y(\varphi)$ by means of Eq. (76),

$$m(\varphi,\varphi_j)=\frac{1}{d}\left[2^{d-1}Y(\varphi_j)-d\frac{Y'(\varphi_j)}{Y(\varphi_j)}+\frac{1-d}{\varphi_j}\right](\varphi_j-\varphi)\equiv\mu(\varphi_j)(\varphi_j-\varphi). \tag{84}$$

The latter result must be substituted into $s^*(m,\varphi)$ to get the behavior close to φ_j. It is easy to see from Eqs. (75)

[32]We recall that the case $\Sigma_j=0$ corresponds to the ideal glass.

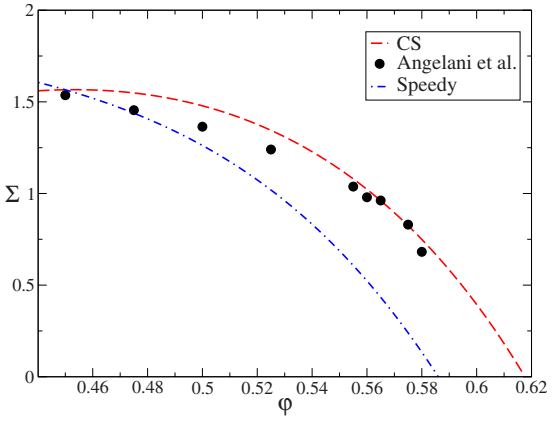

FIG. 16. (Color online) Equilibrium complexity $\Sigma_{eq}(\varphi)$ as a function of φ in $d=3$ using the Carnahan-Starling equation of state in the small cage expansion (Sec. VII). The prediction is compared with data from Speedy (1998) and Angelani and Foffi (2007).

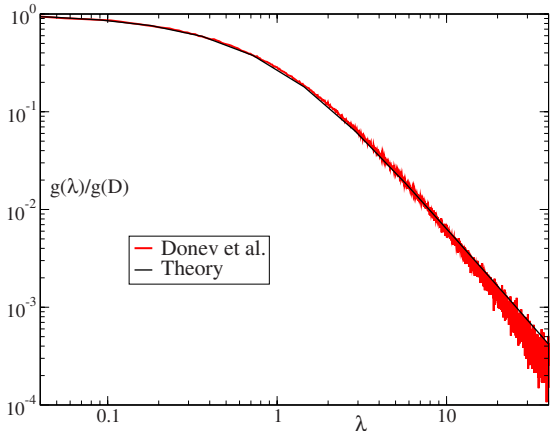

FIG. 17. (Color online) Scaling limit of the delta peak. Numerical data, reproduced from Donev *et al.* (2005a), refer to a packing $\varphi_j \sim 0.64$ and $\varphi_j - \varphi \sim 10^{-12}$. $g_G(r)/g_G(D)$ is plotted vs $\lambda = (r-D)p/D$. The full line is the theoretical prediction (90). Compare with Fig. 9 for a similar result obtained in the HNC approximation.

that for $m \to 0$, $s^*(m,\varphi) \sim d(1-m)\ln m$; therefore,

$$s(\varphi,\varphi_j) \sim d\,\ln(\varphi_j-\varphi) - d\mu(\varphi_j)(\varphi_j-\varphi)\ln(\varphi_j-\varphi) + \cdots \tag{85}$$

close to φ_j, and the (reduced) pressure diverges as

$$p(\varphi,\varphi_j) = -\varphi\frac{\partial s(\varphi,\varphi_j)}{\partial\varphi} \sim \frac{d\varphi_j}{\varphi_j-\varphi} - d\varphi_j\mu(\varphi_j)\ln(\varphi_j-\varphi) + \cdots. \tag{86}$$

It is important to remark that the corrections to the leading order are quite large (logarithmically divergent), as observed in numerical simulations (Skoge *et al.*, 2006).

2. Correlation function

The most interesting results on the scaling close to φ_j are obtained by investigating the pair-correlation function of the spheres in the glass state. At first order we obtained Eq. (70); the first term describes the delta peak, while the other terms do not contribute close to $r=D$. It would be interesting to evaluate them, but this seems a complicated task (see Appendix D for a complete list of these terms). Here we focus on the first term. We then study the asymptotic behavior of $Q(r)$ in the jamming limit. This is done in Appendix C.3, and the result is

$$g_G(r) = g(r)[1+Q(r)] = g(r)\left[1+\frac{1}{m}\Delta_m\left(\frac{r-D}{\sqrt{4mA}}\right)\right], \tag{87}$$

where $g(r)$ is the (extrapolated) correlation function of the liquid at the same density, and $m=m(\varphi,\varphi_j)$, $A=A^*(m(\varphi,\varphi_j))$; the function $\Delta_m(t)$ is defined in Eq. (C38) and shown in Fig. 25.

The function $\Delta_m(t)$ gives the leading contribution to $g_G(r)$ close to contact, which comes from neighboring particles that are in contact with the reference particle exactly at φ_j. This contribution is nonvanishing only for $r-D \lesssim \sqrt{A} \sim \sqrt{\varphi_j-\varphi}$ and becomes a delta peak at φ_j. Other corrections are encoded in the remaining terms in Eq. (70) or are missed by the first-order small cage expansion. A first consequence of this fact is that the integral of $g_G(r)-1$ does not vanish at $\varphi=\varphi_j$ as it should, being proportional to the compressibility. A second consequence of our approximations is that Eq. (76) is not satisfied: this is because from Eq. (87), for $\varphi \to \varphi_j$

$$g_G(D) = Y(\varphi_j)[1+Q(D)] \sim \frac{Y(\varphi_j)}{m} = \frac{Y(\varphi_j)}{\mu(\varphi_j)(\varphi_j-\varphi)} \tag{88}$$

and therefore

$$1 + 2^{d-1}\varphi g_G(D) \sim \frac{2^{d-1}\varphi_j Y(\varphi_j)}{\mu(\varphi_j)(\varphi_j-\varphi)} \neq \frac{d\varphi_j}{\varphi_j-\varphi} = p(\varphi,\varphi_j). \tag{89}$$

This is not a surprise since Eq. (76) is violated in most of the approximate theories for the liquid phase (Hansen and McDonald, 1986). Note, however, that the difference is not so large because the first term in $\mu(\varphi_j)$, given by Eq. (84), dominates as $Y(\varphi)$ is quite large (~ 20) in the density range of interest.

Using again $m(\varphi,\varphi_j)=\mu(\varphi_j)(\varphi_j-\varphi)$ and the expression of $A^*(m)$ we get from Eq. (87) close to φ_j

$$\begin{aligned}\frac{g_G(r)}{g_G(D)} &\sim \Delta_0\left(\frac{(r-D)\sqrt{\pi}2^d\varphi_j Y(\varphi_j)}{D\mu(\varphi_j)(\varphi_j-\varphi)}\right)\\ &= \Delta_0\left(\frac{\sqrt{\pi}}{2}\frac{r-D}{D}[1+2^{d-1}\varphi g_G(D)]\right)\\ &= \Delta_0\left(\frac{\sqrt{\pi}}{2}\lambda\right),\end{aligned} \tag{90}$$

having defined the variable $\lambda=(r-D)[1+2^{d-1}\varphi g_G(D)]/D \sim (r-D)p/D$ [the last equality holds

only if Eq. (76) holds]. Note that the same scaling of the delta peak was already predicted in the HNC approximation (see Fig. 9); thus it is a robust feature that emerges from the replica method independently of the approximations.

This scaling form of the delta peak of $g_G(r)$ close to jamming has been observed numerically by Donev *et al.* (2005a). In Fig. 17 we show numerical data from Donev *et al.* (2005a) on the delta-peak contribution for a packing in $d=3$ with $\varphi_j \sim 0.64$ and $\varphi_j - \varphi \sim 10^{-12}$. We see that our result, given by Eq. (90) for $\varphi_j=0.64$, is in excellent agreement with the numerical data.

In summary, from Eq. (87) and Appendix C.3, we get the following scaling for the delta peak of $g_G(r)$

$$g_G(r) \sim \begin{cases} \dfrac{1}{\varphi_j - \varphi}, & r - D \sim \varphi_j - \varphi, & \lambda \sim 1 \\ \dfrac{1}{(\varphi_j - \varphi)\lambda^2} \sim \dfrac{\varphi_j - \varphi}{(r-D)^2}, & \varphi_j - \varphi < r - D \sim \sqrt{\varphi_j - \varphi}, & \lambda \sim 1/\sqrt{\varphi_j - \varphi} \\ \exp[-(r-D)^2/(\varphi_j - \varphi)], & r - D \gg \sqrt{\varphi_j - \varphi}, & \lambda \gg 1/\sqrt{\varphi_j - \varphi}, \end{cases} \tag{91}$$

where the last line comes from the cutoff on the function $\Delta_m(t)$ at finite m (see Appendix C.3).

In numerical simulations a $(r-D)^{-\alpha}$ divergence of $g_G(r)$ close to D is observed, with $\alpha \sim 0.5$. This leads to a difference with respect to Eq. (91), with the $(r-D)^{-2}$ regime extending only up to $r-D \sim (\varphi_j - \varphi)^{2/3}$. This feature is not present in our calculation; this discrepancy deserves further investigation.

3. Number of contacts

The interpretation of Eq. (91) is that for $\varphi \to \varphi_j$ there is a shell of width $\varphi_j - \varphi$ around a given particle where the probability of finding other particles is very high. These particles become *neighbors* of the particle in the origin at $\varphi = \varphi_j$, and their number is finite as the integral of $g_G(r)$ on this shell is finite.

There is, however, a second shell $\varphi_j - \varphi \leqslant r - D \leqslant \sqrt{\varphi_j - \varphi}$ where the probability of finding particles is very high. The integral of $g_G(r)$ over this shell is of 1 so also in this shell there is a finite number of particles that will become neighbors of the particle in the origin.

The integral of $g_G(r)$ on a shell $D \leqslant r \leqslant D + O(\sqrt{\varphi_j - \varphi})$ then gives the number of contacts for $\varphi \to \varphi_j$,

$$z = \Omega_d \rho D^{d-1} g(D) \int_D^{D+O(\sqrt{A})} dr[1 + Q(r)]. \tag{92}$$

Recall that in the expression above, as everywhere in the paper, $g(D) = Y(\varphi)$ is the contact value of the liquid correlation, which is finite; this should not be confused with $g_G(D)$ which diverges at jamming. For $\varphi_j - \varphi$ finite but small this number can be interpreted as the number of particles that collide with the particle in the origin during a finite but long time τ (Brito and Wyart, 2006).

Remarkably, the integral of the second term in Eq. (92) can be computed exactly using Eq. (C39); since the function $\Delta_m(t)$ contains an exponential cutoff at $r-D \sim \sqrt{A}$ (see Fig. 25), the upper integration limit can be extended up to ∞ and we obtain

$$\Omega_d \rho D^{d-1} g(D) \int_D^{\infty} dr Q(r) = 2d(1-m), \tag{93}$$

i.e., $z = 2d$ for $\varphi = \varphi_j$. Close to φ_j there is a correction $\delta z \propto m \sim \varphi_j - \varphi$ coming from the equation above plus a second correction $\delta z \propto \sqrt{\varphi_j - \varphi}$ coming from the integral of 1 in Eq. (92). The second correction dominates, then we have

$$z = 2d + O(\sqrt{\varphi_j - \varphi}) \tag{94}$$

as found by Brito and Wyart (2006). We can try to give a quantitative estimate of the coefficient by observing that the function $\Delta_m(t)$ starts to drop exponentially at $t = \sqrt{m}$ and drops to 0 for $t = \tau\sqrt{m}$ with τ close to 2. Clearly the upper limit of integration τ plays the role of a fitting parameter, however, the value $\tau = 2$ is reasonable from Fig. 25, given also the uncertainty involved in the numerical estimate. Thus we assume that the integral is done up to $r = D + 2\sqrt{A}$ and we have

$$\begin{aligned} z &= 2d + \Omega_d \rho D^{d-1} g(D) 2\sqrt{A} \\ &= 2d + 2\Omega_d \rho D^{d-1} g(D) \frac{1-m}{Q_m} \frac{D}{\rho V_d(D) g(D)} \\ &= 2d + 2d\frac{1-m}{Q_m} \sim 2d + 2d\sqrt{\frac{4m}{\pi}} \\ &= 2d + 2d\sqrt{\frac{4\mu(\varphi_j)}{\pi}}\sqrt{\varphi_j - \varphi}. \end{aligned} \tag{95}$$

The result is compared with numerical data in Fig. 18. The value of $\mu(\varphi_j)$ is given in Eq. (84). Despite the good agreement, note that the square-root growth of δz was attributed by Brito and Wyart (2006) to the square-root singularity of $g_G(r)$, which is a different mechanism from the one discussed above.

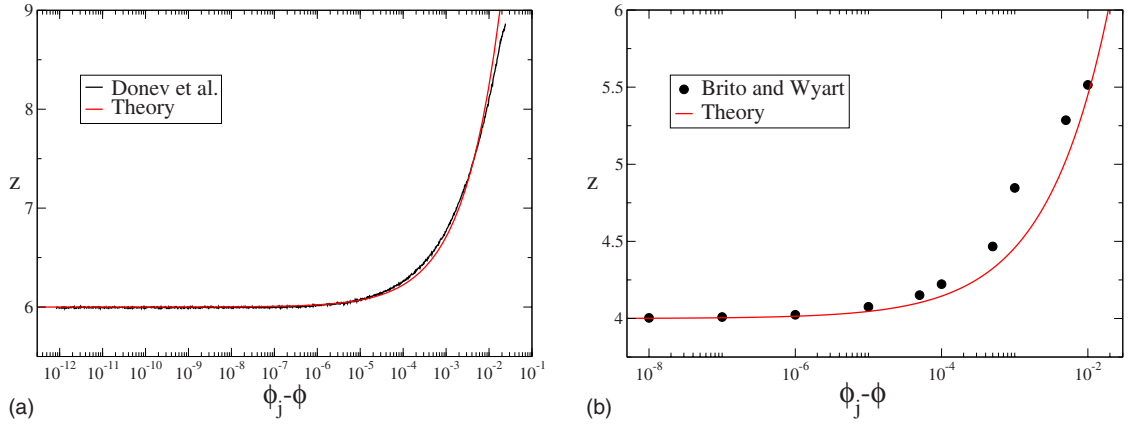

FIG. 18. (Color online) Number of contacts from Eq. (95). (Left) Data from Donev *et al.* (2005a) in $d=3$ and $\varphi_j \sim 0.64$. We have $z \sim 6+20\sqrt{\varphi_j-\varphi}$ for both curves. (Right) Data from Brito and Wyart (2006) in $d=2$ and $\varphi_j \sim 0.83$. The best fit gives $z=4+31\sqrt{\varphi_j-\varphi}$ while the theory gives $z=4+14.5\sqrt{\varphi_j-\varphi}$.

4. Force distribution

Donev *et al.* (2005a) investigated the force distribution of dense amorphous packings generated by using the Lubachevsky-Stillinger algorithm in $d=3$. The interparticle forces are defined in this way: one takes a packing of density φ_j, slightly reduces the density, and measures the average momentum exchanged by two neighboring particles over a large time t. Note that on very large times and if the volume is large enough the packing will be unstable and relax toward a more compact structure (either at φ_{GCP} or at φ_{fcc}) [see Fig. 5 of Donev *et al.* (2005a)]. However, before this happens there is enough time to measure the forces with sufficient accuracy.

The interparticle forces are then normalized such that $\langle f \rangle = 1$ and the distribution $P(f)$ is investigated. The theory of Donev *et al.* (2005a) relates this quantity to the shape of the delta peak close to contact (Fig. 17) by the relation

$$\frac{g_G(\lambda)}{g_G(D)} = \int_0^\infty df f P(f) e^{-\lambda f}, \tag{96}$$

where $\lambda = (r/D-1)p$ as in the previous sections. The previous equation expresses the fact that for small interparticle separation the gap $h \propto 1/f$, as discussed also by Brito and Wyart (2006). Equations (90) and (C40) give

$$\frac{g_G(\lambda)}{g_G(D)} = \Delta_0\left(\frac{\sqrt{\pi}}{2}\lambda\right) = 2\int_0^\infty dy\, y e^{-y^2-\sqrt{\pi}\lambda y} = \frac{2}{\pi}\int_0^\infty df f e^{-f^2/\pi-\lambda f} \tag{97}$$

and finally

$$P(f) = \frac{2}{\pi} e^{-f^2/\pi}. \tag{98}$$

In Fig. 19 we see that this form reproduces well the numerical data for large forces. The discrepancy at small forces can be explained by (i) the fact that the small f behavior of $P(f)$ is related to the large λ behavior of $g_G(\lambda)$, and as discussed above in the large λ region there are corrections to $g_G(\lambda)$ that we are missing; and (ii) a possible finite-size effect (indeed it seems that the data for larger samples are in better agreement with the theory).

We stress again that here we focused only on the results of Donev *et al.* (2005a) that refer to packings produced using slow compressions; these should be related to the infinite pressure glassy states that are the object of this paper. Interestingly, similar results for $P(f)$ have been obtained by Snoeijer, Vlugt, Ellenbroek, *et al.* (2004) and Snoeijer, Vlugt, van Hecke, *et al.* (2004) by using an ensemble approach for the force network based on Gaussian random matrices. O'Hern *et al.* (2002) found a Gaussian tail in $P(f)$ for packings close to the J point; moreover, it has been shown that finite-size fluctuations of the jamming density can introduce self-averaging problems when averaging over many configurations that in turn produce exponential tails in $P(f)$. Therefore some care should be taken when comparing

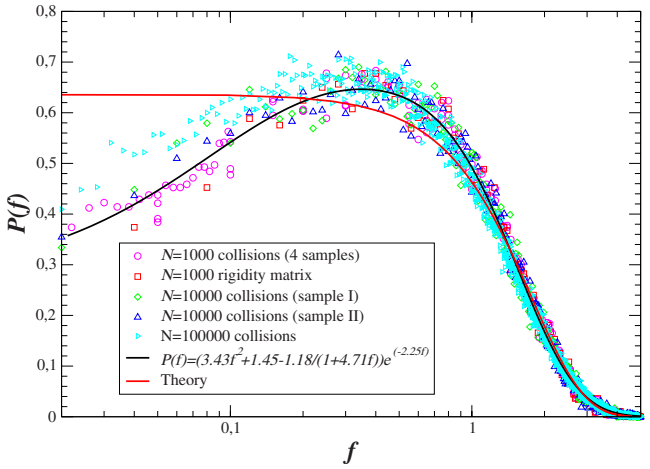

FIG. 19. (Color online) Probability distribution of the forces from Donev *et al.* (2005a). The full line corresponds to the Gaussian form (98). The black line is a fit performed by Donev *et al.* (2005a).

our prediction of a Gaussian shape of $P(f)$ with numerical data. Moreover, the force distribution has been studied in great detail for packings of frictional spheres produced using different protocols and seems to depend strongly on the protocol used. As discussed in the Introduction, covering the relevant literature here is impossible. In particular, friction strongly affects the force network and is expected to have a dramatic effect on $P(f)$.

VIII. BEYOND FIRST ORDER IN THE SMALL CAGE EXPANSION

In order to improve over the first-order expansion, one could try to perform a second-order (and third, etc.) expansion systematically. However, the convergence of this procedure is not clear, and, moreover, the calculation of higher-order corrections becomes increasingly difficult and is already difficult at second order. Following the tradition of theoretical physics, we then try to use resummation techniques for our expansion. Unfortunately, the results presented here are not satisfactory, but still we believe that they are interesting since they illustrate a possible direction one can follow to improve the theory. We believe that a more accurate treatment of the resummation we discuss could indeed lead to much better results.

The simple resummation we discuss in this section has the advantage of being fully analytically solvable but unfortunately gives inconsistent results for the thermodynamics of the ideal glass. The main idea is to fully exploit the resummation discussed in Sec. V, which has been particularly useful to solve the model in the limit $d\to\infty$. Note that the small cage expansion of Sec. VII does not give access to the pair-correlation function of glass, which is one of the most interesting quantities to compute (see Sec. II.D). The advantage of the resummation we discuss here is that it allows, by finding a good approximation to compute the properties of the effective liquid, a full computation of the correlation function of the glass.

A. Percus-Yevick approximation for the Baxter model

To resum a class of terms in the small cage expansion we start from Eq. (39), i.e., we neglect all $n\geqslant 3$-body potentials but try to treat the two-body one as exactly as possible. Then we have to compute the entropy of a liquid with a hard-core repulsion and a small tail given by $\phi_{\rm eff}(r)=-\ln[1+Q(r)]$. The tail is *attractive* for $m<1$ and repulsive for $m>1$ (see Fig. 11).

The advantage of this formulation is that the correlation function of the glass is simply

$$g_G(r)=-\frac{2}{\rho}\left.\frac{\delta S[\rho,\chi(r)e^{-\upsilon(r)}[1+Q(r)]]}{d\upsilon(r)}\right|_{\upsilon=0}=g_{\rm eff}(r), \tag{99}$$

where $g_{\rm eff}(r)$ is the pair correlation of the liquid with the effective potential $\phi_{\rm eff}$. Therefore $g_G(r)$, the correlation of the glass, turns out to be equal to the correlation function of the effective liquid and then automatically has many of the reasonable properties of a correlation function for hard particles (e.g., it is positive, it vanishes inside the hard core, the structure factor is positive, etc.). We can use different approximation schemes [Percus-Yevick (PY), HNC, etc.] to compute the free energy and correlation function of the effective liquid.

To further simplify the problem, we observe that in the limit $m\to 0$ the cage radius vanishes and the strength of the attractive part of the potential diverges. Then we can approximate $Q(r)$ with a delta function as in Eq. (45) and the effective liquid becomes a Baxter model. Note that the approximation (45) strictly holds only for $m\to 0$, where $A\to 0$. However, it might be reasonable for any $m<1$, as in this case the interaction is attractive and its range is anyway much smaller than the hard-core diameter. We run into problems, however, for $m>1$, as in this case the interaction is repulsive and cannot be described by Eq. (45). Therefore in the following discussion we always assume that $m<1$.[33]

Following the notation of Baxter (1968) we have

$$e^{-\phi_{\rm eff}(r)}=\chi(r)[1+Q(r)]\to\chi(r)\left[1+\frac{4\pi D}{12\tau}\delta(r-D)\right]. \tag{100}$$

Comparing this with Eq. (C4), we see that in $d=3$ the effective liquid is finally reduced to a Baxter model at the same density φ and of interaction strength $\tau=1/4G_m(A)$.

1. Free energy and the equation for A

Remarkably, the Percus-Yevick approximation for the Baxter model has been solved exactly in $d=3$ (Baxter, 1968): an analytical expression for the free energy has been given in Eqs. (2.5) and (2.7) of Tejero and Baus (1993), while the correlation function can be computed using the method of Wertheim (1963).

The function $\tau(m,A)$ can be computed in $d=3$ by numerical integration of Eqs. (C4) and (C17). Then we get an analytical (although complicated) expression for $\mathcal{S}(m,\varphi;A)$,

$$\mathcal{S}(m,\varphi;A)=S_{\rm harm}(m,A)+1-\ln\frac{6\varphi}{\pi}-\psi\left[\varphi,\frac{1}{4G_m(A)}\right], \tag{101}$$

where $\psi[\varphi,\tau]$ is given in Eq. (2.7) of Tejero and Baus (1993). The equation for A reads, using the definition of Appendix C.1,

[33] For $m>1$ the strength of the interaction is always finite (and much smaller than for $m<1$). In this case it seems reasonable to use the first-order approximation derived previously.

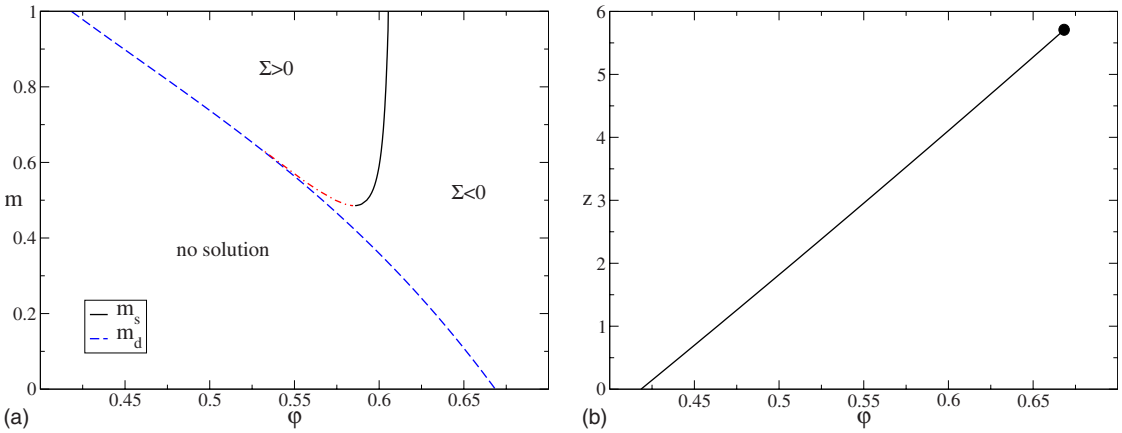

FIG. 20. (Color online) The Baxter resummation. (Left) Phase diagram of the Baxter resummation (Sec. VIII). The dashed line is the boundary of the region where a solution for A is found. The full and dot-dashed lines are the boundary of the region where the complexity is positive. (Right) Number of contacts z as a function of density along the line $m_d(\varphi)$. The black dot corresponds to $m_d(\varphi)=0$. z increases almost linearly from 0 (liquid state) to $z\sim 6$, the value expected for an amorphous jammed phase. Note, however, that the upper part of the line corresponds to negative complexity.

$$1 = -\frac{8}{3}\frac{d\psi}{d\tau^{-1}}\left[\varphi, \frac{1}{4G_m(A)}\right] F_m(A), \tag{102}$$

and it has to be solved numerically for generic m, φ.

However, some simplifications are possible. First, for $m\to 1$ we have $G_m(A)\to 0$ and $\tau\to\infty$. It is possible to show that

$$S_{\mathrm{PY}}(\varphi) = 1 - \ln\frac{6\varphi}{\pi} - \lim_{\tau\to\infty}\psi[\varphi,\tau],$$
$$\lim_{\tau\to\infty}\frac{\partial\psi[\varphi,\tau]}{\partial\tau^{-1}} = -\varphi Y_{\mathrm{PY}}(\varphi). \tag{103}$$

Therefore the equation for A becomes

$$1 = \tfrac{8}{3}\varphi Y_{\mathrm{PY}}(\varphi) F_1(A). \tag{104}$$

In the jamming limit $m\to 0$, $A=\alpha m$, $G_m(A)\to G_0(\alpha)$ that can be computed easily [see Eq. (C34)]. Using Eq. (C35) the equation for α is

$$1 = -\frac{8}{3}\frac{d\psi}{d\tau^{-1}}\left[\varphi, \frac{1}{4G_0(\alpha)}\right] F_0(\alpha). \tag{105}$$

The expression for the complexity can be simplified similarly.

2. Results

Unfortunately, the results of the Baxter resummation are poor in $d=3$. The main problem is that the static value of m, $m_s(\varphi)$ is not a decreasing function of φ. This is inconsistent since it would imply that the ideal glass state has smaller density than the liquid state at $\varphi=\varphi_K$. On the contrary, the behavior of the line $m_d(\varphi)$ is reasonable even if the value of the transition at $m=1$, $\varphi_d=0.418$, is exceedingly smaller than the conjectured one, $\varphi_d\sim 0.58$. For these reasons the phase diagram in this approximation seems unreliable (Fig. 20).

More interesting is the result for the pair-correlation function. Indeed, the pair-correlation function of the Baxter liquid shows many characteristic features which are observed in jammed packings of hard spheres, as discussed by Miller and Frenkel (2004b). The most interesting among them are the peak at $r/D=\sqrt{3}$ and the jump in $r/D=2$ which have been observed by Donev *et al.* (2005a) for random jammed packings of monodisperse spheres. Unfortunately, the values of τ that come from the analysis above seem to be too high for these features to be present in the $g_G(r)$ with the correct order of magnitude so that a quantitative comparison with numerical simulations seems to be impossible at this stage.

Note also that the $g(r)$ of the Baxter liquid is characterized by a delta peak at contact (due to the adhesive potential). From the amplitude of the latter peak, which is analytically known in the Percus-Yevick solution (Baxter, 1968), we can compute a number of neighbors as a function of density. The result is similar to what is expected: the number of neighbors increases from 0 to $z\sim 6=2d$, i.e., an isostatic packing (Fig. 20). However, the upper part of the curve corresponds to negative complexity so that the corresponding packings do not exist.

B. Discussion

This particular simple resummation scheme seems unable to correctly describe the glassy states of hard spheres. However, the idea of resumming all terms corresponding to the two-body interaction seems promising as the resulting $g_G(r)$ shows some features that are observed in real packings and the behavior of the delta peak (number of contacts) is correct.

It is possible that three- (and more) body interactions play a major role, however, it would be worth trying to keep only the simplest two-body interactions and use more refined equations for the effective liquid. For instance, the delta-function approximation for $Q(r)$ might

be too rough as $\sqrt{A}\sim 0.01$ and on this scale the $g(r)$ of hard spheres has strong variations at least close to contact. One could then try to solve numerically the Percus-Yevick approximation for the exact potential ϕ_{eff}. Alternatively, a more precise equation of state [such as the one proposed by Miller and Frenkel (2004a)] could be used for the Baxter model.

One might be worried because of the fact that in the limit $m\to 0$ we do not recover the small cage expansion results (e.g., the complexity was positive for $\varphi<0.68$ at first order in $\sqrt{A}$ while here we always found a negative Σ). The reason is that for $m\to 0$, the small cage parameter is $\alpha=A/m$ and not A. Therefore, even if $A\to 0$ in this limit, the small cage expansion is not recovered because α remains relatively big.

IX. BINARY MIXTURES

In this section we report the recent extension of the theory to binary mixtures that was obtained by Biazzo *et al.* (2009). The extension to binary system is important since in these systems crystallization can be easily avoided; this allowed us to study their glass transition in detail [see, e.g., Santen and Krauth (2000), Foffi *et al.* (2003, 2004), Götze and Voigtmann (2003), and Donev *et al.* (2006) and, in particular, the recent works (Berthier and Witten, 2009a, 2009b; Hermes and Dijkstra, 2010)]. Jamming of binary mixtures has also been investigated [see, e.g., Dodds (1975, 1980), Ouchiyama and Tanaka (1981), and O'Hern *et al.* (2002)]. These investigations allow us to test the prediction of the theory concerning the variation with composition of packing density, structure, etc. Details of the computation of the function $\mathcal{S}(m,\varphi)$ for a general multicomponent mixture, following Coluzzi *et al.* (1999), can be found from Biazzo *et al.* (2009) in the framework of the first-order small cage approximation. Here we report only the results for a binary mixture of two types of three-dimensional spheres $\mu=A,B$ in a volume V, with different diameter D_μ and density $\rho_\mu=N_\mu/V$. We define $r=D_A/D_B>1$ the diameter ratio, $x=N_A/N_B$ the concentration ratio, $\varphi=\rho_A V_3(D_A)+\rho_B V_3(D_B)$ the packing fraction, and $\eta=\rho_B V_3(D_B)/\varphi=1/(1+xr^3)$ the volume fraction of the small (B) component.

As in the monodisperse case, once an equation of state for the liquid has been chosen, one can obtain for a given Σ_j the equation of state of the corresponding metastable glass, as well as its jamming density φ_j. The equation of state used by Biazzo *et al.* (2009) is a generalization of the Carnahan-Starling equation. The theoretical results were compared with numerical results obtained from the Lubachevsky-Stillinger algorithm discussed in Sec. II.A. In Fig. 21 the evolution of the inverse reduced pressure during compression is shown for a mixture with $x=1$ and $r=1.4$, which has been recently studied (O'Hern *et al.*, 2002; Berthier and Witten, 2009a, 2009b). Overall, one observes the same behavior already discussed in the monodisperse case. The curve (numerical 1) corresponds to a relatively fast compression ($\gamma=10^{-2}$). The curve (numerical 2) has been obtained starting the compression (at the same compression rate) from a carefully equilibrated liquid configuration of the same mixture at $\varphi=0.58$ [see Berthier and Witten (2009b) for details on how this configuration was produced and equilibration was checked]. In the latter case, since the relaxation time of the liquid at that density is already long compared to the compression rate, the system falls immediately out of equilibrium and the pressure increases fast until jamming occurs at a higher density compared to the previous case. The numerical equation of state is compared with that of glassy states corresponding to $\Sigma_j=0.5$, 1.2, 1.5. Starting the compression from a high-density-liquid equilibrium configuration produces a glassy state with lower Σ_j. This is confirmation of a prediction of the theory, that different glassy states jam at different densities. Finally, we report, for the same system, the numerically extrapolated value of the reduced pressure $p=\beta P/\rho$ at the ideal glass transition, $p_K=34.4$, obtained by Berthier and Witten (2009b). Again, this corresponds well (within 10%) to the computed value $p_K=31.8$ from the theory (see Fig. 21).

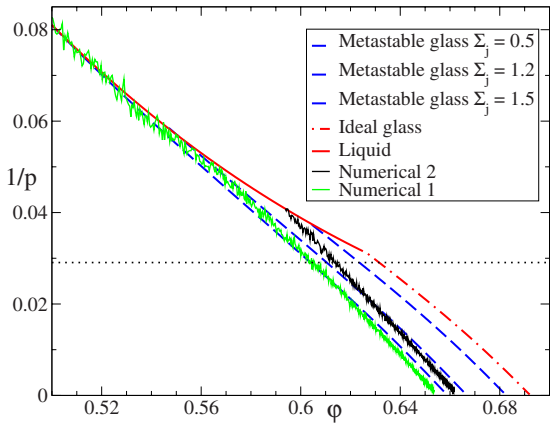

FIG. 21. (Color online) Inverse reduced pressure $\rho/\beta P$ as a function of the packing fraction φ for a mixture with $r=1.4$ and $x=1$. Numerical data are obtained using two different protocols. In the first, compression is started at low density. In the second, compression is started from an equilibrated configuration at $\varphi=0.58$. The equations of state of different metastable glasses, corresponding to different Σ_j, are reported as dashed lines. The dot-dashed line is the pressure of the ideal glass, corresponding to $\Sigma_j=0$. A numerical estimate (Berthier and Witten, 2009b) of the Kauzmann pressure, $p_K=34.4$, is reported as a dotted horizontal line.

In Fig. 22, the jamming density φ_j is shown for different mixtures, putting together numerical results (Biazzo *et al.*, 2009), experimental data (Yerazunis *et al.*, 1965), and the theoretical results. The latter have been obtained by fixing $\Sigma_j=1.7$ for all mixtures, which gives the best agreement. Note that a single "fitting" parameter Σ_j, which is strongly constrained, allows us to describe different sets of independent numerical and experimental data. The prediction of the theory is qualitatively similar to previous ones (Dodds, 1980; Ouchiyama and Tanaka, 1981), but the quantitative agreement is much

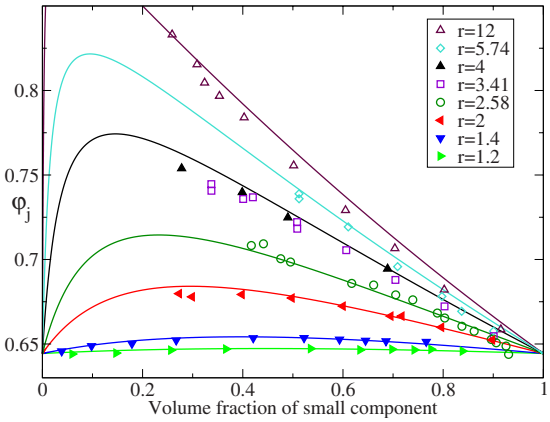

FIG. 22. (Color online) Packing fraction φ_j as a function of $\eta = 1/(1+xr^3)$ at fixed r. Full symbols are numerical data from Biazzo *et al.* (2009). Open symbols are experimental results from Yerazunis *et al.* (1965). Lines are predictions from theory obtained fixing $\Sigma_j = 1.7$. Note that the large r-small η region cannot be explored since for asymmetric mixtures the large spheres form a rigid structure while small spheres are able to move through the pores and are not jammed (Dodds, 1980; Ouchiyama and Tanaka, 1981).

better. Interestingly, a similar qualitative behavior for φ_{MCT} has been predicted by mode-coupling theory (Foffi *et al.*, 2003; Götze and Voigtmann, 2003); although there is no *a priori* reason why the variation with mixture composition of φ_{MCT} and φ_j should be related, it is reasonable to expect that they show similar trends (Foffi *et al.*, 2003).

The average coordination numbers at φ_j are denoted $z_{\mu\nu}(\varphi_j)$, and it was checked by Biazzo *et al.* (2009) that their variations with φ_j are negligible. They are shown in Fig. 23 for different mixtures. The numerical values have been obtained by Biazzo *et al.* (2009) by removing the rattlers from the packing. Experimental data from Pinson *et al.* (1998) are also shown on the right panel of Fig. 23. As discussed, the total coordination is close to the isostatic value $z=6$, which is the value predicted by the theory also for binary mixtures (Biazzo *et al.*, 2009). As can be seen in Fig. 23, the computed values agree well with the outcome of the numerical simulation, at least for r not too large, while some discrepancies are observed in the contacts of the large particles for large r.

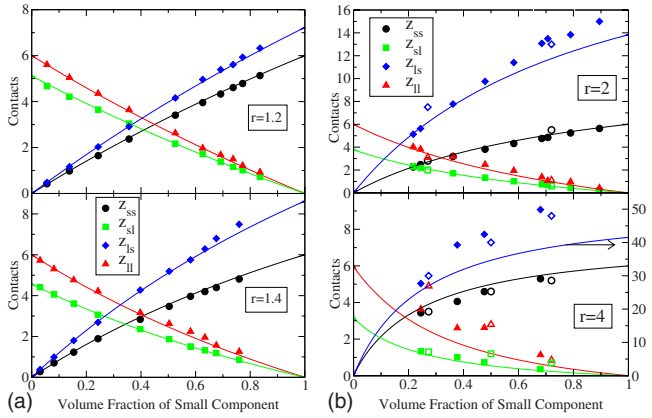

FIG. 23. (Color online) Partial average coordination numbers (small-small, small-large, large-small, and large-large) as a function of volume fraction of the small particles $\eta = 1/(1+xr^3)$ for different values of r. Full symbols are numerical data from Biazzo *et al.* (2009). Open symbols are experimental data from Pinson *et al.* (1998). Note that in the lower right panel a different scale is used for z_{ls}.

X. CONCLUSIONS

This paper is based on the main assumption that amorphous jammed packings of hard spheres can be identified with the infinite pressure limit of glassy states. In addition we assumed that the mean-field scenario for the glass transition holds also in finite dimension, at least on the time and length scales that are currently investigated in numerical simulations (and sometimes also in experiment on colloids and granular systems when the number of particles is not so large) (Bouchaud and Biroli, 2004).

The mean-field picture leads to a nontrivial structure of the phase diagram, whose main consequence is the existence of amorphous jammed packings in a range of densities $[\varphi_{\mathrm{th}}, \varphi_{\mathrm{GCP}}]$. The random close packing density can be any density within this interval and its precise value depends on the details of the protocol used to construct the packings (Krzakala and Kurchan, 2007).

Based on these assumptions we used the replica method to compute the properties of these glassy states. Before concluding we summarize our results and discuss some possible future developments, including how the picture is modified in finite-dimensional systems.

A. Summary of our results

We used different approximation schemes for the replicated liquid. The HNC approximation seems to work well in the moderately dense phase close to φ_d and φ_K at $m=1$. On the contrary, the small cage approximation works better in the regime where cages are small, namely, for $m \sim 0$ close to the ideal glass line and in large dimension. In dimension $d=3$ the mapping of the replicated liquid onto the Baxter adhesive hard sphere model seems a promising way to obtain a satisfactory description in the phase diagram but for the moment gives poor quantitative results.

We list here the main results discussed in this paper; many of them have been compared with numerical results in the figures.

- We presented a consistent description of the glass transition for hard spheres in $d \to \infty$: in particular we give predictions for the clustering [Eqs. (54) and (56)] and Kauzmann [Eq. (59)] densities. We are able to compute the correlation function [Eq. (60)] and the number of contacts [Eq. (62)], which we find equal to $2d$ at least close to φ_{GCP}.
- We computed the Kauzmann and glass close-packing

densities in any finite dimension in the small cage expansion (see Table III and Fig. 13).

- In $d=3$ we obtain an expression [Eq. (97)] for the scaling of the contact peak of $g(r)$ close to jamming. This expression describes well the numerical results (see Fig. 17). From this expression it follows that the distribution of contact forces is Gaussian [see Eq. (98) and Fig. 19] and that the number of neighbors is $z=2d$ at jamming (i.e., packings are isostatic) [see Eq. (95) and Fig. 18]. The form of the scaling function seems particularly robust as it is found both in the small cage expansion and in the HNC approximation.
- We are able to reproduce the equation of state of the glass for slow compression rates (see Figs. 14 and 15) and the equilibrium complexity of the liquid (see Fig. 16).
- In the HNC approximation we have indications for the development in $g(r)$ of a jump in $r=2D$ and of long-range correlations; these features cannot be studied within the small cage approximation but should also be present in the Baxter resummation.
- For binary mixtures, we showed that the theory correctly predicts the variation with mixture composition of the jamming density and the partial coordinations.

Recently strong evidence has been reported for a divergence of the equilibrium relaxation time of a hard sphere liquid at a density φ_0 at which the pressure of the liquid stays finite (Berthier and Witten, 2009a, 2009b; Brambilla *et al.*, 2009). This seems consistent with the existence of a Kauzmann transition at $\varphi_0=\varphi_K$ of the kind discussed in this paper even if a computation of the complexity for this system is still missing. These results seem to exclude the possibility that the equilibrium relaxation time diverges only at random close packing as proposed by some.

B. Discussion and perspectives

There are still many important points that deserve investigation. A tentative list is the following:

- Our theory is based on an equilibrium computation (where we also include metastable long-lived states). Hence, a key role is played by entropy. We stress that in the context of metastable glassy states there are two important concepts related to entropy: the first one is the complexity, which counts the number of such states; the second is the *surface tension* between different amorphous states, which must also be of entropic nature since we are dealing with hard spheres. The existence of a surface tension (a free-energy cost) to match different glassy states is necessary for those states to be well defined [see Appendix A and Xia and Wolynes (2001a), Bouchaud and Biroli (2004), and Cavagna (2009) for complete discussion]. While the complexity can be computed, at least approximately, within the theory presented here, a first-principles method to compute the surface tension is still missing despite preliminary attempts in simplified models (Franz, 2005). However, the study of the latter has recently become the subject of intense numerical effort (Biroli *et al.*, 2008; Cammarota *et al.*, 2009), which will hopefully lead to a more complete understanding of the properties of glassy states.
- Clearly, a major open problem is whether a thermodynamic glass transition really exists in finite-dimensional systems. Our mean-field theory has not much to say on this problem. It might seem that in our theory the existence of a Kauzmann transition is a major assumption. This is indeed not true: going carefully over the discussion, it will become clear that what really matters is the existence of long-lived metastable glassy states. The glass transition might be avoided in finite dimension because of some still unknown mechanism. The existence of metastable glassy states seems well established and mean-field theory provides a precise description of their properties.
- As discussed in Appendix A, in finite dimension, in the limit of infinite volume and if one waits an infinite time, only the ideal glass state (if any) remains stable at finite (but arbitrarily large) pressure; therefore in a finite-dimensional system stable amorphous packings exist strictly only at φ_{GCP}. Here we say that a packing is stable if the system remains close to it for an infinite time when the pressure is made finite by slightly decompressing the particles. It might be useful to elucidate the relation of this notion of stability with the jamming categories of Torquato *et al.* (2000) and Donev *et al.* (2007). On the other hand, the time scale needed to observe the instability should diverge exponentially in the distance from φ_{GCP}, with an associated diverging length scale (Bouchaud and Biroli, 2004); therefore for all practical purposes we expect the mean-field picture to hold in finite systems. A systematic investigation of the stability of packings as a function of system size would be very important in this respect.
- The existence of a further phase transition has recently been recognized in the context of mean-field models defined on random graphs, including for instance the hard sphere model of Biroli and Mézard (2001). It has been called *freezing* or *rigidity* transition and is characterized by the appearance of a finite fraction of frozen particles in the system (Zdeborová and Krzakala, 2007; Semerjian, 2008). In other words, at densities below the freezing transition, even if the structure is frozen, particles can still diffuse out of their cages, while above the freezing transition a finite fraction of them is really stuck inside his cage and can only vibrate; the diffusion coefficient is strictly zero for these particles. This transition is peculiar to mean-field models: indeed, it has been shown (Osada, 1998) that for finite-dimensional

hard spheres the diffusion constant of a tagged particle is always strictly positive at finite pressure. Even if this transition is avoided in finite-dimensional system, it might play some role for finite volumes and finite times. Its role in the context of jamming should be clarified.

- An important result that attracted much attention in the last years is the presence of an anomalous bunch of soft modes in jammed packings at φ_J (O'Hern *et al.*, 2003; Silbert *et al.*, 2005; Wyart, Nagel, and Witten, 2005; Majmudar *et al.*, 2007). These modes are related to isostaticity; they are associated to a diverging length scale and have been related to the boson peak observed in glasses at low temperature. It would be interesting to find out the origin of these soft modes within the approach presented here.
- Another subject of discussion in the community is the role of rattlers (particles that are not blocked by their neighbors) in jammed packings. In our theory the presence of rattlers is ignored due to the simple form we chose for the single-molecule density [Eq. (34)]. A more refined ansatz for this quantity could allow us to compute the fraction of rattlers, and it would be interesting to compare this with numerical simulations. Also, in the presence of rattlers the internal entropy of the glass should remain finite at jamming (even if its derivative, the pressure, should diverge). It would be important to check this explicitly.
- An important role might be played by three- and many-body interactions in the effective replicated liquid, at least in finite dimension. In this paper we ignored these interactions. The inclusion of the three-body interaction will allow us to compute the second order in the small cage expansion and might cure the unsatisfactory behavior of the Baxter resummation. We believe that this is the most important technical point to be studied in the future.
- The result for the number of neighbors in $d\to\infty$ is strange and should be reconsidered with more care. In particular, one should check whether the 1RSB solution is stable and look more carefully to subleading corrections, also coming from many-body interactions.
- Our result for the clustering transition for $d\to\infty$, $\varphi_d \sim d/2^d$, suggests that a dynamical glass transition happens around this density. It would be interesting to study the mode-coupling equations in the limit $d\to\infty$ to investigate this possibility.
- The Baxter resummation can be improved in different ways as discussed in the last section. In particular, there are some features of the $g(r)$ such as the square-root singularity and the peak in $r=\sqrt{3}D$, that we are not able to reproduce at present and might be captured by a more careful resummation.
- An extension to nonspherical particles such as ellipsoids should be possible and interesting since these systems show a nontrivial behavior of packing density with aspect ratio (Donev *et al.*, 2004).
- Potentials made by a hard-core part plus a short-range attractive potential can be investigated: at the mode-coupling level these potentials show an interesting phase diagram characterized by a reentrant glass transition and a glass-glass transition line (characterized by higher-order mode-coupling singularities). These results have been partially reproduced by a static HNC computation by Velenich *et al.* (2006), still with no evidence of a glass-glass transition. It would be interesting to see if better approximation schemes (such as the small cage approximation) could also describe the glass-glass transition.
- Soft repulsive potentials such as those used by O'Hern *et al.* (2002, 2003) and Berthier and Witten (2009a, 2009b) could be studied with this method, but this will require matching between the small cage expansion for hard spheres discussed here with the harmonic expansion of Mézard and Parisi (1999a). This might be technically difficult.

We hope that future work will address at least some of these issues.

ACKNOWLEDGMENTS

We wish to thank, in particular, Donev *et al.* (2005a), Brito and Wyart (2006), Skoge *et al.* (2006), Angelani and Foffi (2007), Schreck and O'Hern (2008), Berthier and Witten (2009b), and van Meel *et al.* (2009) for sending us their numerical data, giving permission to reproduce them here, and patiently answering all our questions about the data. F.Z. greatly benefited from the stimulating environment of two workshops: the "Jamming" workshop in Aspen Center for Physics (August 2007) and the "Dynamical Heterogeneities" workshop held in Lorentz Center, Leiden (September 2008). He wishes to thank both centers for their hospitality and the participants for many useful discussions. Finally, it is a great pleasure for us to thank L. Angelani, L. Berthier, I. Biazzo, G. Biroli, J.-P. Bouchaud, F. Caltagirone, A. Cavagna, P. Charbonneau, B. Coluzzi, O. Dauchot, A. Donev, W. Ellenbroek, G. Foffi, S. Franz, A. Giuliani, P. Goldbart, W. Krauth, F. Krzakala, J. Kurchan, J. L. Lebowitz, A. Liu, R. Mari, M. Mézard, C. O'Hern, D. Ruelle, M. Schröter, B. Scoppola, G. Semerjian, M. Tarzia, S. Torquato, P. Verrocchio, P. G. Wolynes, M. Wyart, and L. Zdeborová for many interesting discussions that were fundamental for the development of this work.

APPENDIX A: METASTABLE GLASSY STATES IN FINITE DIMENSION

In this appendix we discuss how the concepts of metastable glassy state and of complexity should be modified in finite-dimensional systems. We refer the interested reader to the original literature for more details.

1. Metastable states in ferromagnetic systems

As discussed, the key feature of mean-field theory is the existence of an exponential number of metastable glassy states at high density. In the mean field these states can be defined as the minima of a suitable free-energy functional: the TAP functional (Thouless *et al.*, 1977; Mézard *et al.*, 1987) for spin systems or a suitable density functional for particle systems (Kirkpatrick and Wolynes, 1987a; Dasgupta and Valls, 1999; Chaudhuri *et al.*, 2005). These states are stable because in the infinite range case the barriers may be divergent. However, in finite-dimensional systems, states that have a free energy (per particle) greater than the ground state can always decay toward the ground state by a nucleation process by crossing a barrier that may diverge only when the energy difference with the ground state goes to zero.

Therefore we should find a suitable definition of these states. First recall the way this is done, for instance, in a ferromagnetic system. In positive magnetic field, the state (called $-$) with negative magnetization is metastable with respect to the $+$ state. However, one can study the $-$ state by preparing the system in the negative field where this state is stable and then slowly increasing the field toward its final positive value. After some time the $+$ state will nucleate. Still, if one is far enough from the spinodal of the $-$ state, the nucleation time is long enough and one is able to follow the $-$ state into the positive field region and measure its properties (e.g., its magnetization). In dimension d the lifetime of the metastable state diverges for small h as $\tau(h) = \exp(Ah^{1-d})$. This example shows that once the correct order parameter has been identified, one can study metastable states by adding a suitable external field coupled to the order parameter in order to stabilize this state and then change the external field following the evolution of the state into the region where it is metastable.

Actually this can be turned into a practical computational scheme as follows. Suppose we fix the magnetic field to its positive value but then perform an expansion of the free energy in $1+m$, assuming that the system is in the metastable $-$ state and therefore its magnetization m is close to -1. One can check explicitly that below the critical temperature for ferromagnetism the free energy obtained in this way displays a minimum at $m=-m^*$, which gives the magnetization of the $-$ state. One might wonder why a minimum appears as the free energy for positive magnetic field should be convex and have a single minimum at positive m. The key observation is that the decay of the metastable state is nonperturbative in $1+m$, so that it is missed at any order in perturbation theory[34] around $m=-1$. Thus, the expansion around $m=-1$ also stabilizes the metastable minimum for a finite-dimensional system. This might seem an artifact of the approximation, but in some sense it reflects a physical property of the system, the existence of a metastable state, which is relevant for numerical simulations and experiments as far as they are able to probe this state. This is exactly what we are interested in.

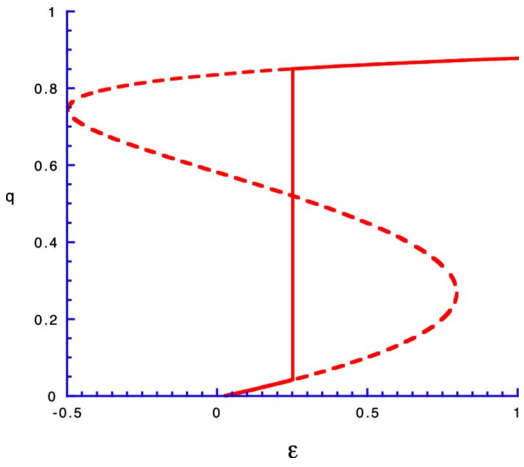

FIG. 24. (Color online) The shape of the function $q=A_0/A$ for $\varphi>\varphi_d$: the full line is the correct result and the dashed line is the output of a mean-field approximation.

2. Free energy functional for metastable glassy states: Order parameter and coupled replicas

In the case of a 1RSB transition to an amorphous state, it is not possible to identify a simple order parameter since the density profile of each state is amorphous and depends on the state. For each state, one should add to the Hamiltonian a specific external potential that favors the specific density profile of that state, but this is impossible since the density profiles are not known *a priori*.

A precise definition of the complexity was given by Franz and Parisi (1997), Mézard (1999), and Mézard and Parisi (2000) and it is based on the same idea discussed above in the case of the ferromagnet: one couples an external field to the order parameter in order to prepare the system in the metastable state. In this case one needs to consider a replicated system, as discussed in Sec. III, since the order parameter is the overlap between replicas (or equivalently the cage radius). The derivation is the same as in Sec. III.B.1. We introduce a parameter ϵ which is coupled to the average distance between replicas and allows us to compute the entropy as a function of the cage radius (see Fig. 7) via a Legendre transform. The physical values of A for a given ϵ are the solutions of $\partial_A \mathcal{S}(m,\varphi;A)=d(m-1)\epsilon$ and we are ultimately interested in the case $\epsilon=0$. The function $\mathcal{S}(m,\varphi;A)$ is therefore the entropy of the system of m copies with the constraint that each pair of copies is at fixed (in the

[34]Technically speaking the free energy is nonanalytic at the point $h=0$, being however, a C^∞ function of h. This fact is practically invisible from the expansion around $m=\pm 1$. If we analytically continue the free energy in the region of a negative magnetic field, it should acquire an imaginary part proportional to $\tau(h)^{-1}$, signaling that a sharp definition of the properties of the metastable phase is not possible. See Parisi (1988) for detailed discussion.

thermodynamic limit) distance A given by Eq. (13).

The typical shape of $\mathcal{S}(m,\varphi;A)$ is shown in Fig. 7. In a mean-field model, at densities below φ_K, the correlated phase is metastable and the system is liquid; at the glass transition it becomes stable as discussed above. In the mean field all this is well defined and one can perform explicit computations (Monasson, 1995; Mézard, 1999). In a finite-dimensional system, however, $\mathcal{S}(m,\varphi;A)$ must be a convex function of A: then the minimum at small A should disappear below φ_K. However, if we compute $\mathcal{S}(m,\varphi;A)$ in a power series expansion around $A=0$, we will find a stable minimum at small A. This is exactly the same effect discussed for the ferromagnetic case. In this way, the properties of the metastable state can also be studied in finite-dimensional systems. We focus on the region where the equation for A has two solutions that correspond to a local minimum of $\mathcal{S}(m,\varphi;A)-d(m-1)\epsilon A$. At fixed density, by varying ϵ one of the two solutions looses its stability and it disappears: these two curves are the equivalent of the spinodal lines in usual first-order transition. The dynamical transition is the point where for the first time the small-A solution exists at $\epsilon=0$: only at higher density the two coupled replicas may remain at a high value of the overlap in absence of a force that keeps them together. On the contrary the static transition is characterized by the fact that the coexistence line of the two solutions touches the axis $\epsilon=0$.

In finite dimension, general arguments tell us that the free energy is a convex function of A, so that the correct shape of the function $\mathcal{S}$ can be obtained by the Maxwell construction. To discuss the consequences of this fact on the definition of the complexity we consider the function $q(\epsilon)=A_0/A(\epsilon)$ (for some reference value of A_0) for densities bigger than φ_d, which is shown in Fig. 24. As can be seen from the figure, the point where we evaluate the complexity (i.e., $\epsilon=0$ and high q) is always in the metastable region for $\varphi<\varphi_K$ where the equilibrium complexity is nonzero. This causes an intrinsic ambiguity in the definition of complexity because the free energy in not defined with infinite precision in the metastable phase. However, we can use the fact that the free energy is a C^∞ function of ϵ near the discontinuity point to extrapolate the high ϵ free energy in the metastable region. This ambiguity becomes smaller and smaller the more we approach the Kauzmann density and in general it is rather small unless we are very near to the clustering phase transition. This ambiguity is not important from practical purposes; however, it implies that there is no sharp infinitely precise definition of the equilibrium complexity. If we forget this intrinsic ambiguity in the definition of the complexity, we may arrive at contradictory results.

It is important to remark once again that this discussion can be turned into a practical computational scheme to obtain the complexity analytically via the small cage expansion or in numerical simulations, where it has been used for both Lennard-Jones (Coluzzi *et al.*, 1999) and hard sphere (Angelani and Foffi, 2007) systems (see the original papers for details).

3. The physical meaning of the small A minimum of the free energy

The previous discussion was based only on the analytic properties of the replicated free energy $\mathcal{S}(m,\varphi;A)$. To complete the description, it is desirable to have an understanding of the mechanism that is beyond the metastability of the small A minimum. This is a key point because the mechanism is completely different in mean-field and in finite dimension.

a. Mean field

We first discuss what happens in the mean field. In this case, glassy states are really stable in the sense that they are local minima of a well-defined free-energy functional, separated by barriers whose height diverges in the thermodynamic limit. In a dynamical perspective, once the system is prepared in a glassy state, it will remain there forever. There is a real "ergodicity breaking" in the liquid state above φ_d, corresponding to the ideal mode-coupling dynamical transition. So why is the small A minimum metastable with respect to the liquid one between φ_d and φ_K?

The reason is that the number of glassy states is exponentially large in system size between φ_d and φ_K. Consider for instance the case of two coupled replicas, $m=2$. If the limit of zero coupling and if both replicas are in the same state, the total entropy will be twice the internal entropy of a state, plus the complexity Σ that represents the contribution of all possible states in which the two copies can be. On the other hand, if the two replicas are uncorrelated, the total entropy is twice the internal entropy, plus twice the complexity, since now each replica can be in each state independently. It is clear that by forcing the two replicas in the same state, one loses entropy. This is why the small A minimum has lower entropy or higher free energy and is metastable as long as the complexity $\Sigma>0$.

Therefore, in the mean field, glassy states are stable but their large number is responsible for the fact that the replicated system finds it more convenient to have each replica in a different state. This situation is very strange: indeed it is specific of the mean-field structure and it changes completely when one considers finite-dimensional systems.

b. Finite dimension

What goes wrong in the above picture when applied to finite-dimensional systems?

The main problem is that, in a finite-dimensional system, an exponential number of equilibrium states cannot exist. This can be argued as follows:

(1) Pure states are defined by taking the thermodynamic limit with a specified sequence of boundary conditions and the number of different boundary conditions scales as $e^{\kappa L^{d-1}}$, i.e., as the exponential of the surface of the system, so that the number of states cannot be exponential in the volume. The pic-

ture of the liquid state split in an exponential number of stable pure states does not make sense in finite dimension. On the contrary, at and above φ_K the number of states is not exponential in the system size even in the mean field. Therefore in this case the picture does not need to be modified in finite dimensions: a subexponential number of pure states are perfectly allowed as the number of possible boundary conditions is still very large.

(2) A better argument can be made for soft particles if we consider the minima of the energy. Of course there can be an exponentially large number of minima of the energy. A true metastable state would be a configuration whose energy cannot be decreased by moving a finite number of particles. It is easy to argue that such a configuration must have the same free energy of the ground state. On the other hand, we can consider local minima of order k, i.e., configurations whose energy cannot be decreased by moving at most k particles. It is quite evident that the associated complexity densities $\Sigma_k(E)$ will be different from zero, although they will tend to zero when k goes to infinity (Biroli and Monasson, 2000). Note that analytic computations based on the small cage expansion discussed in this paper will likely predict something similar to $\Sigma_1(E)$, and the effective value of k will increase with the precision of the computation. However, for not too large times and, in particular, in the experiments it is quite possible that $\Sigma_1(E)$ or $\Sigma_2(E)$ are the relevant quantities.

The two arguments above strongly suggest that the metastability of the small A minimum in finite dimensions is connected to the large-scale properties of the states and, in particular, to large-scale rearrangements. This is at the origin of the ambiguity in the definition of the complexity discussed previously.

Then, in what sense can exponential number of metastable glassy states, giving a finite complexity, exist in this case? A consistent "real-space" formulation of the problem has recently been discussed (Xia and Wolynes, 2001a, 2001b; Bouchaud and Biroli, 2004; Franz, 2005). One first assumes that for a finite (and small) system it is possible to define metastable states and that they initially are exponentially many in system size. Then, one can ask whether these states remain stable on increasing the system size. The key observation is the following (Bouchaud and Biroli, 2004). Consider a ball of size R inside the system. The rest of the system will influence the ball through its boundary, therefore favoring one particular state α of the ball among the exponentially many through a surface contribution $F_\alpha = -\kappa R^{d-1}$ to the free energy of the ball when the latter is in state α. On the other hand, the ball might be in any other state $\beta \neq \alpha$, and in this case it will gain entropy because of the large multiplicity of states: $F_{\text{not }\alpha} = F(\text{all possible } \beta \neq \alpha) = -T\Sigma R^d$. The ball will choose whether to stay in state α or not according to which is the largest between F_α and $F_{\text{not }\alpha}$. It is easy to see that for small enough R, F_α wins, while for large enough R, the other term wins and the ball will choose not to stay in the state α suggested by its boundary. This reasoning shows that, for large R, the assumption of the existence of an exponential number of states is inconsistent since for entropic reasons subsystems will always ignore the influence of their boundary and escape from the state.

See Xia and Wolynes (2001a, 2001b), Franz (2005), and, in particular, Bouchaud and Biroli (2004) for detailed discussion. In this series of papers the discussion above was precisely formulated in a nucleation theory where the driving force is of *entropic* nature. Remarkably, methods to compute the length of the critical nuclei (droplets) and their relaxation time have been proposed; this is a first step toward a quantitative description of activated processes between φ_d and φ_K even if a complete theory is still lacking.

c. Finite dimension, finite volume

The last point to be discussed is the assumption made previously that for finite and small enough systems an exponential number of states still exist and can be taken as the starting point for the nucleation theory discussed by Xia and Wolynes (2001a) and Bouchaud and Biroli (2004).

We discuss this crucial point in the specific case of hard spheres, which is of interest here. Consider a system of hard spheres enclosed in a finite box with, for simplicity, hard walls. It is very easy to see that for a small box and high enough density, there will be disconnected sets of configurations in the sense that there are pairs of configurations that cannot be transformed one into the other simply by continuously moving the spheres. Therefore we can group each set of configurations that can be continuously transformed one into each other in a state. We can say that configurations inside a state are "blocked" in the sense that once the system is prepared in a state it will never escape.[35] We can define a finite-volume complexity as $\Sigma_V = (1/V)\ln \mathcal{N}_V$, where $\mathcal{N}_V$ is the number of such states in a volume V.

Now we can increase the volume of the box while at the same time adding particles in order to keep the density fixed. On a general ground, we expect Σ_V to be a decreasing function of V since by increasing the volume one will open new channels to "unblock" the configurations and connect some states that will be merged in a bigger state. On the basis of the analysis of Bouchaud and Biroli (2004), we expect three possible behaviors of Σ_V:

[35]We use the word blocked in order to avoid confusion with the concept of "jamming." In a jammed configuration no particle can move. Instead, in a blocked configuration particles can move a little but the whole system is unable to visit the phase space; the existence of blocked configurations was shown a long time ago by Ruelle (1977).

(1) For $\varphi<\varphi_d$, in the unclustered liquid phase, we expect Σ_V to fall very rapidly to 0 as for large enough volumes all configurations will be connected and form the unique liquid state.

(2) For $\varphi_d<\varphi<\varphi_K$ we are in the clustered liquid phase; then we expect that Σ_V first decreases to a finite plateau for small enough volume. The plateau corresponds to the mean-field value $\Sigma(\varphi)$. On larger length scales, once the nucleation effect described previously becomes effective, the glassy states are unblocked and the complexity will drop to zero; only the liquid state survives.

(3) For $\varphi>\varphi_K$, the plateau value goes to zero since the mean-field complexity vanishes. Therefore in this case the complexity will go to zero fast as in case (1). Still, even in the $V\to\infty$ limit a large number of amorphous states will survive (but their number is not exponential).

It is interesting to remark that in case (2) "unblocking" a configuration will require a long time since a large number of particles have to rearrange together. Therefore the dynamics in this region will be very slow and the system will stay for a long time close to a configuration that is made by patches of locally blocked configurations, the "mosaic state" of Xia and Wolynes (2001a). Conversely, in case (3), the dynamics will be completely frozen even in the thermodynamic limit.

A consequence of this discussion is that an infinite system of hard spheres at finite pressure, even if very large, will always relax to the ideal glass state, i.e., at density φ_{GCP} (if crystallization is avoided). Therefore the ideal glass states at φ_{GCP} are the only jammed states that remain stable if pressure is made very large but finite in the limit $V\to\infty$. Of course for finite sizes or finite times this will be true also for metastable glasses.

APPENDIX B: THE "LINK" EXPANSION FOR HARD SPHERES

We describe here a formal way to justify the introduction of the effective potentials to integrate over $m-1$ replicas and obtain an expression for the replicated entropy which is formally equal to the one of a nonreplicated liquid. We use one replica, say replica 1, as a reference and integrate over the small displacements of the other $m-1$ replicas. Note that we are not breaking the replica symmetry: we are only looking for a way to expand the entropy for small A. In the following we use the notation $\mathbf{x}=(x_2,\ldots,x_m)$.

The expansion of a given diagram proceeds as follows. At the zeroth order ($A=0$), the function $\rho(\bar{x})$ is a product of delta functions; therefore all replicas coincide. Then we have

$$\mathcal{D}=\mathcal{D}_0=\frac{1}{S}\int\prod_i \rho dx_i\prod_\ell[\chi(\ell)-1], \tag{B1}$$

i.e., $\mathcal{D}_0$ is the corresponding diagram of the nonreplicated system.

The quantities x_1-x_a are of order $\sqrt{A}$. Then the crucial observation is that, for $a\geqslant 2$, the function $\chi(x_{ai}-x_{aj})$ in Eq. (33) is essentially constant if $|x_{1i}-x_{1j}|$ differs from D by a quantity $\gg\sqrt{A}$; in fact it becomes simply equal to $\chi(x_1-y_1)=\theta(|x_1-y_1|-D)$. This means that the integration region in the space x_{1i} such that $||x_{1i}-x_{1j}|-D|\gg\sqrt{A}$ for all links $\ell=(i<j)$ does not give any contribution apart from the zeroth-order one. We call a link ℓ such that $||x_{1i}-x_{1j}|-D|\sim\sqrt{A}$ a "critical link": the idea is to isolate the contribution of the regions such that k links are critical, whose volume is of order $A^{k/2}$.

1. Expansion of the replicated entropy

We define $\mathcal{D}x_1=\Pi_i\rho dx_{1i}$ and $\mathcal{D}\mathbf{x}=\Pi_i[\rho(i)/\rho]d\mathbf{x}_i$ and note that using Eq. (34) we have $\int\mathcal{D}\mathbf{x}=1$. Defining $\chi_a(\ell)=\chi(x_{ai}-x_{aj})$, we have for a diagram $\mathcal{D}$ contributing to $\mathcal{S}$

$$\begin{aligned}
\mathcal{D}=\frac{1}{S}\int\prod_i\rho(i)dx_{1i}d\mathbf{x}_i\prod_\ell[\bar{\chi}(\ell)-1]&=\frac{1}{S}\int\mathcal{D}\mathbf{x}\mathcal{D}x_1\prod_\ell[\chi_1(\ell)-1+\bar{\chi}(\ell)-\chi_1(\ell)]\\
&=\frac{1}{S}\int\mathcal{D}x_1\prod_\ell[\chi_1(\ell)-1]+\frac{1}{S}\int\mathcal{D}x_1\sum_\ell\prod_{\ell'\neq\ell}[\chi_1(\ell')-1]\int\mathcal{D}\mathbf{x}[\bar{\chi}(\ell)-\chi_1(\ell)]\\
&\quad+\frac{1}{S}\int\mathcal{D}x_1\sum_{\ell<\ell'}\prod_{\ell''\neq\ell,\ell'}[\chi_1(\ell'')-1]\int\mathcal{D}\mathbf{x}[\bar{\chi}(\ell)-\chi_1(\ell)][\bar{\chi}(\ell')-\chi_1(\ell')]+\cdots\\
&=\mathcal{D}_0+\int\mathcal{D}x_1\sum_\ell\tilde{Q}(\ell)\prod_{\ell'\neq\ell}[\chi_1(\ell')-1]+\int\mathcal{D}x_1\sum_{\ell<\ell'}\tilde{Q}_2(\ell,\ell')\prod_{\ell''\neq\ell,\ell'}[\chi_1(\ell'')-1]+\cdots\\
&=\mathcal{D}_0+\sum_{n\geqslant 1}\int\mathcal{D}x_1\sum_{\ell_1<\cdots<\ell_n}\tilde{Q}_n(\ell_1,\ldots,\ell_n)\prod_{\ell\neq(\ell_1,\ldots,\ell_n)}[\chi_1(\ell)-1],
\end{aligned} \tag{B2}$$

having defined the functions $\tilde{Q}_n(\ell_1,\ldots,\ell_n)$ from

$$\tilde{Q}_1(\ell) = \tilde{Q}(\ell) = \int \mathcal{D}\mathbf{x}[\bar{\chi}(\ell) - \chi_1(\ell)] = \int d\mathbf{x}_i d\mathbf{x}_j \frac{\rho(i)\rho(j)}{\rho^2}[\bar{\chi}(i,j) - \chi_1(i,j)],$$
$$\tilde{Q}_n(\ell_1,\ldots,\ell_n) = \int \mathcal{D}\mathbf{x}\prod_{i=1}^{n}[\bar{\chi}(\ell_i) - \chi_1(\ell_i)] = \int \prod_{i\in\partial L_n} d\mathbf{x}_i \frac{\rho(i)}{\rho}\prod_{\ell\in L_n}[\bar{\chi}(\ell) - \chi_1(\ell)]. \tag{B3}$$

The integral over $\mathcal{D}\mathbf{x}$ contains all vertices of the original diagram. However, the integrand depends only on the vertices that are adjacent to one of the links $L_n = (\ell_1,\ldots,\ell_n)$; calling this set ∂L_n and because the integrals over the other vertices give 1, we obtained the last equality in Eq. (B3).

Note that, for example, the function $\tilde{Q}_2(\ell,\ell')$ depends on three or four x_i depending whether the two links ℓ,ℓ' are adjacent or not. But if the two links are nonadjacent, then $\tilde{Q}_2(\ell,\ell') = \tilde{Q}(\ell)\tilde{Q}(\ell')$. This motivates the introduction of the connected functions, defined by $\tilde{Q}^c(\ell) = \tilde{Q}(\ell)$,

$$\tilde{Q}_2(\ell,\ell') = \tilde{Q}(\ell)\tilde{Q}(\ell') + \tilde{Q}_2^c(\ell,\ell'),$$
$$\tilde{Q}_3(\ell,\ell',\ell'') = \tilde{Q}(\ell)\tilde{Q}(\ell')\tilde{Q}(\ell'') + \{\tilde{Q}_2^c(\ell,\ell')\tilde{Q}(\ell'') + \text{perm.}\} + \tilde{Q}_3^c(\ell,\ell',\ell''), \tag{B4}$$

and so on, as usual in statistical mechanics. The important property of these functions is that they are nonvanishing only if the subdiagram identified in $\mathcal{D}$ by the links in L_n is connected.

Now we insert the expression of the connected functions in Eq. (B4) into Eq. (B2). It is not difficult to check that we can resum the contributions containing $\tilde{Q}(\ell)$ to obtain

$$\mathcal{D} = \frac{1}{S}\int \mathcal{D}x_1 \prod_{\ell}[\chi_1(\ell) + \tilde{Q}(\ell) - 1] + \frac{1}{S}\int \mathcal{D}x_1 \sum_{\ell<\ell'} \tilde{Q}_2^c(\ell,\ell') \prod_{\ell''\neq\ell,\ell'}[\chi_1(\ell'') + \tilde{Q}(\ell) - 1] + \cdots. \tag{B5}$$

The interpretation of the above equation is the following: the original diagram of the replicated liquid generates a diagram in which the vertices carry a factor ρ and the links carry a function $\chi_1 + \tilde{Q} - 1$, plus a sum of contributions in which a subdiagram made of links L_n is marked and on each of its connected parts an interaction $\tilde{Q}^c$ is placed. The unmarked links carry again the function $\chi_1 + \tilde{Q} - 1$ and the vertices a factor ρ. In fact, it is easy to check on specific examples that the explicit sum over the links in L_n can be rearranged by grouping together, as usual, diagrams with the same topology. In this way the multiplicity factors S are corrected to become the exact-symmetry factors of the diagram with marked links.

In summary, we can write

$$\mathcal{D} = \mathcal{D}_0[\chi_1 + \tilde{Q}] + \mathcal{D}_2[\chi_1 + \tilde{Q}, \tilde{Q}_2^c] + \mathcal{D}_3[\chi_1 + \tilde{Q}, \tilde{Q}_2^c, \tilde{Q}_3^c] + \cdots, \tag{B6}$$

where the $\mathcal{D}_n$ represent diagrams that are built from the original diagram by marking n links in all the possible *topologically inequivalent* ways and placing the interactions Q^c on the marked connected parts. Each diagram has a symmetry factor S which is the number of equivalent relabeling of the vertices, taking into account the presence of the marked links. Clearly, summing the contribution of all the diagrams and Eq. (35) we get

$$\mathcal{S}[\rho(\bar{x}),\bar{\chi}(\bar{x},\bar{y})] = NS_{\text{harm}} + \mathcal{S}_0[\rho,\chi_1(x-y) + \tilde{Q}(x-y)] + \mathcal{S}_2[\rho,\chi_1(x-y) + \tilde{Q}(x-y),\tilde{Q}_2^c(x,y,z)] + \cdots, \tag{B7}$$

where $\mathcal{S}_0[\rho,1+f]$ is defined in the same way as the functional (32), but for one single copy of the system and with f on the links of the diagrams, while the other terms come from interactions involving more than two particles.

It is worth noting at this point that the specific form of the effective potentials $\tilde{Q}_n^c$ depends on the topology of the subdiagram that carries them. For the three-body interactions there is only one possible diagrams (the one in which ℓ,ℓ' are adjacent, i.e., they share one vertex) but for $n \geqslant 3$ there are many possible diagrams that correspond to different interactions.

The $\tilde{Q}^c$ functions are quite difficult to handle. However, from their definition one can show that, for small A, they are nonzero only if for all the links it holds $|x_i - x_j| \sim D + O(\sqrt{A})$, as expected on the basis of the argument put forward at the beginning of this section. Moreover, for $m > 0$ these functions are bounded in the sense that when they are different from zero, they stay finite for $A \to 0$. This implies that, for example, the contribution coming from diagrams containing $\tilde{Q}_2^c$ is of order A because the integrals over the two link variables have to support only on an interval of order $\sqrt{A}$. Therefore, Eq. (B7) is an expansion in powers of $\sqrt{A}$, where the term $\mathcal{S}_n$ is proportional to $A^{n/2}$. Note that this is specific to the

hard sphere potential which is always constant except for the discontinuity in $r=D$. For smooth potentials, the corrections come from all values of $|x_i-x_j|$, and in this case it is more convenient to integrate over the displacement of the replicas at a fixed center of mass [see Mézard and Parisi (1999a)]. Another remarkable property of the effective potentials is that in the limit of infinite dimension only the two-body potential should give important contributions.

2. The effective potentials

To gain physical intuition on the effective liquid described by the entropy functional (B7), it is convenient to compute its partition function. First, we define the potentials Q by

$$Q_n(\ell_1,\dots,\ell_n)=\frac{\tilde{Q}_n(\ell_1,\dots,\ell_n)}{\chi_1(\ell_1)\cdots\chi_1(\ell_n)}=\int\prod_{i\in\partial L_n}d\mathbf{x}_i\frac{\rho(i)}{\rho}\prod_{\ell\in L_n}\left[\prod_{a=2}^{m}\chi_a(\ell)-1\right]=\left\langle\prod_{\ell\in L_n}\left[\prod_{a=2}^{m}\chi_a(\ell)-1\right]\right\rangle_{\partial L_n} \tag{B8}$$

and similarly for the connected potentials. The brackets indicate the average over the $\rho(i)$ of the vertices in ∂L_n.

When constructing the partition function that generates the diagrams in Eq. (B7), we must take into account the fact that if a link is labeled it carries the function $\tilde{Q}_n^c$ instead of the usual function $f(\ell)=\chi_1(\ell)[1+Q(\ell)]-1$. This leads, using standard liquid theory, to the following grancanonical partition function:

$$Z_{\rm eff}[z]=\sum_{N=0}^{\infty}\frac{z^N}{N!}\int d^Nx\prod_{\ell}\chi_1(\ell)[1+Q(\ell)]\prod_{\ell<\ell'}\left[1+\frac{Q_2^c(\ell,\ell')}{[1+Q(\ell)][1+Q(\ell')]}\right]\times\prod_{\ell<\ell'<\ell''}\left[1+\frac{Q_3^c(\ell,\ell',\ell'')}{[1+Q(\ell)][1+Q(\ell')][1+Q(\ell'')]\left\{\left[1+\frac{Q_2^c(\ell,\ell')}{[1+Q(\ell)][1+Q(\ell')]}\right]\times\text{perm.}\right\}}\right]\times\cdots, \tag{B9}$$

where now the links are all possible pairs of particles. This makes it possible to identify the n body potentials of the effective liquid. For instance, we have

$$e^{-\phi_{\rm eff}(x-y)}=\chi(x-y)[1+Q(x-y)]=\chi(x-y)\left\langle\prod_{a=2}^{m}\chi(x_a-y_a)\right\rangle_{x,y},$$
$$e^{-\phi^{(2)}_{\rm eff}(x-y,x-z)}=1+\frac{Q_2^c(x-y,x-z)}{[1+Q(x-y)][1+Q(x-z)]}=\frac{\left\langle\prod_{a=2}^{m}\chi(x_a-y_a)\chi(x_a-z_a)\right\rangle_{x,y,z}}{\left\langle\prod_{a=2}^{m}\chi(x_a-y_a)\right\rangle_{x,y}\left\langle\prod_{a=2}^{m}\chi(x_a-z_a)\right\rangle_{x,z}}, \tag{B10}$$

and so on. As before, the brackets denote averages over the Gaussian distribution of the molecule. The entropy functional (B7) is obtained by expanding $Z_{\rm eff}$ in a Mayer series of z and then Legendre transforming to the density. Then one has

$$\mathcal{S}[\rho(\bar{x}),\bar{\chi}(\bar{x},\bar{y})]=NS_{\rm harm}-\beta NF_{\rm eff}, \tag{B11}$$

where $F_{\rm eff}$ is the canonical free energy of the liquid (B9).

3. Correlation function of the glass

It is interesting to compute the correlation function of the glass state; it is the correlation function of one replica (see Sec. III.B.2). It can be computed as follows. We choose one replica and we add to the hard-core interaction an additional potential $v(x-y)$, only to this replica. Then it is easy to show that

$$\frac{\rho^2}{2}g_G(x-y)=-\left.\frac{\delta\mathcal{S}[\bar{\rho},\bar{\chi}]}{\delta v(x-y)}\right|_{v=0}. \tag{B12}$$

This can be done by looking at the partition function $Z_m(\epsilon)$ [Eq. (11)]. If we add a potential to replica 1, we get an additional term

$$\exp\left\{-\frac{1}{2}\int dxdy v(x-y)\sum_{i\neq j}\delta(x-x_{1i})\delta(y-y_{1j})\right\}. \tag{B13}$$

Then if we differentiate with respect to $v(x-y)$ we get

$$\left.\frac{\delta \ln Z_m(\epsilon)}{\delta v(x-y)}\right|_{v=0} = -\frac{1}{2}\left\langle\sum_{i\neq j}\delta(x-x_{1i})\delta(y-y_{1j})\right\rangle = -\frac{1}{2}\rho_{11}(x,y) = -\frac{\rho^2}{2}g_G(x-y). \tag{B14}$$

The derivative of $\mathcal{S}$ is exactly the same because it is the Legendre transform of $\ln Z_m(\epsilon)$.

The expression of $\mathcal{S}(m,\varphi;A)$ in the presence of the additional interaction v is simple; indeed the only modification is $\chi_1 \to \chi_1 e^{-v}$, which has to be substituted in the final result (B7). Note that the functions Q, Q_2, etc., do not contain χ_1 explicitly because they depend only on the potentials of the replicas $2,\ldots,m$ [see Eq. (B8) so that they will not depend on v]. Therefore the correlation of the glass is given by the correlation of the liquid described by the partition function (B9).

APPENDIX C: THE TWO-BODY EFFECTIVE POTENTIAL

1. Definitions

The function $Q(x,y)=Q(x-y)$ is defined in Eq. (B8). Making use of Eq. (34) we get

$$\begin{aligned} Q(x-y) &= \rho^{-2}\int d\mathbf{x}d\mathbf{y}\rho(x,\mathbf{x})\rho(y,\mathbf{y})\left[\prod_{a=2}^{m}\chi(x_a-y_a)-1\right] \\ &= \int dXdY\gamma_A(x-X)\gamma_A(y-Y)\left\{\left[\int d\xi d\eta\gamma_A(\xi)\gamma_A(\eta)\chi(X+\xi-Y-\nu)\right]^{m-1}-1\right\} \\ &= \int dXdY\gamma_A(x-X)\gamma_A(y-Y)\{q_A(X-Y)^{m-1}-1\}, \end{aligned} \tag{C1}$$

where

$$\begin{aligned} q_A(\vec{r}) &= \int d\xi d\eta\gamma_A(\xi)\gamma_A(\eta)\chi(\vec{r}+\xi-\eta) \\ &= \int d\vec{r}'\gamma_{2A}(\vec{r}')\chi(\vec{r}-\vec{r}'). \end{aligned} \tag{C2}$$

The last equality is obtained by introducing $\vec{r}'=\eta-\xi$ and observing that as ξ and η are independent Gaussian variables with variance A, their difference is also a Gaussian variable of variance $2A$. Following a similar procedure,[36] we obtain

$$Q(\vec{r}) = \int d\vec{r}'\gamma_{2A}(\vec{r}')\{q_A(\vec{r}-\vec{r}')^{m-1}-1\}. \tag{C3}$$

We are particularly interested in the integral

$$\begin{aligned} G_m(A) &= \frac{1}{V_d(D)}\int d\vec{r}\chi(\vec{r})Q(\vec{r}) \\ &= \frac{1}{V_d(D)}\int d\vec{r}[q_A(\vec{r})^m - q_A(\vec{r})] \\ &= \frac{1}{V_d(D)}\int d\vec{r}[q_A(\vec{r})^m - \chi(\vec{r})], \end{aligned} \tag{C4}$$

which is the contribution to the virial of the nontrivial part of the two-body effective potential given in Eq. (B10); the different expressions in Eq. (C4) are obtained starting either from Eq. (C3) or directly from Eq. (C1) and performing similar manipulations to the ones in Eq. (C1).

We are also interested in the following functions:

$$\begin{aligned} F_m(A) &\equiv \frac{A}{1-m}\frac{\partial G_m(A)}{\partial A} \\ &= \frac{mA}{1-m}\frac{1}{V_d(D)}\int d\vec{r}q_A(\vec{r})^{m-1}\frac{\partial q_A(\vec{r})}{\partial A}, \\ H_m(A) &\equiv -m\frac{\partial G_m(A)}{\partial m} \\ &= -\frac{m}{V_d(D)}\int d\vec{r}q_A(\vec{r})^m \ln q_A(\vec{r}). \end{aligned} \tag{C5}$$

In the limit $m\to 1$ we have $G_m(A)\to 0$ while

$$F_m(A) \to F_1(A) \equiv -\frac{A}{V_d(D)}\int d\vec{r}\ln[q_A(\vec{r})]\frac{\partial q_A(\vec{r})}{\partial A}, \tag{C6}$$

[36] We start from the last line of Eq. (C1) and introduce $\xi=x-X$ and $\eta=y-Y$, and then $\vec{r}'=\eta-\xi$.

$$H_m(A) \to H_1(A) \equiv -\frac{1}{V_d(D)} \int d\vec{r} q_A(\vec{r}) \ln q_A(\vec{r}).$$

In the limit $m \to 0$, $A = \alpha m$, we show that $G_m(A) \to G_0(\alpha)$ which is a finite function of α. We also show that

$$F_m(A) \to F_0(\alpha) = \alpha \frac{dG_0(\alpha)}{d\alpha},$$
$$H_m(A) \to H_0(\alpha) = \alpha \frac{dG_0(\alpha)}{d\alpha} = F_0(\alpha). \tag{C7}$$

Finally, we are interested in the large d limit with the following scaling:

$$\mathcal{G}_m(\hat{A}) \equiv \lim_{d\to\infty} G_m(D^2 \hat{A} d^{-2}),$$
$$\mathcal{F}_m(\hat{A}) \equiv \lim_{d\to\infty} F_m(D^2 \hat{A} d^{-2}). \tag{C8}$$

Unfortunately a full analytical evaluation of these integrals is not possible. In the following we will discuss some particular cases in which analytical calculations are possible.

2. The function $q_A(r)$ and the virial coefficient $G_m(A)$

The function $q_A(r)$ defined in Eq. (C2) is the convolution of a Gaussian and the theta function $\chi(r)$. This integral can be reduced to a one-dimensional integral by means of d-dimensional bipolar coordinates. This will be proved in the next section.

a. Bipolar coordinates

To compute the convolution (C2) we introduce d-dimensional bipolar coordinates in the space $\vec{r}' = (x_1, \ldots, x_d)$. We assume, without loss of generality, thanks to rotational invariance that $\vec{r}$ is directed along the axis x_1 in $\mathbb{R}^d$, and we define $u = |\vec{r}'|$, $v = |\vec{r} - \vec{r}'|$, and $R = \sqrt{x_2^2 + \cdots + x_d^2}$ the distance between $\vec{r}'$ and the axis x_1. We then look to the projection $r'_\perp$ of $\vec{r}'$ on the hyperplane $P_\perp = (x_2, \ldots, x_d)$ perpendicular to x_1; the distance of $r'_\perp$ from the origin in this plane is just R, and we can introduce polar coordinates (R, θ_{d-1}) on this plane, thus defining a set θ_{d-1} of $d-2$ angles that specify the position of $r'_\perp$ on the sphere of radius R in $P_\perp$. We define in this way the change to bipolar coordinates $\vec{r}' \to (u, v, \theta_{d-1})$.

We compute the Jacobian of such a transformation. It is easy to show that

$$\frac{\partial(u, v, \theta_{d-1})}{\partial(x_1, \cdot, x_d)} = \begin{pmatrix} \frac{x_1}{u} & \frac{x_2}{u} \cdots \frac{x_d}{u} \\ \frac{x_1 - r}{v} & \frac{x_2}{v} \cdots \frac{x_d}{v} \\ \vec{0} & \left[\frac{\partial \theta_{d-1}}{\partial(x_2, \ldots, x_d)}\right] \end{pmatrix}. \tag{C9}$$

The reason for the zeros in the first column is that the angles θ_{d-1} are independent of x_1 as they describe the position of $r'_\perp$ in $P_\perp$. We can write the determinant of this matrix as

$$J^{-1} = \left|\frac{\partial(u, v, \theta_{d-1})}{\partial(x_1, \ldots, x_d)}\right| = \frac{x_1 R}{uv} \left| \begin{bmatrix} \frac{x_2}{R} \cdots \frac{x_d}{R} \\ \frac{\partial \theta_{d-1}}{\partial(x_2, \ldots, x_d)} \end{bmatrix} \right| - \frac{(x_1 - r)R}{uv} \left| \begin{bmatrix} \frac{x_2}{R} \cdots \frac{x_d}{R} \\ \frac{\partial \theta_{d-1}}{\partial(x_2, \ldots, x_d)} \end{bmatrix} \right| = \frac{rR}{uv} \left| \begin{bmatrix} \frac{x_2}{R} \cdots \frac{x_d}{R} \\ \frac{\partial \theta_{d-1}}{\partial(x_2, \ldots, x_d)} \end{bmatrix} \right|. \tag{C10}$$

The matrix appearing in the previous equation is just the Jacobian matrix for the change to spherical coordinates in $P_\perp$ and its determinant is given by

$$\left| \begin{bmatrix} \frac{x_2}{R} \cdots \frac{x_d}{R} \\ \frac{\partial \theta_{d-1}}{\partial(x_2, \ldots, x_d)} \end{bmatrix} \right| = \frac{dR d\theta_{d-1}}{d^{d-1} r'_\perp} = \frac{1}{R^{d-2} J_{d-1}(\theta_{d-1})}. \tag{C11}$$

From the two previous equations we obtain the desired Jacobian

$$d\vec{r}' = \frac{uv}{r} R^{d-3} du dv J_{d-1}(\theta_{d-1}) d\theta_{d-1}$$
$$= \frac{uv}{r} R^{d-3} du dv d\Omega_{d-1}, \tag{C12}$$

where the integral of $d\Omega_{d-1}$ is just the $(d-1)$-dimensional solid angle Ω_{d-1}. The radius R is easily expressed as a function of u, v by elementary geometrical considerations,

$$R(u,v;r) = \frac{\sqrt{2u^2v^2 + 2u^2r^2 + 2v^2r^2 - u^4 - v^4 - r^4}}{2r}. \tag{C13}$$

The (positive) variables u,v,r have to respect the triangular inequalities, so the domain of integration is for instance $u \in [0,\infty)$, $v \in [|r-u|, r+u]$.

Then, performing the change of variable $w = v^2 - (r-u)^2$ and using $R(u,w;r)^2 = w(4ru-w)/4r^2$, we get

$$\begin{aligned} q_A(r) &= \Omega_{d-1} \int_0^\infty du \int_{|r-u|}^{r+u} dv \frac{uv}{r} \\ &\quad \times R(u,v;r)^{d-3} \theta(u-D) \gamma_{2A}(v) \\ &= \frac{\Omega_{d-1}}{2r} \int_D^\infty du u \frac{e^{-(u-r)^2/4A}}{(4\pi A)^{d/2}} \\ &\quad \times \int_0^{4ru} dw \left(\frac{w(4ru-w)}{4r^2}\right)^{(d-3)/2} e^{-w/4A}. \end{aligned} \tag{C14}$$

We now make use of the relation

$$\begin{aligned} \int_0^1 e^{-Bx}[x(1-x)]^{(d-3)/2} &= B^{(2-d)/2} e^{-B/2} \sqrt{\pi} \Gamma\left(\frac{d-1}{2}\right) \\ &\quad \times I_{(d-2)/2}(B/2) \end{aligned} \tag{C15}$$

and of the definition $\Omega_{d-1} = 2\pi^{(d-1)/2}/\Gamma[(d-1)/2]$ to obtain the final result

$$\begin{aligned} q_A(r) &= \int_D^\infty du \left(\frac{u}{r}\right)^{(d-1)/2} \frac{e^{-(r-u)^2/4A}}{\sqrt{4\pi A}} \\ &\quad \times \left[e^{-ru/2A} \sqrt{\pi \frac{ru}{A}} I_{(d-2)/2}\left(\frac{ru}{2A}\right) \right]. \end{aligned} \tag{C16}$$

b. Three dimensions

Remarkably, in $d=3$ the integrand simplifies and a full calculation of $q_A(r)$ is possible,

$$\begin{aligned} q_A(r) &= \frac{1}{r\sqrt{4\pi A}} \int_D^\infty du u [e^{-(r-u)^2/4A} - e^{-(r+u)^2/4A}] \\ &= \frac{1}{2}\left[\mathrm{erf}\left(\frac{r-D}{\sqrt{4A}}\right) - \mathrm{erf}\left(\frac{r+D}{\sqrt{4A}}\right) \right. \\ &\quad \left. + \frac{2}{r}\sqrt{\frac{A}{\pi}}(e^{-(r-D)^2/4A} - e^{-(r+D)^2/4A}) + 2 \right], \end{aligned} \tag{C17}$$

with

$$\mathrm{erf}(t) \equiv \frac{2}{\sqrt{\pi}} \int_0^t dx e^{-x^2}, \tag{C18}$$

$$\Theta(t) = \frac{1}{2}[1 + \mathrm{erf}(t)] = \frac{1}{\sqrt{\pi}} \int_{-\infty}^t dx e^{-x^2}.$$

Given that $q_A(r) \to 1$ for $r - D \gg \sqrt{A}$, this allows for a simple numerical evaluation of the integral in Eq. (C4) to compute $G_m(A)$. A full computation of $Q(r)$ is also possible using Eq. (C3). It is also easy to check that uniformly in r we have,[37]

$$q_A(r) \sim \Theta\left(\frac{r-D}{\sqrt{4A}}\right) + O(\sqrt{A}) + O(e^{-D/\sqrt{A}}). \tag{C19}$$

c. Finite dimension: Expansion in powers of $\sqrt{A}$

In general finite dimension the integral (C16) cannot be explicitly evaluated. However, an expansion in powers of $\sqrt{A}$ similar to Eq. (C19) holds. In fact, when A is very small it is easy to realize that the main contribution to $q_A(r)$ comes from the integration over the component of $\vec{r}'$ which is parallel to $\vec{r}$: in the orthogonal directions $\theta(|\vec{r}-\vec{r}'|-D)$ is essentially constant and the integration over these components gives a correction $O(e^{-D/\sqrt{A}})$. Then we have

$$q_A(r) \sim \int_{-\infty}^\infty dr' \frac{e^{-r'^2/4A}}{\sqrt{4\pi A}} \theta(r - r' - D) = \Theta\left(\frac{r-D}{\sqrt{4A}}\right). \tag{C20}$$

The same result can be derived from Eq. (C16) by observing that for $A \to 0$, $r \sim D$, one has $z = ur/2A \to \infty$ and for all n (Abramowitz and Segun, 1965)

$$e^{-z}\sqrt{2\pi z} I_n(z) \to 1. \tag{C21}$$

Thus we have, changing variables to $t = (r-D)/\sqrt{4A}$ and $s = (u-D)/\sqrt{4A}$,

$$\begin{aligned} q_A(t) &= \frac{1}{\sqrt{\pi}} \int_0^\infty ds \left(\frac{D + s\sqrt{4A}}{D + t\sqrt{4A}}\right)^{(d-1)/2} e^{-(t-s)^2} \\ &\sim \frac{1}{\sqrt{\pi}} \int_0^\infty ds e^{-(t-s)^2} = \Theta(t). \end{aligned} \tag{C22}$$

The next-to-leading orders in $\sqrt{A}$ can in principle be computed using the large z expansion of the Bessel functions (Abramowitz and Segun, 1965).

In this way we can derive the leading-order contribution to $G_m(A)$: substituting $q_A(t) = \Theta(t)$ into Eq. (C4) we get

[37] Note that $\Theta(t)$ is a "smoothed" theta function.

$$G_m(A) = \frac{d\sqrt{4A}}{D}\int_{-D/\sqrt{4A}}^{\infty} dt \times\left(\frac{D+t\sqrt{4A}}{D}\right)^{d-1}[\Theta(t)^m-\theta(t)] \sim \frac{d\sqrt{4A}}{D}\int_{-\infty}^{\infty} dt[\Theta(t)^m-\theta(t)] = \frac{d\sqrt{4A}}{D}Q_0(m), \tag{C23}$$

defining

$$Q_0(m) = \int_{-\infty}^{\infty} dt[\Theta(t)^m-\Theta(t)]. \tag{C24}$$

One can check that the function $Q_0(m)$ is given by

$$Q_0(m) = Q_0(1-m) + O((1-m)^2), \qquad Q_0 = -\int_{-\infty}^{\infty} dt\Theta(t)\ln\Theta(t) \tag{C25}$$

close to $m=1$ and that

$$Q_0(m) \sim \sqrt{\pi/4m}(\sqrt{m})^m \tag{C26}$$

for $m\to 0$ using the $t\to-\infty$ expansion of the error function.

d. Infinite dimension

In the limit of infinite dimension, we are interested in the scaling $A=D^2\hat{A}/d^2$. One could then naively expect the small cage expansion of the previous section to work well. However, one has $z=(ur/2D^2\hat{A})d^2$, and an inspection of the large z expansion of the Bessel function $I_n(z)$ (Abramowitz and Segun, 1965) shows that it is indeed an expansion in powers of n^2/z. Then, for $n=(d-2)/2$ as in Eq. (C16) one has to resum all orders in this large z expansion.

This can be done without difficulty either by looking at the large z expansion or by a saddle-point evaluation of the integral representation,

$$I_n(z) = \frac{1}{2\pi i}\int_C dt t^{-n-1}e^{(z/2)(t+1/t)}, \tag{C27}$$

and one can show that

$$\lim_{d\to\infty} e^{-d^2z}\sqrt{2\pi d^2 z}I_{(d-2)/2}(d^2z) = e^{-1/8z}. \tag{C28}$$

Using this result in Eq. (C16), we have

$$q_A(r) = \int_D^{\infty} du\left(\frac{u}{r}\right)^{(d-1)/2}\frac{e^{-(r-u)^2/4A}}{\sqrt{4\pi A}}e^{-D^2\hat{A}/4ru}. \tag{C29}$$

Changing variables again to $t=(r-D)/\sqrt{4A}$ and $s=(u-D)/\sqrt{4A}$ and using

$$\left(\frac{u}{r}\right)^{(d-1)/2} = \left(\frac{1+\frac{s\sqrt{4\hat{A}}}{d}}{1+\frac{t\sqrt{4\hat{A}}}{d}}\right)^{(d-1)/2} \sim e^{(s-t)\sqrt{4\hat{A}}}, \tag{C30}$$

we get

$$q_A(t) \sim e^{-\hat{A}/4}\frac{1}{\sqrt{\pi}}\int_0^{\infty} dse^{(s-t)\sqrt{4\hat{A}}-(t-s)^2} = \Theta\left(t+\frac{\sqrt{\hat{A}}}{2}\right). \tag{C31}$$

We can use this result to compute $\mathcal{G}_m(\hat{A})$ as defined in Eq. (C8). Similarly to Eq. (C23), we get

$$\mathcal{G}_m(\hat{A}) = \lim_{d\to\infty}\sqrt{4\hat{A}}\int_{-d/\sqrt{4\hat{A}}}^{\infty} dt\left(1+t\frac{\sqrt{4\hat{A}}}{d}\right)^{d-1} \times\left[\Theta\left(t+\frac{\sqrt{\hat{A}}}{2}\right)^m-\theta(t)\right] \sim \sqrt{4\hat{A}}\int_{-\infty}^{\infty} de^{t\sqrt{4\hat{A}}}\left[\Theta\left(t+\frac{\sqrt{\hat{A}}}{2}\right)^m-\theta(t)\right] = \int_{-\infty}^{\infty} dye^y\left[\Theta\left(\frac{y+\hat{A}}{\sqrt{4\hat{A}}}\right)^m-\theta(y)\right]. \tag{C32}$$

Note that if we expand the second line of Eq. (C32) for small $\hat{A}$ (which amounts to setting $\hat{A}=0$ in the integrand) we obtain exactly the leading term (C23), which indicates that the two limits $d\to\infty$ and $A\to 0$ can be safely exchanged.

e. Jamming limit

The jamming limit corresponds to $m\to 0$ and $A=\alpha m$. Note that $G_m(A)$ is not analytic in $A=m=0$, so the limits $m\to 0$ and $A\to 0$ cannot be exchanged.

However, the integral (C4) is uniformly convergent in the jamming limit so we can exchange the limit with the integral. As $A\to 0$, we can use Eq. (C20) for $q_A(r)$; using then the asymptotic expansion of the error function for $|t|\to\infty$, we can show that

$$\lim_{m\to 0,A=\alpha m}\Theta\left(\frac{r-D}{\sqrt{4A}}\right)^m = \begin{cases} e^{-(r-D)^2/4\alpha}, & r<D \\ 1, & r\geq D. \end{cases} \tag{C33}$$

Then we have

$$G_0(\alpha) = \lim_{m\to 0,A=\alpha m} G_m(A) = \frac{d}{D^d}\int_0^D drr^{d-1}e^{-(r-D)^2/4\alpha}. \tag{C34}$$

It is also possible to show that

$$F_0(\alpha) = \alpha \frac{dG_0(\alpha)}{d\alpha} = \lim_{m\to 0, A=\alpha m} \frac{A}{1-m}\frac{\partial G_m(A)}{\partial A}$$
$$= -\lim_{m\to 0, A=\alpha m} m\frac{\partial G_m(A)}{\partial m}$$
$$= \frac{d}{4\alpha D^d}\int_0^D dr r^{d-1}(r-D)^2 e^{-(r-D)^2/4\alpha}. \quad \text{(C35)}$$

In the limit $d\to\infty$, $\alpha = D^2\hat{\alpha}/d^2$, Eq. (C34) becomes, by changing variable to $y = d(D-r)/D$,

$$\mathcal{G}_0(\hat{\alpha}) = \lim_{d\to\infty} G_0(D^2\hat{\alpha}/d^2) = \lim_{m\to 0, \hat{A}=\hat{\alpha}m} \mathcal{G}_m(\hat{A})$$
$$= \int_0^\infty dy e^{-y-y^2/4\hat{\alpha}}, \quad \text{(C36)}$$

which can also be directly derived from Eqs. (C32) and (C33), confirming that the limits $d\to\infty$ and $A\to 0$ can be exchanged without problems.

3. The function $Q(r)$ in the jamming limit

Even if $q_A(r)$ can be fully computed, the function $Q(r)$, defined in Eq. (C3), cannot be computed analytically in finite dimension. Therefore we limit ourselves here to the computation at first order in $\sqrt{A}$. In this case we have $q_A(r) \sim \Theta((r-D)/\sqrt{4A})$; the integration over the components of $\vec{r}'$ orthogonal to $\vec{r}$ gives 1 neglecting subleading corrections and we get

$$Q(r) = \int_{-\infty}^{\infty} dr' \frac{e^{-(r')^2/4A}}{\sqrt{4\pi A}}\left[\Theta\left(\frac{r-r'-D}{\sqrt{4A}}\right)^{m-1} - 1\right]$$
$$\equiv \frac{1}{m}\Delta_m\left(\frac{r-D}{\sqrt{4mA}}\right), \quad \text{(C37)}$$

where

$$\Delta_m(t) = m\int_{-\infty}^{\infty} \frac{ds}{\sqrt{\pi}} e^{-(t\sqrt{m}-s)^2}[\Theta(s)^{m-1} - 1]. \quad \text{(C38)}$$

It is easy to show that

$$\int_0^\infty dt \Delta_m(t) = \sqrt{m}\int_{-\infty}^{\infty} ds[\Theta(s)^m - \Theta(s)]$$
$$= \sqrt{m}Q_0(m) \underset{m\to 0}{\to} \sqrt{\pi/4}. \quad \text{(C39)}$$

Using, for $s\to-\infty$, $\Theta(s)\sim e^{-s^2}/2\sqrt{\pi}|s|$, it is easy to show that for $m\to 0$, $\Delta_m(0)\to 1$, for $1 \ll t \ll 1/\sqrt{m}$, $\Delta_0(t)\sim 1/2t^2$, and for very large $t \gg 1/\sqrt{m}$, $\Delta_m(t)\sim e^{-mt^2}$. Indeed, we have for any finite t

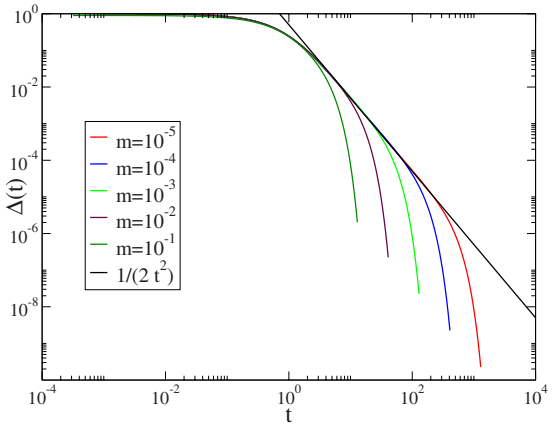

FIG. 25. (Color online) The function $\Delta_m(t)$ for different values of m compared with the asymptotic behavior for $m\to 0$ and large t.

$$\Delta_0(t) \equiv \lim_{m\to 0}\Delta_m(t) = 2\int_0^\infty dy y e^{-y^2-2ty}$$
$$= 1 - \sqrt{\pi}te^{t^2}[1-\mathrm{erf}(t)] \underset{t\gg 1}{\sim} \frac{1}{2t^2} - \frac{3}{4t^4} + \cdots. \quad \text{(C40)}$$

The (one-dimensional) Fourier transform of $\Delta_0(t)$ is given by

$$\hat{\Delta}_0(q) = \int_{-\infty}^{\infty} dt e^{iqt}\Delta_0(|t|)$$
$$= \sqrt{\pi}\left\{1 - e^{q^2/4}\frac{\sqrt{\pi}}{2}|q|\left[1 - \mathrm{erf}\left(\frac{|q|}{2}\right)\right]\right\}$$
$$= \sqrt{\pi}\Delta_0\left(\frac{|q|}{2}\right). \quad \text{(C41)}$$

The function $\Delta_m(t)$ is shown in Fig. 25 for different values of m.

APPENDIX D: DERIVATIVES OF THE CORRELATION FUNCTIONS

In this appendix we show how to compute the derivative $dg(u,v)/d\ln\chi(x,y)$ that is needed to compute the correlation function in the first-order small cage approximation [Eq. (68)]. We start from the partition function as a function of the activity,

$$Z[z(x),\chi(x,y)] = \sum_{N=0}^{\infty}\int \frac{d^N x}{N!}\prod_i z(x_i)\prod_{i<j}\chi(x_i,x_j)$$
$$= \int \exp\left(\int dx\hat{\rho}(x)\ln z(x) + \frac{1}{2}\int dxdy\hat{\rho}_2(x,y)\ln\chi(x,y)\right), \quad \text{(D1)}$$

where the $\int$ sign is a shorthand for $\Sigma_{N=0}^{\infty}\int d^N x/N!$ and $\hat{\rho}(x) = \Sigma_i\delta(x-x_i)$, $\hat{\rho}_2(x,y) = \Sigma_{i\neq j}\delta(x-x_i)\delta(y-x_j)$. From the last expression it is straightforward to show that

$$\frac{\partial \ln Z}{\partial \ln z(x)} = \langle \hat{\rho}(x) \rangle = \rho(x),$$
$$\frac{\partial \ln Z}{\partial \ln \chi(x,y)} = \frac{1}{2}\langle \hat{\rho}_2(x,y) \rangle = \frac{\rho^2}{2} g(x,y). \tag{D2}$$

We define the entropy functional, the Legendre transform of Z,

$$\mathcal{S}[\rho(x), \chi(x,y)] = \max_{z(x)} \left[\ln Z[z(x), \chi(x,y)] - \int dx \rho(x) \ln z(x) \right]. \tag{D3}$$

From this it follows that

$$\frac{\partial \mathcal{S}}{\partial \rho(x)} = -\ln z(x),$$
$$\frac{\partial \mathcal{S}}{\partial \ln \chi(x,y)} = \frac{\partial \ln Z}{\partial \ln \chi(x,y)} = \frac{\rho^2}{2} g(x,y) \tag{D4}$$

because the explicit derivative with respect to $z(x)$ vanishes due to the maximum condition.

Therefore we need to compute $\partial^2 \mathcal{S} / \partial \ln \chi(x,y) \partial \ln \chi(u,v)$. To simplify the notation we write $\ln \chi(x,y) = J_1$, $\ln \chi(u,v) = J_2$, and $\ln z(x) = j(x)$. Then

$$\frac{\partial^2 \mathcal{S}}{\partial J_1 \partial J_2} = \frac{\partial^2 \ln Z}{\partial J_1 \partial J_2} + \int dt \frac{\partial^2 \ln Z}{\partial J_1 \partial j(t)} \frac{dj(t)}{dJ_2} = \frac{\partial^2 \ln Z}{\partial J_1 \partial J_2} - \int dt ds \frac{\partial^2 \ln Z}{\partial J_1 \partial j(t)} \left[\frac{\partial^2 \ln Z}{\partial j(t) \partial j(s)} \right]^{-1} \frac{\partial^2 \ln Z}{\partial J_2 \partial j(s)}, \tag{D5}$$

where we computed $dj(t)/dJ_2$ as follows. Recalling that the derivatives in the last equation are done at constant ρ we can write

$$0 = \frac{d}{dJ_2}\rho(t) = \frac{d}{dJ_2}\frac{\partial \ln Z}{\partial j(t)} = \frac{\partial^2 \ln Z}{\partial j(t) \partial J_2} + \int ds \frac{\partial^2 \ln Z}{\partial j(t) \partial j(s)} \frac{dj(s)}{dJ_2} \tag{D6}$$

from which

$$\frac{dj(t)}{dJ_2} = -\int ds \left[\frac{\partial^2 \ln Z}{\partial j(t) \partial j(s)} \right]^{-1} \frac{\partial^2 \ln Z}{\partial j(s) \partial J_2}. \tag{D7}$$

The explicit derivatives of Z that appear in Eq. (D5) can be explicitly related to correlation functions of the liquid as follows (Hansen and McDonald, 1986):

$$\frac{\partial^2 \ln Z}{\partial \ln \chi(x,y) \partial \ln \chi(u,v)} = \frac{1}{4}[\langle \hat{\rho}_2(x,y)\hat{\rho}_2(u,v) \rangle - \langle \hat{\rho}_2(x,y) \rangle \langle \hat{\rho}_2(u,v) \rangle] = \frac{\rho^2}{4}[\delta(x-u)\delta(y-v) + \delta(x-v)\delta(y-u)]g(x,y) + \frac{\rho^4}{4}\{g_4(x,y,u,v) + \rho^{-1}[\delta(u-x)g_3(y,u,v) + 3 \text{ perm.}] - g(x,y)g(u,v)\},$$
$$\frac{\partial^2 \ln Z}{\partial \ln \chi(x,y) \partial \ln z(t)} = \frac{1}{2}[\langle \hat{\rho}_2(x,y)\hat{\rho}(t) \rangle - \langle \hat{\rho}_2(x,y) \rangle \langle \hat{\rho}(t) \rangle] = \frac{\rho^3}{2}(g_3(x,y,t) + \{\rho^{-1}[\delta(x-t) + \delta(y-t)] - 1\}g(x,y)),$$
$$\frac{\partial^2 \ln Z}{\partial \ln z(t) \partial \ln z(s)} = \langle \hat{\rho}(t)\hat{\rho}(s) \rangle - \langle \hat{\rho}(t) \rangle \langle \hat{\rho}(s) \rangle = \rho\{\delta(t-s) + \rho h(t,s)\},$$
$$\left[\frac{\partial^2 \ln Z}{\partial \ln z(t) \partial \ln z(s)} \right]^{-1} = \frac{1}{\rho}\delta(t-s) - c(t,s), \tag{D8}$$

where the last equation follows from the Ornstein-Zernicke relation (Hansen and McDonald, 1986).

Finally, we have

$$\frac{dg(u,v)}{d \ln \chi(x,y)} = \frac{2}{\rho^2} \frac{\partial^2 \mathcal{S}}{\partial \ln \chi(x,y) \partial \ln \chi(u,v)} = \frac{1}{2}[\delta(x-u)\delta(y-v) + \delta(x-v)\delta(y-u)]g(x,y) + \frac{\rho^2}{2}\{g_4(x,y,u,v) + \rho^{-1}[\delta(u-x)g_3(y,u,v) + 3 \text{ perm.}] - g(x,y)g(u,v)\} - \frac{\rho^4}{2}\int dt ds (g_3(x,y,t) + \{\rho^{-1}[\delta(x-t) + \delta(y-t)] - 1\}g(x,y)) \left[\frac{1}{\rho}\delta(t-s) - c(t,s) \right] \times (g_3(u,v,s) + \{\rho^{-1}[\delta(u-s) + \delta(v-s)] - 1\}g(u,v)). \tag{D9}$$

By inspection of these contribution to Eq. (68) one can show that only the first one is relevant to describe the delta peak of $\tilde{g}(x,y)$, which gives Eq. (70).

APPENDIX E: SCALING CLOSE TO JAMMING

We will show here how to compute the behavior of $m(\varphi,\varphi_j)$ for $\varphi\to\varphi_j$. For this we will need the asymptotic behavior of $Q_0(m)$ for $m\to 0$; one can show that

$$Q_0(m) \sim \sqrt{\frac{\pi}{4m}} e^{(m/2)\ln m} R_m + S_m, \tag{E1}$$

where R_m and S_m are C^∞ functions of m with $R_m=1+R_1 m+\cdots$ and $S_m=S_1 m+S_2 m^2+\cdots$, so that

$$\ln Q_0(m) \sim \frac{1}{2}\ln\frac{\pi}{4} - \frac{1}{2}\ln m + \frac{m}{2}\ln m + \ln R_m + O(m^{3/2}), \tag{E2}$$

where $O(x^\alpha)$ represents a quantity which is bounded by Cx^α for $x\to 0$. From this relation it follows that

$$\frac{Q_0'(m)}{Q_0(m)} = -\frac{1}{2m} + \frac{\ln m}{2} + \frac{1}{2} + \frac{R_m'}{R_m} + O(m^{1/2}),$$
$$\frac{d}{dm}\frac{Q_0'(m)}{Q_0(m)} = \frac{1}{2m^2} + \frac{1}{2m} + O(m^{-1/2}). \tag{E3}$$

We have then from Eq. (75)

$$\begin{aligned}\partial_m \Sigma(m,\varphi) &= \frac{d}{2m} + \frac{d}{1-m} + 2dm\frac{Q_0'(m)}{Q_0(m)} \\ &\quad - d - dm(1-m)\frac{d}{dm}\frac{Q_0'(m)}{Q_0(m)} \\ &= -d + O(\sqrt{m}).\end{aligned} \tag{E4}$$

On the other hand,

$$\begin{aligned}\partial_\varphi \Sigma(m,\varphi) &= S'(\varphi) + d\frac{\partial_\varphi [A^*(m)]^{-1/2}}{[A^*(m)]^{-1/2}} \\ &= S'(\varphi) + d\frac{\partial_\varphi[\varphi Y(\varphi)]}{\varphi Y(\varphi)} \\ &= S'(\varphi) + \frac{d}{\varphi} + d\frac{Y'(\varphi)}{Y(\varphi)},\end{aligned} \tag{E5}$$

and we obtain, close to φ_j,

$$m(\varphi,\varphi_j) \sim -\frac{1}{d}\left[S'(\varphi) + \frac{d}{\varphi} + d\frac{Y'(\varphi)}{Y(\varphi)}\right](\varphi_j-\varphi), \tag{E6}$$

i.e., Eq. (84).

REFERENCES

Abate, A., and D. Durian, 2006, Phys. Rev. E **74**, 031308.
Abramowitz, H., and I. Segun, 1965, *Handbook of Mathematical Functions* (Dover, New York).
Alder, B. J., and T. E. Wainwright, 1957, J. Chem. Phys. **27**, 1208.
Alexander, S., 1998, Phys. Rep. **296**, 65.
Angelani, L., and G. Foffi, 2007, J. Phys.: Condens. Matter **19**, 256207.
Anikeenko, A. V., and N. N. Medvedev, 2007, Phys. Rev. Lett. **98**, 235504.
Anikeenko, A. V., N. N. Medvedev, and T. Aste, 2008, Phys. Rev. E **77**, 031101.
Aste, T., 2005, J. Phys.: Condens. Matter **17**, S2361.
Aste, T., and A. Coniglio, 2004, Europhys. Lett. **67**, 165.
Aste, T., M. Saadatfar, and T. J. Senden, 2005, Phys. Rev. E **71**, 061302.
Ball, K., 1992, Int. Math. Res. Notices **1992**, 217.
Barrat, A., S. Franz, and G. Parisi, 1997, J. Phys. A **30**, 5593.
Barthel, W., A. K. Hartmann, and M. Weigt, 2003, Phys. Rev. E **67**, 066104.
Baxter, R. J., 1968, J. Chem. Phys. **49**, 2770.
Bengtzelius, U., W. Gotze, and A. Sjolander, 1984, J. Phys. C **17**, 5915.
Bennett, C. H., 1972, J. Appl. Phys. **43**, 2727.
Bernal, J., and J. Mason, 1960, Nature (London) **188**, 910.
Bernal, J., J. Mason, and K. Knight, 1962, Nature (London) **194**, 957.
Berryman, J. G., 1983, Phys. Rev. A **27**, 1053.
Berthier, L., and T. A. Witten, 2009a, EPL **86**, 10001.
Berthier, L., and T. A. Witten, 2009b, Phys. Rev. E **80**, 021502.
Biazzo, I., F. Caltagirone, G. Parisi, and F. Zamponi, 2009, Phys. Rev. Lett. **102**, 195701.
Binder, K., and W. Kob, 2005, *Glassy Materials and Disordered Solids: An Introduction to their Statistical Mechanics* (World Scientific, Singapore).
Biroli, G., J. Bouchaud, A. Cavagna, T. Grigera, and P. Verrocchio, 2008, Nat. Phys. **4**, 771.
Biroli, G., and M. Mézard, 2001, Phys. Rev. Lett. **88**, 025501.
Biroli, G., and R. Monasson, 2000, Europhys. Lett. **50**, 155.
Bishop, M., and P. A. Whitlock, 2005, J. Chem. Phys. **123**, 014507.
Bouchaud, J. P., and G. Biroli, 2004, J. Chem. Phys. **121**, 7347.
Brambilla, G., D. E. Masri, M. Pierno, L. Berthier, L. Cipelletti, G. Petekidis, and A. B. Schofield, 2009, Phys. Rev. Lett. **102**, 085703.
Brito, C., and M. Wyart, 2006, Europhys. Lett. **76**, 149.
Brumer, Y., and D. Reichman, 2004, J. Phys. Chem. B **108**, 6832.
Cammarota, C., A. Cavagna, G. Gradenigo, T. Grigera, and P. Verrocchio, 2009, J. Stat. Mech. **2009**, L12002.
Cardenas, M., S. Franz, and G. Parisi, 1998, J. Phys. A **31**, L163.
Cardenas, M., S. Franz, and G. Parisi, 1999, J. Chem. Phys. **110**, 1726.
Castellani, T., and A. Cavagna, 2005, J. Stat. Mech.: Theory Exp. **2005**, P05012.
Cavagna, A., 2009, Phys. Rep. **476**, 51.
Cavagna, A., A. Attanasi, and J. Lorenzana, 2005, Phys. Rev. Lett. **95**, 115702.
Cavagna, A., T. S. Grigera, and P. Verrocchio, 2007, Phys. Rev. Lett. **98**, 187801.
Chaudhuri, P., L. Berthier, and S. Sastry, 2009, e-print arXiv:0910.0364.
Chaudhuri, P., S. Karmakar, C. Dasgupta, H. R. Krishnamurthy, and A. K. Sood, 2005, Phys. Rev. Lett. **95**, 248301.
Clarke, A. S., and H. Jónsson, 1993, Phys. Rev. E **47**, 3975.
Coluzzi, B., M. Mézard, G. Parisi, and P. Verrocchio, 1999, J. Chem. Phys. **111**, 9039.

Conway, J. H., and N. J. A. Sloane, 1993, *Sphere Packings, Lattices and Groups* (Spriger-Verlag, New York).
Cugliandolo, L. F., and J. Kurchan, 1993, Phys. Rev. Lett. **71**, 173.
Daniels, K. E., and R. P. Behringer, 2006, J. Stat. Mech.: Theory Exp. **2006**, P07018.
Dasgupta, C., and O. T. Valls, 1999, Phys. Rev. E **59**, 3123.
Dauchot, O., G. Marty, and G. Biroli, 2005, Phys. Rev. Lett. **95**, 265701.
Debenedetti, P. G., and F. H. Stillinger, 2001, Nature (London) **410**, 259.
De Dominicis, C., and P. C. Martin, 1964, J. Math. Phys. **5**, 31.
Dodds, J., 1975, Nature (London) **256**, 187.
Dodds, J., 1980, J. Colloid Interface Sci. **77**, 317.
Donev, A., I. Cisse, D. Sachs, E. Variano, F. Stillinger, R. Connelly, S. Torquato, and P. Chaikin, 2004, Science **303**, 990.
Donev, A., R. Connelly, F. H. Stillinger, and S. Torquato, 2007, Phys. Rev. E **75**, 051304.
Donev, A., F. H. Stillinger, and S. Torquato, 2006, Phys. Rev. Lett. **96**, 225502.
Donev, A., S. Torquato, and F. H. Stillinger, 2005a, Phys. Rev. E **71**, 011105.
Donev, A., S. Torquato, and F. H. Stillinger, 2005b, Phys. Rev. Lett. **95**, 090604.
Donth, E., 2001, *The Glass Transition: Relaxation Dynamics in Liquids and Disordered Materials* (Springer, New York).
Dress, C., and W. Krauth, 1995, J. Phys. A **28**, L597.
Ediger, M. D., C. A. Angell, and S. R. Nagel, 1996, J. Phys. Chem. **100**, 13200.
Edwards, S., and R. Oakeshott, 1989, Physica A **157**, 1080.
Edwards, S. F., 1998, Physica A **249**, 226.
Finney, J. L., 1970, Proc. R. Soc. London, Ser. A **319**, 479.
Foffi, G., W. Götze, F. Sciortino, P. Tartaglia, and T. Voigtmann, 2003, Phys. Rev. Lett. **91**, 085701.
Foffi, G., W. Götze, F. Sciortino, P. Tartaglia, and T. Voigtmann, 2004, Phys. Rev. E **69**, 011505.
Franz, S., 2005, J. Stat. Mech.: Theory Exp. **2005**, P04001.
Franz, S., and G. Parisi, 1997, Phys. Rev. Lett. **79**, 2486.
Franz, S., and F. Tria, 2006, J. Stat. Phys. **122**, 313.
Frisch, H. L., and J. K. Percus, 1999, Phys. Rev. E **60**, 2942.
Gao, G.-J., J. Blawzdziewicz, and C. S. O'Hern, 2006, Phys. Rev. E **74**, 061304.
Goldbart, P., N. Goldenfeld, and D. Sherrington, 2005, Eds., *Stealing the Gold–A Celebration of the Pioneering Physics of Sam Edwards* (Oxford University Press, Oxford).
Götze, W., 1999, J. Phys.: Condens. Matter **11**, A1.
Götze, W., and T. Voigtmann, 2003, Phys. Rev. E **67**, 021502.
Grigera, T., and G. Parisi, 2001, Phys. Rev. E **63**, 045102.
Gross, D. J., and M. Mézard, 1984, Nucl. Phys. B **240**, 431.
Hales, T. C., 2005, Ann. Math. **162**, 1065.
Hall, R. W., and P. G. Wolynes, 2003, Phys. Rev. Lett. **90**, 085505.
Hall, R. W., and P. G. Wolynes, 2008, J. Phys. Chem. B **112**, 301.
Hansen, J.-P., and I. R. McDonald, 1986, *Theory of Simple Liquids* (Academic, London).
Hatano, T., M. Otsuki, and S. Sasa, 2007, J. Phys. Soc. Jpn. **76**, 023001.
Henderson, D., 1975, Mol. Phys. **30**, 971.
Hermes, M., and M. Dijkstra, 2010, EPL **89**, 38005.
Jerkins, M., M. Schröter, H. L. Swinney, T. J. Senden, M. Saadatfar, and T. Aste, 2008, Phys. Rev. Lett. **101**, 018301.
Jodrey, W. S., and E. M. Tory, 1985, Phys. Rev. A **32**, 2347.
Kabatiansky, G. A., and V. I. Levensthein, 1978, Probl. Inf. Transm. **14**, 1.
Kamien, R. D., and A. J. Liu, 2007, Phys. Rev. Lett. **99**, 155501.
Kansal, A. R., S. Torquato, and F. H. Stillinger, 2002, Phys. Rev. E **66**, 041109.
Kauzmann, W., 1948, Chem. Rev. (Washington, D.C.) **43**, 219.
Kim, K., and T. Munakata, 2003, Phys. Rev. E **68**, 021502.
Kirkpatrick, T. R., and D. Thirumalai, 1987, Phys. Rev. Lett. **58**, 2091.
Kirkpatrick, T. R., D. Thirumalai, and P. G. Wolynes, 1989, Phys. Rev. A **40**, 1045.
Kirkpatrick, T. R., and P. G. Wolynes, 1987a, Phys. Rev. A **35**, 3072.
Kirkpatrick, T. R., and P. G. Wolynes, 1987b, Phys. Rev. B **36**, 8552.
Krauth, W., 2006, *Statistical Mechanics: Algorithms and Computations* (Oxford University Press, New York).
Krivelevich, M., S. Litsyn, and A. Vardy, 2004, Int. Math. Res. Notices **2004**, 2271.
Krzakala, F., and J. Kurchan, 2007, Phys. Rev. E **76**, 021122.
Krzakala, F., A. Montanari, F. Ricci-Tersenghi, G. Semerjian, and L. Zdeborova, 2007, Proc. Natl. Acad. Sci. U.S.A. **104**, 10318.
Krzakala, F., M. Tarzia, and L. Zdeborová, 2008, Phys. Rev. Lett. **101**, 165702.
Lechenault, F., O. Dauchot, G. Biroli, and J. Bouchaud, 2008, EPL **83**, 46003.
Leuzzi, L., and T. Nieuwenhuizen, 2007, *Thermodynamics of the Glassy State* (Taylor & Francis, London).
Liu, A., and S. Nagel, 2001, *Jamming and Rheology: Constrained Dynamics on Microscopic and Macroscopic Scales* (Taylor & Francis, London).
Lochmann, K., A. Anikeenko, A. Elsner, N. Medvedev, and D. Stoyan, 2006, Eur. Phys. J. B **53**, 67.
Lubachevsky, B. D., and F. H. Stillinger, 1990, J. Stat. Phys. **60**, 561.
Luding, S., 2001, Phys. Rev. E **63**, 042201.
Majmudar, T. S., M. Sperl, S. Luding, and R. P. Behringer, 2007, Phys. Rev. Lett. **98**, 058001.
Mari, R., F. Krzakala, and J. Kurchan, 2009, Phys. Rev. Lett. **103**, 025701.
Mason, G., and W. Clark, 1965, Nature (London) **207**, 512.
Mason, G., and W. Clark, 1966, Nature (London) **211**, 957.
Matheson, A. J., 1974, J. Phys. C **7**, 2569.
Mézard, M., 1999, Physica A **265**, 352.
Mézard, M., and G. Parisi, 1996, e-print arXiv:cond-mat/9602002.
Mézard, M., and G. Parisi, 1999a, J. Chem. Phys. **111**, 1076.
Mézard, M., and G. Parisi, 1999b, Phys. Rev. Lett. **82**, 747.
Mézard, M., and G. Parisi, 2000, J. Phys.: Condens. Matter **12**, 6655.
Mézard, M., G. Parisi, and M. A. Virasoro, 1987, *Spin Glass Theory and Beyond* (World Scientific, Singapore).
Miller, M. A., and D. Frenkel, 2004a, J. Chem. Phys. **121**, 535.
Miller, M. A., and D. Frenkel, 2004b, J. Phys.: Condens. Matter **16**, S4901.
Möller, J., I. Gutzow, and J. Schmelzer, 2006, J. Chem. Phys. **125**, 094505.
Monasson, R., 1995, Phys. Rev. Lett. **75**, 2847.
Montanari, A., and F. Ricci-Tersenghi, 2004, Phys. Rev. B **70**, 134406.
Montanari, A., and G. Semerjian, 2006, J. Stat. Phys. **125**, 23.
Morita, T., and K. Hiroike, 1961, Prog. Theor. Phys. **25**, 537.

O'Hern, C. S., S. A. Langer, A. J. Liu, and S. R. Nagel, 2002, Phys. Rev. Lett. **88**, 075507.
O'Hern, C. S., L. E. Silbert, A. J. Liu, and S. R. Nagel, 2003, Phys. Rev. E **68**, 011306.
Olsson, P., and S. Teitel, 2007, Phys. Rev. Lett. **99**, 178001.
Onoda, G. Y., and E. G. Liniger, 1990, Phys. Rev. Lett. **64**, 2727.
Osada, H., 1998, Probab. Theory Relat. Fields **112**, 53.
Ouchiyama, N., and T. Tanaka, 1981, Ind. Eng. Chem. Fundam. **20**, 66.
Parisi, G., 1988, *Statistical Field Theory* (Addison-Wesley, Reading, MA).
Parisi, G., 2008, J. Stat. Phys. **132**, 207.
Parisi, G., and F. Slanina, 2000, Phys. Rev. E **62**, 6554.
Parisi, G., and F. Zamponi, 2005, J. Chem. Phys. **123**, 144501.
Parisi, G., and F. Zamponi, 2006a, J. Stat. Mech.: Theory Exp. **2006**, P03017.
Parisi, G., and F. Zamponi, 2006b, J. Stat. Phys. **123**, 1145.
Phan, S.-E., W. B. Russel, Z. Cheng, J. Zhu, P. M. Chaikin, J. H. Dunsmuir, and R. H. Ottewill, 1996, Phys. Rev. E **54**, 6633.
Pica Ciamarra, M., M. Nicodemi, and A. Coniglio, 2007, Phys. Rev. E **75**, 021303.
Pica Ciamarra, M., M. Tarzia, A. de Candia, and A. Coniglio, 2003, Phys. Rev. E **67**, 057105.
Pinson, D., R. P. Zou, A. B. Yu, P. Zulli, and M. J. McCarthy, 1998, J. Phys. D **31**, 457.
Powell, M. J., 1979, Phys. Rev. B **20**, 4194.
Pusey, P., and W. Van Megen, 1986, Nature (London) **320**, 340.
Richard, P., L. Oger, J.-P. Troadec, and A. Gervois, 1999, Phys. Rev. E **60**, 4551.
Rintoul, M. D., and S. Torquato, 1996, J. Chem. Phys. **105**, 9258.
Rivoire, O., G. Biroli, O. Martin, and M. Mézard, 2004, Eur. Phys. J. B **37**, 55.
Robles, M., and M. L. de Haro, 2003, Europhys. Lett. **62**, 56.
Rogers, C. A., 1964, *Packing and Covering* (Cambridge University Press, Cambridge).
Ruelle, D., 1977, private communication.
Santen, L., and W. Krauth, 2000, Nature (London) **405**, 550.
Santen, L., and W. Krauth, 2001, e-print arXiv:cond-mat/0107459.
Schreck, C. F., and C. S. O'Hern, 2008, unpublished.
Schröter, M., D. I. Goldman, and H. L. Swinney, 2005, Phys. Rev. E **71**, 030301.
Scott, G., 1962, Nature (London) **194**, 956.
Scott, G. D., and D. M. Kilgour, 1969, Br. J. Appl. Phys. **2**, 863.
Sellitto, M., G. Biroli, and C. Toninelli, 2005, Europhys. Lett. **69**, 496.
Semerjian, G., 2008, J. Stat. Phys. **130**, 251.
Semerjian, G., and R. Monasson, 2003, Phys. Rev. E **67**, 066103.
Shundyak, K., M. van Hecke, and W. van Saarloos, 2007, Phys. Rev. E **75**, 010301.
Silbert, L., A. Liu, and S. Nagel, 2005, Phys. Rev. Lett. **95**, 098301.
Silbert, L. E., A. J. Liu, and S. R. Nagel, 2006, Phys. Rev. E **73**, 041304.
Singh, Y., J. P. Stoessel, and P. G. Wolynes, 1985, Phys. Rev. Lett. **54**, 1059.
Skoge, M., A. Donev, F. H. Stillinger, and S. Torquato, 2006, Phys. Rev. E **74**, 041127.
Sloane, N. J. A., 2007, http://www.research.att.com/~njas/
Snoeijer, J. H., T. J. H. Vlugt, W. G. Ellenbroek, M. van Hecke, and J. M. J. van Leeuwen, 2004, Phys. Rev. E **70**, 061306.
Snoeijer, J. H., T. J. H. Vlugt, M. van Hecke, and W. van Saarloos, 2004, Phys. Rev. Lett. **92**, 054302.
Somfai, E., M. van Hecke, W. G. Ellenbroek, K. Shundyak, and W. van Saarloos, 2007, Phys. Rev. E **75**, 020301.
Song, C., P. Wang, and H. Makse, 2008, Nature (London) **453**, 629.
Song, Y., E. A. Mason, and R. M. Stratt, 1989, J. Phys. Chem. **93**, 6916.
Speedy, R. J., 1994, J. Chem. Phys. **100**, 6684.
Speedy, R. J., 1998, Mol. Phys. **95**, 169.
Stevenson, J. D., A. M. Walczak, R. W. Hall, and P. G. Wolynes, 2008, J. Chem. Phys. **129**, 194505.
Stillinger, F. H., and T. A. Weber, 1982, Phys. Rev. A **25**, 978.
Stillinger, F. H., and T. A. Weber, 1985, Phys. Rev. B **31**, 5262.
Stoessel, J. P., and P. G. Wolynes, 1984, J. Chem. Phys. **80**, 4502.
Talagrand, M., 2003, *Spin Glasses: A Challenge for Mathematicians—Cavity and Mean Field Models* (Springer, New York).
Talbot, J., G. Tarjus, P. R. V. Tassel, and P. Viot, 2000, Colloids Surf., A **165**, 287.
Tarzia, M., 2007, J. Stat. Mech.: Theory Exp. **2007**, P01010.
Tarzia, M., A. de Candia, A. Fierro, M. Nicodemi, and A. Coniglio, 2004, Europhys. Lett. **66**, 531.
Tejero, C. F., and M. Baus, 1993, Phys. Rev. E **48**, 3793.
Thouless, D., P. Anderson, and R. Palmer, 1977, Philos. Mag. **35**, 593.
Torquato, S., 1995, Phys. Rev. Lett. **74**, 2156.
Torquato, S., 2002, *Random Heterogeneous Materials: Microstructure and Macroscopic Properties* (Springer-Verlag, New York).
Torquato, S., and F. H. Stillinger, 2006a, Phys. Rev. E **73**, 031106.
Torquato, S., and F. H. Stillinger, 2006b, Exp. Math. **15**, 307.
Torquato, S., T. M. Truskett, and P. G. Debenedetti, 2000, Phys. Rev. Lett. **84**, 2064.
Torquato, S., O. U. Uche, and F. H. Stillinger, 2006, Phys. Rev. E **74**, 061308.
van Meel, J. A., D. Frenkel, and P. Charbonneau, 2009, Phys. Rev. E **79**, 030201.
van Megen, W., and S. M. Underwood, 1993, Phys. Rev. Lett. **70**, 2766.
van Megen, W., S. M. Underwood, and P. N. Pusey, 1991, Phys. Rev. Lett. **67**, 1586.
Velenich, A., A. Parola, and L. Reatto, 2006, Phys. Rev. E **74**, 021410.
Wertheim, M. S., 1963, Phys. Rev. Lett. **10**, 321.
Wood, W. W., and J. D. Jacobson, 1957, J. Chem. Phys. **27**, 1207.
Woodcock, L. V., and C. A. Angell, 1981, Phys. Rev. Lett. **47**, 1129.
Wyart, M., 2005, Ann. Phys. **30**, 1.
Wyart, M., S. Nagel, and T. Witten, 2005, Europhys. Lett. **72**, 486.
Wyart, M., L. Silbert, S. Nagel, and T. Witten, 2005, Phys. Rev. E **72**, 051306.
Xia, X., and P. G. Wolynes, 2001a, Proc. Natl. Acad. Sci. U.S.A. **97**, 2990.
Xia, X., and P. G. Wolynes, 2001b, Phys. Rev. Lett. **86**, 5526.
Xu, N., J. Blawzdziewicz, and C. S. O'Hern, 2005, Phys. Rev. E **71**, 061306.

Yerazunis, S., S. Cornell, and B. Wintner, 1965, Nature (London) **207**, 835.
Yoshidome, T., A. Yoshimori, and T. Odagaki, 2007, Phys. Rev. E **76**, 021506.
Zamponi, F., 2007, Philos. Mag. B **87**, 485.
Zdeborová, L., and F. Krzakala, 2007, Phys. Rev. E **76**, 031131.
Zeravcic, Z., W. van Saarloos, and D. R. Nelson, 2008, EPL **83**, 44001.